TESIS DOCTORAL

MEDIDA DE LA TEMPERATURA SUPERFICIAL DE COMBUSTIÓN DEL CARBONIZADO MEDIANTE PIROMETRÍA CON CÁMARA DIGITAL PARA ESTUDIAR EL EFECTO DEL CO_2 EN SU OXI-CONVERSIÓN EN REACTORES DE LECHO FLUIDO

POR PARTE DE

JESÚS SALINERO GONZÁLEZ

PARA OBTENER EL GRADO DE DOCTOR INTERNACIONAL

DIRECTOR: DR. ALBERTO GOMEZ BAREA

Departamento de Ingeniería Química y Ambiental
ESCUELA SUPERIOR DE INGENIERÍA, UNIVERSIDAD DE SEVILLA
Sevilla, España 2017

THESIS FOR DEGREE OF DOCTOR OF PHILOSOPHY

MEASUREMENT OF CHAR TEMPERATURE IN A FLUIDIZED BED REACTOR USING PYROMETRY WITH A DIGITAL CAMERA: APPLICATION TO OXY-FUEL COMBUSTION

BY

JESÚS SALINERO GONZÁLEZ

DIRECTOR: DR. ALBERTO GOMEZ BAREA

Chemical and Environmental Engineering Department
SCHOOL OF ENGINEERING, UNIVERSITY OF SEVILLE
Seville, Spain 2017

A Mis Padres

MEDIDA DE LA TEMPERATURA SUPERFICIAL DE COMBUSTIÓN DEL CARBONIZADO MEDIANTE PIROMETRÍA CON CÁMARA DIGITAL PARA ESTUDIAR EL EFECTO DEL CO_2 EN SU OXI-CONVERSIÓN EN REACTORES DE LECHO FLUIDO

JESÚS SALINERO GONZÁLEZ

Departamento de Ingeniería Química y Ambiental
ESCUELA SUPERIOR DE INGENIERÍA, UNIVERSIDAD DE SEVILLA
Sevilla, España 2017

RESUMEN

A pesar del trabajo en oxi-combustión de partículas de carbón/carbonizado en reactores de lecho fluido, el efecto de cambiar la atmósfera de O_2/N_2 a O_2/CO_2, con una elevada concentración de O_2, sobre el proceso de conversión no está totalmente claro. Ello se debe (i) a que la mayoría de los trabajos experimentales utilizaron concentraciones de O_2 menores al 21 $\%_{v/v}$; (ii) a que algunas de las técnicas de medida de temperaturas empleadas, tales como los termopares, podría haber alterado la conversión; y (iii) a que la mayoría de los estudios teóricos asumen que la partícula de carbón/carbonizado está únicamente en la fase emulsión, obviando las observaciones experimentales que la sitúan tanto en la fase burbuja como en la zona splash (chapoteo) del lecho durante parte del tiempo de fluidización. Por lo tanto, el objetivo principal de esta Tesis es aclarar la oxi-combustión de partículas de carbonizado (varios milímetros) en lecho fluido con una elevada concentración de O_2 en CO_2.

Para ello, se diseñó y construyó un reactor de lecho fluido de geometría bidimensional (escala laboratorio, 18 x 50 x 1.8 cm) equipado con una ventana de cuarzo (20 x 20 cm) que permitió realizar medidas ópticas. Además, se utilizó un segundo reactor de lecho fluido cilíndrico (escala laboratorio, 7 cm diámetro interno x 50 cm). En todos los tests, tanto de combustión (O_2/N_2) como de oxi-combustión (O_2/CO_2), se alimentó al reactor una única partícula de carbonizado, la cual en algunos ensayos tenía un termopar insertado. Las partículas de carbonizado utilizadas se generaron a partir de partículas irregulares de madera de haya, y carbón bituminoso y sub-bituminoso, cuyos tamaños y pesos se fijaron en función del test donde fueran a ser utilizados. Como gente de fluidización se utilizó mezclas de O_2 y N_2 u O_2 y CO_2, así como aire, con una concentración de O_2 del 11, 21, 30, 40, y 50 $\%_{v/v}$.

En el primero de los estudios se desarrolla un método de medida de temperaturas superficiales del carbonizado, que se aplica a la combustión en un reactor de lecho fluido. La técnica se basa en la captura e interpretación de la radiación térmica contenida en las bandas espectrales visibles roja, verde, y azul que hace una cámara digital (Pirometría con Cámara Digital). Se muestra que el uso secuencial de la radiación contenida en los tres colores mencionados mejora la precisión de la temperatura medida respecto el uso tradicional simultáneo. Además, el método permite medir temperaturas del carbonizado menores a las del fondo (limitación en el uso simultáneo de dos colores). En el segundo estudio se analiza el efecto del termopar sobre la combustión del carbonizado en lecho fluido, encontrando que el termopar altera el movimiento del carbonizado a través del lecho, variando el tiempo de residencia en

cada una de las fases del lecho. En concreto el termopar aumenta el tiempo de la partícula en la fase burbuja por la mayor resistencia del conjunto termopar-partícula al arrastre de las partículas del lecho. Este aumento en el tiempo del carbonizado en las burbujas aumenta la temperatura de combustión, reduce el tiempo de consumo y hace que el consumo superficial no sea homogéneo (la rotación de la partícula está impedida). En el tercer trabajo se analiza el efecto del movimiento del carbonizado a través de las diferentes fases del lecho sobre su temperatura, mostrándose que la temperatura superficial de combustión varía decenas de grados en tan solo centésimas de segundos. Este movimiento es experimentalmente caracterizado y se implementa en el modelo teórico de combustión de una partícula de carbonizado en un lecho fluido. Las predicciones ajustan bastante bien las oscilaciones de temperatura y tiempos de consumos. En el último estudio se analiza la influencia del CO_2 y O_2 en la oxi-combustión de las partículas de carbonizado, concluyéndose que la oxi-combustión del carbonizado en un lecho fluido está controlada por la trasferencia de O_2 desde el seno de la fase fluida hacia el carbonizado, y que el consumo por gasificación no es despreciable. Se encuentra que el consumo por gasificación del carbón compensa la menor difusividad del O_2 en CO_2 reduciendo las diferencias entre los consumos aparentes medios del carbonizado (g/m^2s) en O_2/CO_2 y en O_2/N_2 para temperaturas del carbonizado menores a los 925 °C, y haciendo el consumo en O_2/CO_2 mayor para temperatura del carbonizado mayores a 925 °C. Finalmente, las temperaturas registradas en el carbonizado durante conversión en O_2/CO_2 son menores a las registradas en la atmósfera equivalente (igual concentración de O_2) de O_2/N_2, registrándose las mayores diferencias cuando las partículas están en la fase burbuja o zona splash (capoteo) del lecho.

PALABRAS CLAVE: Lecho fluido, Oxi-combutión, Temperatura del carbonizado, Pirometría, Carbón

MEASUREMENT OF CHAR TEMPERATURE IN A FLUIDIZED BED REACTOR USING PYROMETRY WITH A DIGITAL CAMERA: APPLICATION TO OXY-FUEL COMBUSTION

JESÚS SALINERO GONZÁLEZ

Chemical and Environmental Engineering Department
SCHOOL OF ENGINEERING, UNIVERSITY OF SEVILLE
Seville, Spain 2017

ABSTRACT

Despite all work carried out on coal/char oxy-combustion in fluidized bed (FB), the effect of changing the atmosphere from O_2/N_2 to O_2/CO_2 at high O_2 concentration is not well understood yet. Most of the experimental work has been carried out with O_2 concentration lower than 21 $\%_{v/v}$ and some of the techniques used to measure the fuel particle temperature, such as thermocouples, could interfere with the conversion. Theoretical studies assume that the coal/char particle is always in the emulsion phase, although experimental observations confirm that the particle is also in the bubbles and splash zone. These different char particle's location in the bed could involve oscillations in the char particle's temperature during the oxy-combustion process. On the other hand, controlling and measuring the char particle's temperature is one of the main challenges, but neither thermocouples nor pyrometry with an optical probe are accurate enough to be used for that purpose.

Addressing those questions, a bi-dimensional fluidized bed reactor (lab scale, 18 x 50 x 1.8 cm) was designed and constructed with a quartz window in its bottom for optical measurements. Moreover, another cylindrical fluidized bed reactor (lab scale, 7 (i.d) x 50 cm) was occasionally used. All tests carried out were single char particle combustion (O_2/N_2) or oxy-combustion (O_2/CO_2), most of them the particle was freely fluidized (without an embedded thermocouple). Char particles from three different fuels were used: Beech wood, and Sub-bituminous and Bituminous coal, whose sizes and weights were set as a function of the tests where they were going to be used. The fluidization flow was either a pre-heated mixture of O_2 and N_2 or O_2 and CO_2, where the O_2 concentration could be 11, 21, 30, 40 and 50 $\%_{v/v}$.

In the first study, a method is presented to measure the temperature of the char particle's surface during conversion in a FB using a digital camera. The method applies one-color pyrometry sequentially for the three spectral bands red, green and blue (instead of the widespread used two-color pyrometry), changing from one band to another automatically as a function of the radiation intensity received by the digital camera's sensor. In the second study, the pyrometric measurement is used to analyze the impact of using an embedded thermocouple into a char particle in a FB, finding that the thermocouple increases the combustion temperature and involve a non-homogeneous surface carbon consumption. In the third study, it is experimentally measured oscillations in the char's temperature of tens degrees in hundredths of second resulting from its movement through the different bed's phases. That char's movement is experimental characterized and implemented in a theoretical model of a single char particle conversion in a FB, predicting quite well the experimental oscillations of the temperature and

the overall conversion process. In the last study, the pyrometric char temperatures and their predictions (from the theoretical approach presented previously) were used to clarify the influence of the CO_2 concentration gas in a high O_2 concentration atmosphere. The results showed that the transfer of O_2 to the particle controls the overall rate of char conversion in O_2/CO_2 (as in O_2/N_2), being the carbon consumption by gasification significant even a relatively low char temperature (850 °C). This additional carbon consumption makes the apparent consumption rate in both atmosphere roughly equal (for the same O_2 concentration), for temperature below 925 °C, and higher in O_2/CO_2 than in O_2/N_2 for char temperature above 925 °C. It is concluded that the difference in char conversion rate, observed in both atmospheres, is mainly controlled by the time in which the char particle is out of the emulsion phase. These results underline the importance of considering movement of the char particle through different phases of the bed to improve the understanding of oxy-fuel behavior in FB.

KEYWORD: Fluidized bed, Oxy-combustion, Char temperature, Pyrometry, Coal

PAPERS

This thesis in based on a number of papers already published or submitted to journals:

Paper 1. Salinero J, Gómez-Barea A, Tripiana M, Leckner B. Measurement of char surface temperature in a fluidized bed combustor using pyrometry with digital camera. Chemical Engineering Journal 2016; 288: 441-450

Paper 2. Salinero J, Gómez-Barea A, Fuentes-Cano D, Leckner B. The effect of using thermocouples on the char particle combustion in a fluidized bed reactor. Fuel 2017; 207; 615-624

Paper 3. Salinero J, Gómez-Barea A, Fuentes-Cano D, Leckner B. Measurement and theoretical prediction of char temperature oscillation during fluidized bed combustion. Paper submitted in Combustion and flame at October, 2017 as CBF-D-17-00750

Paper 4. Salinero J, Gómez-Barea A, Fuentes-Cano D, Leckner B. The influence of CO_2 gas concentration on the char temperature and conversion during oxy-fuel combustion in a fluidized bed. Paper submitted in Applied Energy at November, 2017 as APEN-D-17-09652

and international conferences:

Paper 5. Salinero J, Goméz-Barea A, Leckner B, Tripiana M, Bu B, Gómez-González E. Improving char temperature measurement by pyrometry with digital camera. Proceedings of 22nd International Conference on Fluidized Bed Conversion at June 14-17, 2015 in Turku (Finland); 2; 375-383 (ISBN 978-952-12-3223-7)

Paper 6. Salinero J, Gómez-Barea A, Fuentes-Cano D, Leahy JJ, Leckner B. Impact of using thermocouples to measure char particle temperature in a fluidized bed combustor. 12nd International Conference on Fluidized Bed Technology at My 23-26, 2017 in Kraków (Poland); 1; 655-662 (ISBN 978-83-62079-16-2)

Paper 7. Salinero J, Gómez-Barea A, Leckner B, Bu C. Application of one-color pyrometry with digital camera for the measurement of fuel temperature in fluidized bed combustion. 4th International Workshop on Oxy-fuel FBC Technology at November 5–7, 2014 in Nanjing (China)

The author has participated in others publication submitted to international conferences and journals, which are not considered direct publication from this work

Paper 8. Ronda A, Ferreira V, Arroyo J, Haro P, Fuentes-Cano D, Nilsson S, Salinero, J, Gómez-Barea A. Heavy Metals Partitioning during Thermal Conversion of Sewage Sludge in a Fluidized Bed under Conditions Relevant for Pyrolysis and Gasification. Proceedings of 25th European Biomass Conference and Exhibition at June 12-15, 2017 in Copenhagen (Denmark); 751–754 (ISBN:978-88-89407-17-2)

Paper 9. Fuentes-Cano D, Salinero J, Haro P, Nilsson S, Gómez-Barea A. Influence of the Stoichiometric Ratio on Tar Composition during Fluidized Bed Gasification. Proceedings of 25th European Biomass Conference and Exhibition at June 12-15, 2017 in Copenhagen (Denmark); 772–775 (ISBN:978-88-89407-17-2)

Paper 10. Fuentes-Cano D, Salinero J, Haro P, Nilsson S, Gómez-Barea A .The influence of volatiles to carrier gas ratio on gas and tar yields during fluidized bed pyrolysis tests. Paper submitted in Fuel at Agst, 2017 as JFUE-D-17-03078

During the thesis the author have been granted by the following projects

- Oxi-Combustión y Oxi-Gasificación en Lecho Fluidizado: Estudio de la Conversión del Carbonizado para el Diseño y Optimización de Equipos de Captura de CO2 de Segunda Generación

  Plan Nacional. ENE2012-37999. 2012-2015

  Main researcher: Alberto Gómez Barea

- Fletgas2

  Proyecto de excelencia de la Junta de Andalucía. P12-TEP-1633. 2014-2017

  Main researcher: Pedro Ollero de Castro

- ENFORBIOM: Aprovechamiento de biomasa forestal para generación de electricidad distribuida,

  Ref. : PI-1363/2014

TABLE OF CONTENT

Every Achievement Begin when you Refuse to Give Up,
Rocky Balboa

RESUMEN DE LA TESIS DOCTORAL EN CASTELLANO

1. ANTECEDENTES Y JUSTIFICACIÓN

La necesaria reducción en las emisiones de CO_2 es de tal magnitud, que no es posible conseguirla únicamente mediante la mejora en la eficiencia de las actuales plantas de energía, haciéndose necesario el desarrollo de soluciones complementarias basadas en tecnologías de captura y almacenamiento de CO_2. La oxi-combustión es una las alternativas para la captura de CO_2 en consideración, mediante la cual se obtiene una alta concentración de CO_2 (del orden del 90% en volumen) en los gases de combustión, facilitando el secuestro y almacenamiento del CO_2 contenido en la misma. Para ello se realiza la combustión con oxígeno puro y parte de los gases de salidas, ricos en CO_2, recirculados para mantener el control de la temperatura en la caldera. De esta forma se consigue una razonable eficiencia neta en la planta, siendo la tecnología con mayores emisiones de CO_2 evitadas.

La 1ª generación de oxi-calderas consiste en el retrofitting de las plantas de producción de energía, donde la concentración de O_2 en el interior de la caldera: 25–35 $\%_{v/v}$, se mantiene en condiciones similares a las de combustión ordinaria con aire (cambiando el N_2 por CO_2). Aunque esta 1ª generación supone una reducción de las emisiones de CO_2, esta tecnología podría utilizarse con una mayor concentración de O_2 en la caldera. Sin embargo, existen una serie de desafíos antes del diseño y construcción de este tipo de calderas de oxi-combustión, también llamadas de 2ª generación. Entre otras cuestiones, está la de aclarar la influencia del CO_2 sobre el modo de conversión de la partícula de carbón, y el control de la temperatura en un reactor con menor volumen para intercambiadores de calor y donde la concentración de O_2 es elevada.

Las principales investigaciones se centran en calderas de carbón pulverizado al ser la caldera más común en la mayoría de las plantas eléctricas. Sin embargo, los reactores de lecho fluido pueden ser mucho más adecuados para la 2ª generación de oxi-calderas debido al control de la temperatura que brinda la circulación de sólidos y su capacidad de trabajar con combustibles de bajo rango, como son los residuos y la biomasa. Las investigaciones fundamentales de oxi-combustión en reactores de lecho fluido se han centrado en condiciones de 1ª generación, y aunque recientemente se ha tratado de dilucidar el efecto del CO_2 para condiciones de 2ª generación, la técnica de medida de temperatura empleada en estos trabajos se basaron en métodos intrusivos como termopares, de tal forma que el proceso de oxi-combustión podría verse afectado. Por otro lado, los principales estudios teóricos asumen que la partícula de

carbón/carbonizado reside únicamente en la fase emulsión, sin tener en cuenta observaciones experimentales que la sitúan en la fase burbuja y zona splash del lecho durante parte de la fluidización. En estas zonas, la combustión puede ser mucho más intensa (transferencia de masa) y las condiciones de transferencia de calor muy diferentes, por lo que las velocidades de consumo de las partículas de carbonizado y su temperatura pueden ser mucho mayores. Los modelos desarrollados hasta la fecha no han tenido presente explícitamente estas consideraciones, por lo que existen significativas discrepancias entre las predicciones y los resultados experimentales (típicamente superiores al 15 %).

El control de la temperatura de las partículas de carbón/carbonizado es especialmente importante para evitar la aglomeración y defluidización del lecho. Esta importancia se incrementa al aumentar la concentración de O_2 dado que se podrían alcanzar temperaturas muy superiores a la del lecho que produzcan la fusión de las cenizas. Es por ello que se han realizado algunos trabajos para aclarar la velocidad de combustión en condiciones de oxi-combustión con altas concentraciones de CO_2 con distintas concentraciones de O2. Sin embargo, la mayoría de los trabajos se han centrado en condiciones de oxi-combustión de primera generación, con concentraciones de O_2 típicamente por debajo de 35%$_{V/V}$.

Durante las investigaciones realizadas para esclarecer la velocidad de combustión en estas nuevas condiciones de reacción, una de las principales técnicas de medida consiste en introducir uno o varios termopares en el interior de la partícula de combustible, que posteriormente se arroja al lecho para medir la temperatura de la partícula con el tiempo, hasta que la partícula alcanza un tamaño aproximado de 3 mm o se desprende del termopar. Además, de la limitación en el tamaño mínimo cuya temperatura puede medirse y de los problemas de desprendimiento partícula-termopar, el movimiento de la partícula fluidizada con un termopar se ralentiza. Sin embargo, su uso se justifica asumiendo que la temperatura de una partícula fluidizada con un termopar es similar a la de una partícula libremente fluidizada, y que el proceso de conversión no se ve afectado. Se han empleado otras técnicas basadas en medidas ópticas como la pirometría, donde se solventan estos inconvenientes, pero si la captura de la radiación térmica emitida por la partícula se realiza por medio de una sonda óptica inmersa en el lecho, los resultados presentan una gran dispersión que los hace difícil de interpretar. Esta captura e interpretación de la radiación podría realizarse por medio de una cámara digital si el lecho es visualmente accesible desde el exterior del reactor. De esta forma, además de no afectar al movimiento de la partícula, los resultados serían mucho más claros y fáciles de interpretar. No obstante, esta técnica tan solo se ha utilizado recientemente para analizar el efecto del CO_2 sobre le temperatura de llama en la devolatización de partículas de distintos tipos de carbón aisladas en una corriente de gas. Es decir, hasta la fecha no se disponen de medidas fiables y precisas de la oxi-combustión de partículas de carbonizado en reactores de lecho fluido y, a pesar de que la técnica de pirometría con cámara digital podría ser adecuada, ésta aún no se ha aplicado debido a las complejidades de visualizar adecuadamente las partículas de combustible durante el proceso de combustión lecho fluidizado.

2. OBJETIVOS

El objetivo de esta tesis es aclarar el proceso de oxi-combustión de partículas de carbonizado en lecho fluido, y para ello, desarrollar y poner a punto la técnica de medida de la temperatura superficial de carbonizado con pirometría con cámara digital en un lecho fluidizado. Para ello, se ha diseñado y construido una instalación experimental basada en un lecho fluidizado bidimensional donde se ha puesto a punto la técnica anterior, realizándose experimentos con distintas partículas de carbonizado de carbón y biomasa en condiciones de oxi-combustión. El trabajo experimental se ha completado con el desarrollo de un modelo teórico que tiene en cuenta de forma explícita el movimiento del carbonizado a través de las diferentes fases del lecho (movimiento que también se ha caracterizado experimentalmente). Adicionalmente, la investigación ha permitido aclarar el efecto del termopar sobre la medida de la temperatura de la partícula, así como mostrar la influencia que el movimiento de la partícula de char a través del lecho tiene sobre la temperatura superficial del char, y en particular, sobre la frecuencia y amplitud de las fluctuaciones de ésta durante la combustión en lecho fluidizado.

3. EQUIPOS Y METODOLOGÍA EXPERIMENTAL

La medida de la temperatura del carbonizado durante los ensayos (tanto de oxi-combustión (O_2/CO_2) como de combustión (O_2/N_2) se basa en la captura e interpretación de la radiación térmica contenida en las bandas espectrales visibles roja, verde y azul que realiza la cámara digital. El software proporciona tres valores para cada uno de los píxeles de la imagen, conocidos como números digitales (DN), que cuantifican la radiación que recibieron en cada una de las bandas espectrales mencionadas (ver Fig. 3.1, Capítulo 3). Si la radiación visible que alcanza al sensor se debe a la temperatura de los objetos presentes en el campo de visión de la cámara (Ley de Planck), es posible utilizar la información contenida en esos números digitales junto con el modelo matemático de la radiación que alcanza el sensor para determinar la temperatura de dichos objetos.

La temperatura pirométrica de las partículas de carbón/carbonizado o de llama en reactores de lecho fluido se miden en la literatura mediante la relación simultanea de la información contenida en dos bandas espectrales o colores (pirometría en dos colores, P2C). De esta forma, se determina la temperatura de la partícula de combustible si esta es mayor a la del fondo (background) y su emisividad no cambia con las longitudes de ondas de los colores utilizados (superficie gris). Sin embargo, si se conoce la emisividad de la partícula en esos colores es posible utilizar la información contenida en cada uno de los colores de forma secuencial y se pueden medir temperaturas del carbonizado menores a las del fondo. Por otro lado, la relación entre los pixeles ocupados por el diámetro de la partícula en los primeros instantes del ensayo y su medida en mm permite estimar el tamaño del carbonizado durante toda la conversión.

En este trabajo se utilizaron partículas de carbonizado de madera de haya y carbón sub-bituminoso y bituminoso (análisis aproximado en la Tabla 3.1, Capítulo 3), cuya forma y masa dependen del tipo de estudio y objetivo. En cada uno de los ensayos se realizó la oxi-combustión (O_2/CO_2) o combustión (O_2/N_2) individual de una de estas partículas. Para desarrollar este trabajo se diseñó y construyó la planta FBC 2D (ver Fig. 3.2, capítulo 3), compuesta por un reactor de lecho fluido de geometría bi-dimensional (18 x 1.8 x 50 cm) equipado con una ventana

de cuarzo en el bottom. Este se situó en el centro de un horno eléctrico (11 kW, 50 x 30 x 70 cm) rodeado por una superficie negra que homogeniza la radiación procedente de las resistencias del horno. El horno eléctrico también está equipado con una ventana de cuarzo desde la cual se realizaron las grabaciones con una cámara digital comercial (JVC Everio HD, 2 Mpx). También se utilizó una planta de lecho fluidizado de laboratorio (FBC 3D), con un reactor de lecho fluido cilíndrico (51 mm de diámetro interno en la parte inferior) situado en el centro de un horno eléctrico circular (9 kW, 30 cm de diámetro x 70 cm altura). En ambos reactores se utilizó arena de sílice como material del lecho (d_i: 0.32-0.5 mm, u_{mf}: 0.18 m/s), cuya temperatura, así como la composición y velocidad del flujo de fluidización dependieron del estudio dentro que se llevase a cabo (ver descripción de los equipos en la Tabla. 3.1).

4. Estudio Teórico (Modelo) de la Combustión de una Partícula de Carbonizado en un Lecho Fluido

Las predicciones de temperatura y conversión realizadas en este trabajo tienen en cuenta el movimiento del carbonizado a través de las diferentes fases del lecho (emulsión, burbuja y splash). Para ello se caracteriza experimentalmente este movimiento cuantificando el tiempo que la partícula de carbonizado está en cada una de las fases en función de su tamaño. De esta manera se añade una variable adicional a la simulación que indica la posición del carbonizado en cada instante. Básicamente, lo que se realiza es la descripción del movimiento aleatorio de la partícula durante su fluidización como un movimiento cíclico que se repite durante la conversión, cuyo periodo y tiempo en cada una de las fases del lecho varía con el tamaño del carbonizado (ver Fig. 2.2, Capítulo 2). Dado que el tamaño de la partícula varía durante la simulación, la caracterización del ciclo también lo hace. Este enfoque, que podemos denominar dinámico, permite simular el cambio en la trasferencia de masa y calor desde/hacia la partícula de carbonizado en función de su posición en el lecho. Este enfoque contrasta con el "tradicional" o "estático" donde se asume que la partícula reside siempre en la fase emulsión. Dada las características experimentales bajo las cuales se obtienen las correlaciones de trasferencia de masa y calor de la literatura, se utilizan correlaciones teóricas (ver Ecs. 2.22-2.27, Capítulo 2).

5. Metodología Específica y Condiciones de Operación en los Ensayos Realizados

En el presente trabajo se realizaron diferentes estudios para investigar aspectos de la combustión de partículas de carbonizado en lecho fluido. Todos ellos utilizan la técnica pirométrica con cámara digital pero con propósitos diferentes. A continuación se resumen las condiciones de operación y ajuste de cada uno de los cuatro estudios principales llevados a cabo.

5.1. Calibración y Validación de la Medida de Temperatura Mediante Pirometría con Cámara Digital en Lecho Fluido

Se realizó la combustión (O_2/N_2) de partículas de carbonizado de madera de haya con forma de paralelepípedo en el centro del horno eléctrico de la planta FBC 2D. En estos ensayos la partícula tenía un termopar alojado en una ranura superficial que permite medir la temperatura de una determinada región de la superficie del carbonizado durante parte del tiempo de combustión. De esta forma fue posible relacionar los números digitales que la cámara asociaba a

una radiación/temperatura conocida (ver Fig. 3.3, Capítulo 3 o Fig. 4.1 capítulo 4), necesarios para la calibración de la cámara digital. Una vez calibrada la técnica de medida se compararon sus resultados (temperaturas pirométricas) haciendo uso de la información contenida en los diferentes colores de forma simultanea (P2C) y de forma secuencial (P1C) con la medida de la temperatura superficial mediante un termopar.

5.2. Influencia del Termopar sobre la Temperatura de Combustión y consumo Superficial del Carbonizado en Lecho Fluido

En este estudio se realiza y graba la combustión (O_2/N_2) de partículas individuales esféricas (~ 10 mm) de carbonizado de madera de Haya, carbón Sub-Bituminoso y Bituminoso en el reactor de lecho fluido FBC 2D fluidizadas libremente (sin termopar), y con un termopar insertado en su centro. Del análisis (clasificación) de las imágenes de estos ensayos (ver fig. 3.6, Capítulo 3 y Fig. 4.9, Capítulo 4), se cuantifica el tiempo de la partícula en cada una de las fases del lecho (emulsión, burbuja y zona splash), y como ese tiempo varía por efecto del termopar. La medida de la temperatura por pirometría con cámara digital, permitió comparar las temperaturas superficiales registradas durante la conversión, y mediante la extracción de las partículas de carbonizado del reactor FBC 2D y del reactor FBC 3D a distintos tiempos de combustión se analizó su efecto sobre el consumo superficial del carbonizado.

5.3. Oscilación de la Temperatura del Carbonizado durante su Combustión en Lecho Fluido

En este estudio se realiza la combustión (O_2/N_2) de partículas individuales esféricas (~ 8 mm) de carbonizado de madera de haya y carbón sub-bituminoso en el reactor de lecho fluido FBC 2D. La temperatura del lecho se fijó a 800 °C, y la concentración de O_2 fue del 11 o 21 $\%_{v/v}$. La medida de la temperatura de las partículas de carbonizado en secuencias de imágenes donde el carbonizado cambia de posición en el lecho: fase emulsión ↔ fase burbuja ↔ zona splash, permitió cuantificar la amplitud de las oscilaciones de las temperaturas y el tiempo en el cual se producen. Además, se implementó la caracterización experimental del movimiento del carbonizado a través de las diferentes fases del lecho en el estudio teórico de conversión del carbonizado en lecho fluido, mostrando su capacidad predictiva de las variaciones de temperatura.

5.4. Influencia del CO_2 en la Oxi-Conversión del Carbonizado en Lecho Fluido

En este estudio se realiza la oxi-combustión (O_2/CO_2) y combustión (O_2/N_2) de partículas individuales esféricas de carbonizado de madera de haya y carbón sub-bituminosos en el reactor de lecho fluido FBC 2D. El peso de las partículas de carbonizado se fijó de forma que las partículas tuvieran un tamaño inicial aproximado de 8 y 13 mm. La temperatura del lecho de arena fue de 800 ó 850 °C, y la concentración de O_2 entre 11 y 50 $\%_{v/v}$ en N_2 o en CO_2. Todos los ensayos fueron grabados lo que permitió medir la temperatura superficial del carbonizado por pirometría con cámara digital (P1C). Además, se midió la conversión mediante el análisis del cambio de tamaño del carbonizado durante todo el proceso de conversión. Se compararon las predicciones

del modelo con los resultados experimentales de temperatura, tiempos de consumo y tasa de consumo aparente (ver Eq. 3.7, Capítulo 3) de este estudio y de otros estudios de la literatura.

6. DISCUSIÓN DE RESULTADOS

Una vez calibrada la cámara digital, esto es, conocido como los parámetros ópticos y electrónicos de la configuración experimental se relacionan con los números digitales generados por el software, se midió la temperatura superficial del carbonizado de madera de haya mediante el uso simultaneo (pirometría en dos colores, P2C) y secuencial (pirometría en un color, P1C) de los números digitales (DN), y mediante un termopar alojado en su superficie (ver Fig. 4.5, Capítulo 4). El resultado muestra que el uso secuencial propuesto mejora la precisión de la temperatura medida, y aumenta el rango de temperaturas que puede medirse, incluyendo temperaturas del carbonizado inferiores a las del fondo. Aunque el principal inconveniente de esta medida (P1C) es que la emisividad del carbonizado debe conocerse, la incertidumbre en el resultado (temperatura medida) cuando la emisividad varía entre los principales valores de la literatura, es inferior al 1 % si la temperatura del carbonizado es mayor a la del fondo (ver Fig. 4.8b, Capítulo 4). No obstante, si la temperatura del carbonizado es inferior a la del fondo es importante realizar una buena estimación de la emisividad (ver Fig. 4.8a, Capítulo 4).

La clasificación de las imágenes de los ensayos de combustión de las partículas de carbonizado fluidizadas con y sin termopar mostró que su uso hunde la partícula en el lecho, aumentando el tiempo que ésta está en la fase burbuja (ver Fig. 4.11, Capitulo 4). El conjunto carbonizado-termopar resiste el arrastre de las partículas del lecho (que tienden a mantener al carbonizado en la fase emulsión) y mantiene al carbonizado enfrentado al flujo ascendente de las burbujas (ver Fig. 4.13, Capítulo 4). El aumento en el tiempo dentro de la fase burbuja (superior al 40, 60, y 100 % para un termopar de 0.25, 0.5, y 0.75 mm de vaina) lleva consigo el aumento de la temperatura de combustión durante la fluidización, reduciendo el tiempo de consumo en más del 5 % respecto del registrado para una partícula de carbonizado fluidizada libremente (ver Fig. 4.14, Capítulo 4). Además, dado que la rotación libre de la partícula está impedida por el termopar, es la misma superficie de la partícula la que enfrenta el flujo de gas que asciende desde el plato distribuidor (ver Fig. 4.16, Capítulo 4). Por lo tanto, esta región es la que sufre las mayores temperaturas y consumos superficiales durante toda la conversión y produce un consumo superficial no homogéneo del carbonizado (ver Figs. 4.16 y 4.17, Capítulo 4).

La interpretación de las imágenes de los ensayos de combustión por pirometría detectó variaciones en la temperatura superficial del carbonizado de decenas de grado en tan solo centésimas de segundo (ver Fig. 4.19, Capítulo 4). Estas oscilaciones de temperatura que se producen durante toda la conversión, son consecuencia del cambio de posición del carbonizado en el lecho, y su amplitud aumenta con la concentración de oxígeno y disminuye con el tamaño de partícula (ver Fig. 4.20, Capítulo 4). Los resultados indican que la temperatura de la partícula de carbonizado es más estable cuando ésta reside en la fase emulsión que cuando está en la fase burbuja o en la zona de chapoteo (splash). Por otro lado, la implementación del movimiento del carbonizado a través del lecho (caracterizado experimentalmente, ver Fig. 4.12 en Capítulo 4) en el modelo, mostró la gran capacidad predictiva del modelo para describir las oscilaciones de temperaturas observadas experimentalmente.

La medida experimental de la temperatura y consumo de una partícula de carbonizado durante su oxi-combustión (O_2/CO_2) y combustión convencional (O_2/N_2) en el reactor FBC 2D ha mostrado que la transferencia de O_2 desde el seno de la fase fluida a la partícula controla el proceso global de conversión, y que el consumo del carbonizado por gasificación no puede despreciarse en ningún caso. Este consumo adicional por gasificación compensa la menor difusividad del O_2 en CO_2 respecto la del O_2 en N_2 reduciendo las diferencias en el consumo en ambas atmósferas (O_2/N_2 y O_2/CO_2) cuando la temperatura del carbonizado es inferior a los 925 °C, o haciendo que el consumo en la atmósfera O_2/CO_2 sea mayor si la temperatura del carbonizado es mayor a los 925 °C. Además, cuando el carbonizado reside en la fase emulsión la temperatura es similar en ambas atmósferas, registrándose las mayores diferencias cuando la partícula está en la fase burbuja o zona splash. Por lo tanto, las principales diferencias en la conversión se deben al tiempo durante el cual la partícula está fuera de la fase emulsión, lo que muestra la importancia de considerar de forma explícita el movimiento del carbonizado a través de las fases del lecho en el estudio teórico. La comparación de los resultados experimentales y de otros trabajos de la literatura con las predicciones del estudio teórico dinámico planteado muestra una incertidumbre menor al 15 %, mejorando algunos de los resultados que pueden encontrarse en la literatura.

7. CONCLUSIONES

El trabajo realizado y discutido puede agruparse en cuatro grandes estudios que aun compartiendo un mismo objetivo general, que es aclarar el proceso de oxi-combustión de partículas de carbonizado en lecho fluido, tuvieron objetivos particulares. A continuación se resumen las conclusiones y contribuciones más destacables de cada uno de los cuatro estudios (publicados en 4 artículos y 2 aportaciones/proceedings a congresos internacionales, ver § PAPERS).

El primero de los estudios consiste en el desarrollo de un método de medida de temperaturas superficiales del carbonizado durante su oxi-combustión y/o combustión en un reactor de lecho fluido, basado en la captura e interpretación de la radiación térmica en las tres bandas espectrales visibles roja, verde, y azul que hace una cámara digital (pirometría con cámara digital), mostrándose que:

I. El uso secuencial de la radiación contenida en los tres colores mencionados mejora la precisión de la temperatura medida respecto el uso tradicional simultáneo (uso simultáneo de dos colores).

II. Se pueden medir temperaturas del carbonizado menores a las del fondo (cosa que no se puede hacer con el uso de varios colores simultáneamente), siempre que se conozca la emisividad del carbonizado.

En el segundo estudio analiza el efecto del termopar sobre la combustión de una partícula en lecho fluido: temperatura y consumos superficiales del carbonizado, mostrándose que:

III. El termopar altera el movimiento del carbonizado a través del lecho, variando el tiempo de residencia en cada una de las fases. El hundimiento de la partícula en el lecho causado por el termopar incrementa su tiempo en la fase burbuja, dada la mayor

resistencia que el conjunto termopar-partícula ofrece al arrastre de las partículas del lecho.

IV. El aumento del tiempo en la burbuja incrementa la temperatura superficial de combustión y reduce el tiempo de consumo.

V. El consumo superficial no es homogéneo, dado que la rotación de la partícula está impedida.

El tercer trabajo aborda el efecto del movimiento del carbonizado a través de las diferentes fases del lecho sobre su temperatura de combustión, e implementa su caracterización experimental en el estudio teórico

VI. Se muestra que la temperatura superficial de combustión varía decenas de grados en tan solo centésimas de segundos como consecuencia de las diferentes posiciones de la partícula en el lecho. Por otro lado, las predicciones del modelo permiten describir estas oscilaciones durante la conversión, mejorando los modelos existentes.

El último estudio analiza la influencia del CO_2 y O_2 en la oxi-combustión de las partículas de carbonizado, concluyendo que:

VII. La oxi-combustión del carbonizado en un lecho fluido está controlada por la trasferencia de O_2 desde el seno de la fase fluida hacia el carbonizado, y que el consumo por gasificación no es despreciable.

VIII. El consumo adicional por gasificación del carbón compensa la menor difusividad del O_2 en CO_2 reduciendo las diferencias entre los consumos aparentes del carbonizado (g/m^2s) en O_2/CO_2 y en O_2/N_2 para temperaturas del carbonizado menores a los 925 °C, y hace mayor el consumo en O_2/CO_2 que en O_2/N_2 para temperatura del carbonizado mayores a 925 °C.

IX. Las temperaturas registradas en el carbonizado durante conversión en O_2/CO_2 son menores a las registradas en la atmósfera equivalente (igual concentración de O_2) de O_2/N_2, registrándose las mayores diferencias cuando las partículas están en la fase burbuja o zona splash del lecho.

Measurement of Char Temperature in a Fluidized Bed Reactor using Pyrometry with a Digital Camera: Application to Oxy-Fuel Combustion

CHAPTER 1. INTRODUCTION

This chapter presents the objectives and methodology followed in this thesis work. To understand the framework of the thesis, the need for development of the combustion technology to reduce the CO_2 emissions is firstly presented. Among all proposal technologies, oxy-fuel combustion in a fluidized bed (FB) is one of the most promising routes. One of the main challenges for the development of this technology is to clarify the influence of changing the fluidization flow from O_2/N_2 to O_2/CO_2 on the fuel particle temperature and conversion.

1.1. OXY-COMBUSTION IN FLUIDIZED BED REACTORS

While more than 25 % of the global electric energy demand is covered by coal combustion and it could be expected an increase in its use since coal is the main source of energy for developing countries [1], the need for reduction of the CO_2 emission involves both the increase in the power plants efficiency as CO_2 capture and storage (CCS) [2,3]. Among all proposal technologies, oxy-combustion stands out with a reasonable net plant efficiency and avoided CO_2 emissions [4, 5]. As shown Fig. 1.1, in this process the coal/char particle conversion is carried out by mixing almost pure O_2 with CO_2 from the recirculation of the flue gases in order to control the conversion temperature and to avoid the dilution of the flue gases with the N_2 from the air [5]. In that way the CO_2 concentration at the exit of the boiler is higher than 90 % and allows capturing the flue gases without a CO_2 separation unit [6]. Moreover, the NO_x and SO_x emission are also reduced [7].

The 1st generation of oxy-boilers involves the retrofitting of the combustion power plants where the flue gases recirculation keeps almost similar conditions inside the boiler: O_2 concentration between 25 and 35 $\%_v$ [3]. Although this 1st generation reduces the CO_2 emissions, oxy-boilers can be conceived with higher O_2 concentration. This 2nd generation oxy boiler would increase the plant efficiency and reduce the volume of the gases through the boiler. However, in spite of all international groups and projects [8], as well as pilot plant [9-11], there are still a number of challenges before designing and building a 2nd generation oxy boiler. Among these questions are clarifying the impact of changing from O_2/N_2 atmosphere (air-firing conditions) to O_2/CO_2 one (oxy-firing conditions) and controlling the conversion temperature inside a reactor with less room (volume) to put heat exchangers [6, 12, 13]. Since pulverized coal is the main type of boiler in existing power plants, most of the research works from literature are focused in these boilers [14-19]. However, FB reactors could be much suitable technology for a 2nd generation of oxy-boilers because the sand particles of the bed moderates the conversion

temperatures (by its large thermal capacity) reducing the flue gases recirculation and the reactor size [12, 13]. Moreover, they can be used with low-grade fuels having low heating value and high ash content, including not only coals but also biomasses and/or wastes.

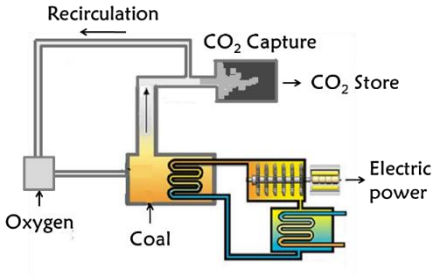

Fig. 1.1. Sketch of an oxy-fuel power plant

Most of the research works about oxy-combustion in FB have addressed environmental or technical aspects, such as pollutant emissions or the switching from air-firing conditions to oxy-firing [20, 21]. They have shown the viability of the process in these reactors with no particular barriers. The fundamental studies about the char/coal particle conversion in an O_2/CO_2 gas atmosphere have addressed the importance of the carbon consumption by gasification of coarse char particles from different types of coals and the excess of their temperature over that of the bed. However, most of them were focused at 1st oxy-firing conditions, that is, O_2 concentration lower than 25-35 % [22-26]. It has been recently studied the devolatilization and conversion of different types of coals at 2nd oxy-firing conditions, that is, O_2 concentration higher than 25-35 % [27-30]. These works compared the devolatilization and burnout times, as well as the flame and char particle maximum temperatures when the gas atmospheres changed from O_2/N_2 to O_2/CO_2. However, these studies used thermocouples as measurement technique and, as it is pointed out below (see § 1.2), they could affect the char/coal particle behavior during conversion, influencing the maximum temperature of the char and the burnout time achieved. On the other hand, reasonable theoretical models have been proposed and their predictions have been checked with the experimental measurements of temperatures and burnout times [26, 28, 30]. However, the differences between these predictions and those experimental results are higher than 15 % and do not clarify the conversion of the coarse char/coal particle in FBs at 2nd oxy-firing conditions [31].

In addition to the uncertainties in the experimental measurements, the disagreement between predicted and experimental results could be explained by the standardized hypothesis assumed in most of theoretical works: they usually assume that the char/coal particle is always in the emulsion phase, in spite of the experimental observations which confirm that the char is burned occasionally in the bubble phase and splash zone during fluidization [32-34]. Moreover, it can be found a few experimental works [32, 35] pointing out the impact of the char particle movement through the emulsion phase, bubble phase, and splash zone on the combustion temperature, showing that this temperature would oscillate tens of degrees as consequence of the mentioned change in the position of the char particle in the bed. These temperature oscillations were recorded by an embedded thermocouple in a coarse coke particle [32, 35] or

by pyrometry with an optical probe inside a FB during combustion of a batch of coke particles [32]. Although the remaining questions about these temperature oscillations are discussed below (see § 1.2), it seems clear that the char particle is not always in the emulsion phase. Therefore, that assumption, which is commonly used most theoretical combustion studies (models) [30, 36-38], do not take explicitly into account that the mass and heat transfer [39-41], the heat generated by CO oxidation to CO_2 close to a char surface [42], and the combustion temperature [43] vary with the different char particle position in the bed].

1.2. MEASUREMENTS OF THE CHAR/COAL PARTICLES' TEMPERATURE IN FLUIDIZED BED REACTORS

The coal/char particle temperatures is a key aspect of the coal combustion technology because of its importance on the efficiency of the boiler, pollutant emissions, and operation problems such as slagging and fouling among others [44]. In a FB reactor, it is also responsible for segregation, agglomeration, and defluidization of the bed that are produced from melting of ashes [45] whose viscosity varies even with small changes in temperature [43]. This aspect is one of the main challenge for oxy-combustion technology since the high O_2 concentration in the entering gas could produce unacceptable temperature levels both globally on the reactor and locally in a fuel particle, especially in the regions where the gas is injected (bottom and secondary-feed gas ports). Therefore, it is essential to measure the coal/char particle temperatures in an accurate and reliable way for further development and safe operation of 2nd generation of oxy-boilers.

Among all techniques used to measure the conversion temperatures of the fuel particles in a FB reactors, the embedding of thermocouple(s) inside the particle is one of the most widespread techniques. As it is shown in Fig. 1.2a, by throwing the particle into the FB, its temperature is recorded until the particle is detached from the thermocouple [35]. By this contact technique, the excess of the temperature of the fuel particle has been quantified for different types of coals, particle sizes, bed temperatures, and different O_2 concentration [35, 46-48]. It has been also used to estimate the heat [49, 50] and mass [51] transfer from/to the fuel particle inside of a fluidized sand bed. While the fuel particle was fluidized with an embedded thermocouple, the CO/CO_2 products rate generated by oxidation on the char particle's surface has been studied for different bed-particle sizes and temperatures [42, 52, 53]. Moreover, theoretical conversion models have been validated using temperatures recorded by thermocouple (in order to simulate the combustion of a batch of particles) [36, 54]. However, because of its intrusive nature that influences on the fuel particle's fluidization movement through the bed [35, 49, 50, 52], its local measurements and the minimum fuel particle's size whose temperature can be measured (~ 3 mm) [36, 47], and the possible effect on the burnout time [42] and combustion temperature [55], non-contact techniques could be a better options to overcome these inconveniences.

These non-contact techniques, which are commonly called optical pyrometry, are based on the capture and interpretation of the thermal radiation emitted from the char particles [32, 56-61]. As it is shown in the Fig. 1.2a, the thermal radiation could be captured by an optical probe [32, 56-58] or by a digital camera [28, 59-61]. By using an optical probe inside the bed, it has been quantified the excess of the coal/char particles' temperatures over that of the bed [58].

However, this technique yields widely scattered results that are difficult to interpret. The field of view of the optical probe sketched in the Fig. 1.2b can help to explain this scatter; since the measured temperature is the average of the bodies present in the field of view, and it also depends on the fraction of the field of view that is occupied by the fuel particle, which also depends on the particle size and its distance to the probe. It is difficult to reduce these uncertainties since there is a particle size distribution in the bed after feeding a batch of coal particles into an FB (or when it is continuously fed), where smaller particles reach higher temperature, and the estimation of the particle size whose temperature is measured by this technique is uncertain [56, 57]. Moreover, the temperature of the particle could vary tens of degrees if it is in the emulsion phase instead of in the bubbles. These weaknesses are overcome by using a digital camera (if the reactor is visibly accessible from outside) since the radiation from the particle surface is effectively separated from that of the adjacent regions, improving the accuracy of the measured surface temperature (see sketch in Fig. 1.2b, where the radiation from the scene captured by one pixel is represented). This technique has been previously used to measure the temperature field inside a FB reactor generated during combustion of an air-propane mixture, and recently it has also has been applied to analyze the effect of changing the fluidization flow from O_2/N_2 to O_2/CO_2 on the flame temperature during the devolatilization of different coal particles [28]. By infrared cameras, the heat transfer and the temperature profiles between the solid bed-particles and the fluidizing gas have been studied [62-64].

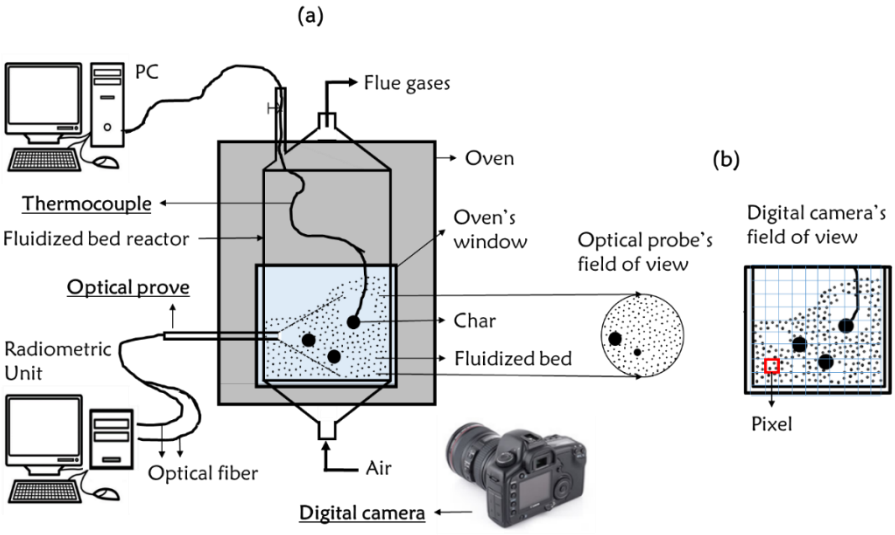

Fig. 1.2. Sketches of the experimental measurements of coal/char particles' temperatures by thermocouple, and pyrometry with an optical probe or digital camera (a), and comparison of the field of view from an optical probe versus the one from a digital camera (b)

The accuracy of the temperature measured by pyrometry not only depends on the simplifications and hypothesis of the heat transfer problem, but it is also affected by the optical and electronic parameters of the devices that capture and interpret the thermal radiation [28]. Although such accuracy is analyzed in literature when the radiation in captured by an optical

probe [58, 65-67], there are limited information when the capture is carried out by a digital device [60]. On the other hand, this technique is based on the capture of the thermal radiation in two (or more) spectral bands and their simultaneous use [68]. In that way, the temperature of the coal/char particle or that in the flame are measured, if this temperature is higher than the background and grey behavior is assumed [32, 56-61, 68]. However, if the surface emissivity is known and the thermal information in the spectral bands are sequentially used (instead of simultaneously), it can be measured the temperature even when it is lower than the background [69].

It could be argued that results obtained by thermocouples and by pyrometry with an optical probe have been used above to pointed out that the movement of the char particle through the bed is important in its conversion and it should be taken into account in the theoretical model (see § 1.1). However, it has just pointed out that the temperatures measured by these techniques could be affected by the measurement technique itself (thermocouples case) or their interpretation is uncertain (pyrometry case). By an embedded thermocouple in a coarse coke particle, an average oscillation of combustion temperature of 75 °C in periods shorter than one minute has been recorded [32]. By the same technique and also for a coarse coke particle, an increase in its combustion temperature higher than 20 °C has been quantified after few seconds after having taken it from the bed at minimum fluidization velocity and put it on the bed surface [35]. By pyrometry with an optical probe inside a sand bed, a more stable and lower particle temperature was observed when coarse coke particles were in the emulsion phase than when they were in the bubble phase [32]. The differences between the average temperatures of the particles in these different phases range from 15 to 150 °C. However, it is uncertain whether these temperature differences (typically measured by this technique [32, 56-58]) are just due to the intermittent interaction of the particle with the emulsion and bubble phases, or they are associated with the weaknesses of the technique that affect its measurement (pointed out above). That is why these results are used to point out the need for taking into account the char particle location in the bed, but there are remaining questions about the effects of these different char particle's locations in the bed on its temperature and conversion.

1.3. OBJECTIVES AND CONTEND OF THIS THESIS

The above discussion has shown that not only remains questions about the impact of a high O_2 concentration in CO_2 on the conversion of a coarse char particle in a FB reactor, but also the surface temperature of the fuel particle still has not been measured in an accurate and reliable way. The oscillations of these temperatures caused by the movement of the char particle through the bed, as well as the time during which these take place, are not well understood. Moreover, this movement is not usually taken explicitly into account in the theoretical conversion studies. On the other hand, in spite of all published evidences about the effect of using thermocouples on the char particle's movement and burnout times, it is assumed that the temperature and consumption of a char particle fluidized with an embedded thermocouple are similar to those of a freely fluidized char particle. The present thesis addresses all these issues relevant to oxy-firing conditions. The main objective is to clarify the conversion of a single char particle in a FB reactor working at 2nd generation oxy-firing conditions, i.e., O_2 concentration higher than 25-35 $\%_v$ in CO_2. To do that:

1) It is developed and demonstrated the application of pyrometry with a digital camera to measure the surface temperature of char particles during combustion in a FB, discussing the capability of the technique to detect further details such as surface temperature gradients or particle's shrinkage.

2) Using this technique a comprehensive analysis of the effect of the thermocouples on the char particle's conversion and the experimental characterization of the char particle's movement through the bed are carried out.

3) Moreover, the amplitude of the temperature oscillations caused by this movement is analyzed both experimentally and theoretically by the implementation of the mentioned experimental characterization of the char particle's positions in the bed during fluidization in the conversion model proposed by Biggs et al. [43].

4) The temperatures and consumptions of char particles during their single combustion (O_2/N_2) and oxy-combustion (O_2/CO_2) in a FB, working at different conditions (O_2 concentration, char particle's size, bed temperature, and types of chars), are measured and analyzed. Moreover, these experimental measurements are compared with our own theoretical predictions and with those from published work in literature, concluding favorably about the ability of the theoretical treatment developed in this thesis with respect to existing models published up to date.

CHAPTER 2. THEORETICAL PREDICTIONS OF A SINGLE CHAR PARTICLE OXY-COMBUSTION IN A FLUIDIZED BED

The theoretical approach for the conversion of the char particle in a fluidized bed (FB) under oxy-fuel conditions taking explicitly into account the movement of the char particle through the bed is presented. The experimental characterization of this movement between different phases of a FB and its effect on the transfer phenomena are established and discussed.

2.1. THEORETICAL APPROACH

Single char/coal particle conversion in a FB has been widely studied over the past decades, where have been proposed different theoretical approaches attending to the way in which the carbon conversion proceeds inside the char particle [70]. Among of these theoretical models and it is justified below (see § 2.3), in this work is assumed that the char consumption (by carbon oxidation and gasification) proceed in a very narrow char layer that separates the unreacted char particle from the bulk phases of the bed since the ash generated is detached (shrinking unreactive particle model). Although a single char particle conversion in a FB is carried out, involving the same concentration of the different species (O_2, N_2, CO_2, and CO) in all bed phases: emulsion phase, bubble phase, and splash zone; the heat and mass transfer from/to the char particle varies depending on char's place/location in the bed. Therefore, taking into account the char's place in the bed for each time, the mass transfer is solved providing the diffusion of the different species (fluxes) from/to the char. These fluxes are then used to calculate the char consumption and temperature using the heat transfer conditions in the corresponding bed phase. It should be noted that before solving the theoretical approach, the characterization of the char particle's movement through the emulsion phase, bubble phase, and splash zone has to be set (see § 2.4).

2.2. MOLAR FLOWS

The char particle consumption in an O_2/N_2 or O_2/CO_2 atmosphere is given by oxidation

$$C(s) + \frac{2+\xi}{2\,(1+\xi)} O_2(g) \rightarrow \frac{\xi}{(1+\xi)} CO(g) + \frac{1}{(1+\xi)} CO_2(g) \tag{2.1}$$

and by gasification

$$C(s) + CO_2(g) \rightarrow 2CO(g) \tag{2.2}$$

where

$$\xi = A_{co/co2}\ \exp\left(-\frac{E_{co/co2}}{R_g Tc}\right) \tag{2.3}$$

is the CO/CO_2 molar ratio produced by the carbon oxidation [71]. As it is shown in Fig. 2.1, the char consumption occurs in a multicomponent gas atmosphere where equimolar counter-diffusion is likely not established [72-74]. Although this phenomenon is often neglected during calculation of single char particle combustion [26, 36-38], errors is introduced in the estimation of mass transfer [72-74] (errors up to 10 % for a 21 %$_v$ O_2 concentration in N_2 have been found [74]). To consider the multicomponent diffusion, the Stefan-Maxwell equations are used:

$$\frac{dx_i}{dr} = \sum_{\substack{j=1 \\ j\neq i}}^{n} \frac{1}{CD_{ij}}\left(x_j N_i - x_i N_j\right) \tag{2.4}$$

relating the molar fluxes of species i (N_i) from/to the char particle's surface and the molar fractions (x_k) at any point of the gas film surrounding the particle. The boundary conditions are:

$$x_i(r = r_c) = x_{i,c}$$

$$x_i(r = r_c + \delta) = x_{i,bed} \tag{2.5}$$

where $x_{i,c}$ and $x_{i,bed}$ are the molar concentration at the char particle surface and that in the bulk gas and

$$D_{ij} = \frac{\varepsilon_{mf}}{\tau} d_{ij} \tag{2.6}$$

the effective mass diffusivity, being d_{ij} the gas binary diffusivity (of the i-th compound through j) [75] and τ tortuosity ($D_{ij} = d_{ij}$ when the char particle is in the bubble phase and splash zone).

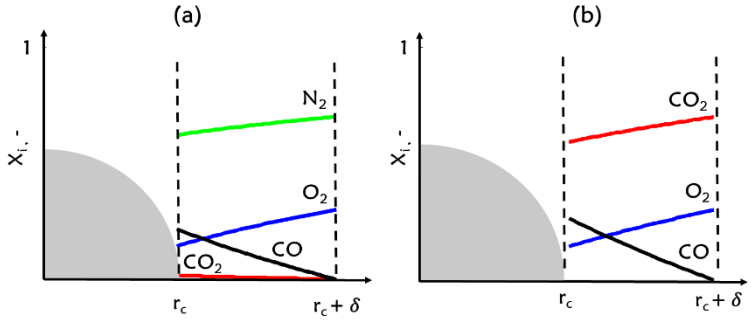

Fig. 2. 1. Sketched of the Molar fractions of the gaseous compounds around a char particle during its conversion in an O_2/N_2 (a) or O_2/CO_2 (b) atmosphere

Taking the mass-transfer resistance into account, the thickness of the gas film around the particle (δ) has been estimated by [76]

$$\delta = \frac{r_c}{\frac{\theta Sh_{cdeq}}{Sh_o} - 1} \tag{2.7}$$

where Sh_o is the Sherwood number during equimolar counter-diffusion without no mass-convective flux ($Sh_o = 2\varepsilon_{mf}$ if the particle is in the emulsion phase and $Sh_o = 2$ if the particle is in the bubble phase or splash zone). Sh_{cdeq} is the Sherwood number when there are equimolar

counter-diffusion and mass-convective fluxes. When there is no equimolar counter-diffusion, a correction factor θ have been estimated elsewhere [76] by

$$\theta = \frac{\xi+2}{\xi}\frac{1}{x_{i,bed}}\ln\left(1+\frac{\xi}{\xi+2}x_{i,bed}\right) \quad (2.8)$$

assuming that the O_2 concentration at the char/coal surface [76] is negligible and equal diffusivities of CO_2, CO and O_2 through N_2 [72, 74] (note in Eq. 2.7 θSh_{cdeq} instead of Sh_{cdeq}).

Applying the conservation of the i-th compound through the gas-film (considering no chemical reaction)

$$r^2 N_i = r_c^2 N_{i,c} \quad (2.9)$$

where $N_{i,c}$ is the molar flux at the char particle's surface, and taking into account that the oxygen is consumed at the external char surface at a rate given by a first-order kinetic combustion reaction

$$r_{O2,cb} = -\frac{2+\xi}{2\,(1+\xi)}K_{cb}Cx_{O2,c} \quad (2.10)$$

and by gasification reaction

$$r_{CO2,gf} = -K_{gf}Cx_{CO2,c} \quad (2.11)$$

where the kinetic coefficients (based on external particle surface) are given by

$$k_{cb} = A_{cb}T_c\exp\left(-\frac{E_{cb}}{T_c R_g}\right) \quad (2.12)$$

for combustion and

$$k_{gf} = A_{gf}T_c\exp\left(-\frac{E_{gf}}{T_c R_g}\right) \quad (2.13)$$

for gasification, the flux of the various species (CO, CO_2 an O_2) at the char particle's surface can be calculated by

$$N_{CO,c} = -\frac{2\xi}{2+\xi}r_{O2,cb} + 2r_{CO2,gf} \quad (2.14)$$

$$N_{CO2,c} = -\frac{2}{2+\xi}r_{O2,cb} - r_{CO2,gf} \quad (2.15)$$

$$N_{O2,c} = r_{O2,cb} \quad (2.16)$$

It should be noted that the flux of N_2 is null at any point of the gas-film surrounding the particle since there is no consumption and production.

2.3. SHRINKING PARTICLE MODEL

As it will be shown in the experimental results (see § 4.2), for the various char tested in this work, the ash detaches rapidly during conversion in fluidized bed and the char particle's density remains approximately constant. Assuming that the temperature gradient inside the particle is small [30], an isothermal shrinking particle model can be applied to a spherical particle to predict char consumption with time. This theoretical model has been successfully applied for different biomasses [77, 78] and coals [53]. The change of char particle's size and temperature with time is predicted by solving the two-coupled equations

$$\frac{dr_c}{dt} = -\frac{1}{\rho_{m_c}}\left(r_{CO2,gf} - \frac{2\,(\xi+1)}{2+\xi} r_{O2,cb}\right) \tag{2.17}$$

$$\frac{dT_c}{dt} = \frac{3}{\rho_{m,c} C_P}\frac{1}{r_c}\left(\left((-\Delta H_{gf}) r_{CO2,gf} - (-\Delta H_{cb}) r_{O2,c}\right) - \left(\frac{Nu^{j}_{cdeq}}{K d_g 2 r_c}(T_c - T_\infty) + \sigma\omega_c\left({T_c}^4 - {T_\infty}^4\right)\right)\right) \tag{2.18}$$

with the initial condition at t = 0

$$r_c = r_{c,o}$$

$$T_c = 298\ K \tag{2.19}$$

where

$$\Delta H_{cb} = \left(\frac{1}{(1+\xi)}\Delta H_{CO2} + \frac{\xi}{(1+\xi)}\Delta H_{CO}\right) - \left(\Delta H_C + \frac{2+\xi}{2\,(1+\xi)}\Delta H_{O2}\right) \tag{2.20}$$

is the combustion heat (exothermic) and

$$\Delta H_{gf} = (2\Delta H_{CO}) - (\Delta H_C + \Delta H_{CO2}) \tag{2.21}$$

the gasification one (endothermic), and Nu^{j}_{cdeq} is the Nusselt number when the char particle is in the emulsion phase (j = ePh), bubble phase (j = bPh), or in the splash zone (j = sPh) as it is explained below (see § 2.4).

It could be argued that the gasification of the char particle with CO_2, which could occur during oxy-fuel combustion with high CO_2 concentration and char particle's temperature higher than 900 °C, is controlled by intrinsic kinetic [24] and takes places throughout the entire particle as the particle is porous and the reaction relatively slow. However, in the treatment given here, char gasification is assumed to effectively occur in a narrow layer near the external surface of the char particle and therefore an externally surface-based kinetic equation rate is used (see Eq. 2.11, 2.13, and Table 2.1). Consistently, the intrinsic kinetic parameters commonly obtained in a Thermo gravimetric Analyzer [18] are extrapolated to apparent ones (externally-based and taking diffusion effects into account) [77]. As a result, apparent kinetic used elsewhere [80-82] for different types of fuel particles has been taken for gasification reaction. It is known that the gasification reaction weakens the internal structure of the char particle by pore enlargement [24], and this could change the conversion rate and density of particles especially at high conversion. However, here is assumed that the char particle density remains approximately constant since the conversion conditions handled involve that the gasification contribution is much lower than oxidation one. Therefore, the possible char particle's density change is assumed to be small supported by our experimental observations. In summary the approach followed in the present work by implementing the gasification as a heterogeneous reaction taking place in parallel with oxidation in a thin shell layer close to external particle, is justified.

2.4. CHAR PARTICLE'S MOVEMENT THROUGH A FLUIDIZED BED

As it is pointed out above (see § 1.1), there are experimental observations indicating that the char particle is in the emulsion phase a large part of the conversion time, but that it is also in the bubble phase and splash zone [32-34, 82]. This period is a fraction of the fluidization time not negligible (it could be higher than 20 % [32, 33]), during which the heat and mass transfer

from/to the char particle vary, and possibly other phenomena such as the CO oxidation close to the char particle. This idea is sketched in Fig. 2.2a by "zooms" in the different char particle's locations in the bed. As it has been theoretically proposed elsewhere [43], the "random" char particle's movement through the bed could be implemented into the conversion model treating this "random" movement as a cyclic one (see Fig. 2.2a). It links the downward motion of the char particle through the emulsion phase until a certain depth from the bed surface, followed by its upward motion from there to the bed surface where it resides some time before starting a new cycle. During the upward motion of the char particle, it stays most of the time in the emulsion phase with intermittent penetration into the bubbles. It should be pointed out that the char particle in the emulsion phase is assumed to be stopped or moved downward because that phase is assumed to be under minimum fluidization condition. The bubbles move sand particles upward and it is assumed that the char also moves upward when it is in the bubble phase or close to it.

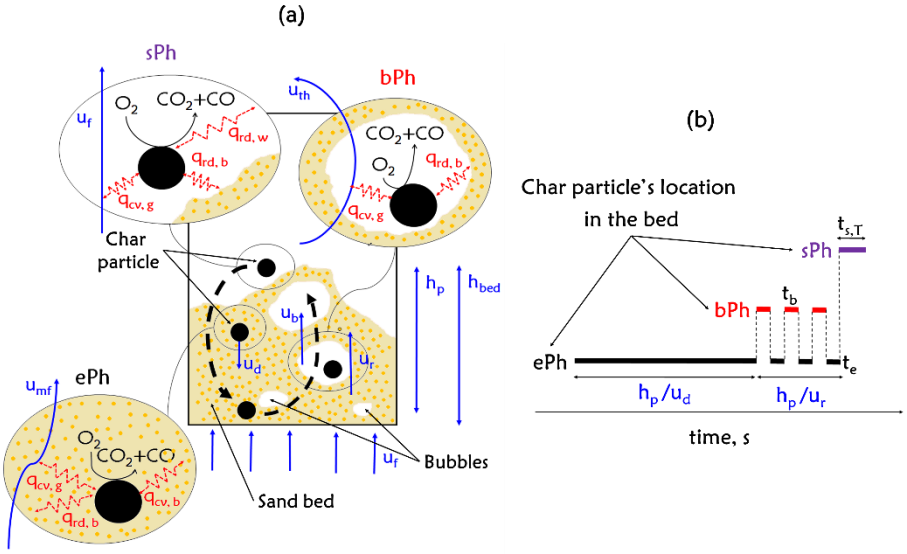

Fig. 2.2. Sketch (a) and temporal characterization (b) of the char particle's movement through the emulsion phase (sPh), bubble phase (bPh) and splash zone (sPh) and the heat and mass transfer and CO/CO_2 ratio in each place

As it is shown in Fig. 2.2b, the characterization of this cycle by fluid-dynamic parameters required the upward and downward char particle's velocities through the bed (u_r and u_d), the depth reached by the char (h_p), the bubble velocity and diameter (u_b and d_b) among others [33]. However, if the depth reached by the char and the fractions of the time (θ_i) during which it is in the emulsion phase (i = ePh), bubble phase (i = bPh), and splash zone (i = sPh) can be experimentally established (see § 3.2.2), the cycle's characterization can be calculated by estimating the bubble velocity and the upward char velocity (see Appendix I). It should be noted that a new time-dependent variable becomes involved in the presented theoretical description: the location of the char particle in the bed. This approach, which can be called "dynamic",

contrasts from the classical approach used in the literature where the char particle is assumed to remain always in the emulsion phase (see § 1.1), here called "static". Therefore, it is needed the estimates of the mass and heat transfers for each one of the char particle's positions in the bed.

2.5. HEAT AND MASS TRANSFERS AND CO/CO_2 RATIO

Mass transfer estimates in a fluidized bed (for experimental conditions handled in this work, see Table 3.1) applied techniques based on the consumption of mass or drying of an active particle, such as naphthalene [83, 84], wet porous particle [85], or coal [51], quantifying the change in the particle mass and/or in the concentration of gaseous compounds, such as naphthalene, water vapor, or CO and CO_2. Moreover, CO oxidation in a gas fluidizing a sand bed with few Pt catalyst spheres immersed, has also been used to estimate mass-transfer coefficients [86]. Heat transfer has been estimated by an energy balance during the cooling of warm metal particles [55, 84, 87], or during water evaporation from a wet porous particle [85]. In all these studies, the particles were freely fluidized, or with an embedded thermocouple, having likely stayed in the emulsion phase most of the time, but also in the bubble/splash regions. Therefore, all these experimental heat and mass transfer estimations implicitly lumped the effect of the active particle's movement through the bed, and none of them can be formally used for just one of the char particle's positions in the bed. Consequently, here it is used theoretical correlations for the mass and heat transfer estimates [39-41, 43] when the char particle is in the emulsion phase (ePh)

$$\mathrm{Sh}_{\mathrm{cdeq}}^{\mathrm{ePh}} = \frac{2\varepsilon_{\mathrm{mf}}}{\tau^2} + 0.3465\left(\mathrm{Re}_{\mathrm{ePh}}\mathrm{C}_{\mathrm{d,ePh}}\right)^{0.33}(\tau/\varepsilon_{\mathrm{mf}})^{0.66}((1+\mathrm{Re}_{\mathrm{ePh}}\mathrm{Sc})^{0.33}-1) \tag{2.22}$$

$$\mathrm{Nu}_{\mathrm{cdeq}}^{\mathrm{ePh}} = \frac{2k_{\mathrm{d,ePh}}}{k_{\mathrm{d,g}}} + 0.3465\left(\mathrm{Re}_{\mathrm{ePh}}\mathrm{C}_{\mathrm{d,ePh}}\right)^{0.33}(\tau/\varepsilon_{\mathrm{mf}})^{0.66}((1+\mathrm{Re}_{\mathrm{ePh}}\mathrm{Pr})^{0.33}-1) + \left(\frac{d_c}{k_{\mathrm{d,g}}}\right)\Big/\left(\frac{d_i}{\psi K_{\mathrm{d,g}}} + 0.5\sqrt{\frac{\pi t_{\mathrm{ePh,T}}}{K_{\mathrm{d,ePh}}\rho_{\mathrm{mf}}Cp_i}}\right) \tag{2.23}$$

bubble phase (bPh)

$$\mathrm{Sh}_{\mathrm{cdeq}}^{\mathrm{bPh}} = 2 + 0.3465\left(\mathrm{Re}_{\mathrm{bPh}}\mathrm{C}_{\mathrm{d,bPh}}\right)^{0.33}((1+\mathrm{Re}_{\mathrm{bPh}}\mathrm{Sc})^{0.33}-1) \tag{2.24}$$

$$\mathrm{Nu}_{\mathrm{cdeq}}^{\mathrm{bPh}} = 2 + 0.3465\left(\mathrm{Re}_{\mathrm{bPh}}\mathrm{C}_{\mathrm{d,bPh}}\right)^{0.33}((1+\mathrm{Re}_{\mathrm{ePh}}\mathrm{Pr})^{0.33}-1) \tag{2.25}$$

and splash zone (sPh)

$$\mathrm{Sh}_{\mathrm{cdeq}}^{\mathrm{sPh}} = 2 + 0.69(\mathrm{Re}_{\mathrm{sPh}})^{0.5}\mathrm{Sc}^{0.33} \tag{2.26}$$

$$\mathrm{Nu}_{\mathrm{cdeq}}^{\mathrm{sPh}} = 2 + 0.69(\mathrm{Re}_{\mathrm{sPh}})^{0.5}\mathrm{Pr}^{0.33} \tag{2.27}$$

The detailed description of these correlations is in Appendix II.

It could be said that the dependence of mass transfer on the minimum fluidization velocity and not on the fluidization velocity, claimed in several investigations [83, 84, 86, 87], is related to the fact that the char particle is mainly in the emulsion phase [83, 86]. However, using one of the experimental correlation could involve taking into account twice the effect of the char particle in the bubble/splash phase on the mass transfer, since that the proposed model account for separately the mass transfer when the particle is in each of these phases. Moreover, other investigations found influence of the fluidization velocity on mass transport rates [39, 85]. This

contradiction could be understood if the effect of the fluidization velocity on the position of the coal/char particle in the bubbling bed changes slightly when the sand bed is at bubbling conditions. In such cases, an increasing fluidization velocity enhances the mass transfer rate because the convective flow in the splash zone and bubble phase is increased (emulsion phase is at minimum fluidization conditions). If the time in these positions for the experimental conditions used in the mentioned works (d_a/d_i: 1 – 200; Ar: 10 – 10^8) varies just a little, it is possible that the measurement techniques used in the estimation are not accurate enough to detect the corresponding small change in the mass transfer [86]. In chapter 4 (§ 4.2.1), the change in the char particle's location in the bed for two different fluidization velocities is quantified, proving that in such conditions (bubbling regime) these locations are barely affected.

Publications addressing the CO/CO_2 ratio generated by carbon oxidation agree on the difficulty of avoiding the oxidation of CO before measuring it. There is also a dependence on the fuel temperature, but if the combustion takes place in a FB, the ratio is independent of the bed temperature and the fluidization velocity [32, 42]; the inert bed particles inhibit the CO oxidation close to the char particle [42]. The CO/CO_2 ratio estimated by Arthur [71] is used here, because in his study different coal ranks and an effective inhibitor of the CO oxidation were investigated. This estimation (Eq. 2.3, Table 2.1) is assumed independent of the position of the char particle in the bed, because there is a slight cloud of bed particles around the char particle when it is in the bubble phase and splash zone, as it is discussed in chapter 4 (see Fig. 4.14 and Fig. 4.18).

In summary, the model used here to estimate the temperature and burnout times includes Eqs 2.1 – 2.27, along with the values of the parameters shown in Tables 2.1, and Eq. AII.1 in Appendix II.

2.6. NUMERICAL METHOD AND SOLUTION PROCEDURE

In addition to the values of the char particle's and fluidization flow's properties summarized in Table 2.1, and the operating conditions of the bed for each test, the theoretical approach requires the char particle's movement through the bed. This movement, whose characterization is in Appendix I, gives the needed time to complete a cycle (T, see Fig. 2.2) and the residence time in each bed phase ($t_{i,T}$) as a function of the char particle's size (diameter). Therefore, given the initial size of the char particle, it is known the place occupied for it during the next T seconds. For every 0.04 seconds, it is calculated all fluxes from/to the char particle's surface ($N_{i,c}$) solving Eqs. 2.3 - 2.16, along with 2.22 if the char is at the emulsion phase, 2.24 if the char is in the bubble phase, and 2.26 if the char is in the splash zone. Eq. 2.17 and 2.18 are then simultaneously solved giving the size of the char particle (r_c) and temperature (T_c) after 0.04 seconds of conversion. Noted that the energy balance (Eq. 2.18) used the heat transfer correlation corresponding to the char's place in the bed at this moment time: 2.23 for emulsion phase, 2.25 for bubble phase, and 2.27 for splash zone.

Table 2.1. Parameters of the model

	Symbol	Value		Unit	Ref.
Char Particle					
Density	ρ_c	405	@ BW*	kg/m^3	
		1090	@ SBC*		
Emissivity	ω_c	0.85	@ BW	-	[60]
		0.9	@ SBC	-	[93]
Specific heat	c_p	13.3	@ BW	J/mol K	[28]
		12.6	@ SBC	J/mol K	[28]
Enthalpy	ΔH_c	c_p (T_c - 298)		J/kg	-
Fluidized bed					
Bed particles' density	ρ_i	2560		kg/m^3	[24]
Bed's density	ρ_b	1440		kg/m^3	-
Bed's Porosity	ε_{mf}	0.44		-	
Bed particles' specific heat	$c_{p,i}$	798		J/kg K	[41]
Bed particles' conductivity	k_i	0.33		W/mK	[41]
Minimum fluidization velocity	u_{mf}	0.18		m/s	-
Diffusivitties*					
O_2 diffusivity in N_2	$d_{O2\text{-}N2}$	$2.15 \cdot 10^4$ $(T/1073)^{1.81}$		m^2/s	[101]
O_2 diffusivity in CO_2	$d_{O2\text{-}CO2}$	$1.67\ 10^4$ $(T/1073)^{1.81}$		m^2/s	[101]
O_2 diffusivity in CO	$d_{O2\text{-}CO}$	$d_{O2\text{-}N2}$		m^2/s	[72]
CO_2 diffusivity in N_2	$d_{CO2\text{-}N2}$	$1.7\ 10^4$ $(T/1073)^{1.81}$		m^2/s	[101]
CO diffusivity in N_2	$d_{CO\text{-}N2}$	$d_{O2\text{-}N2}$		m^2/s	[72]
CO_2 diffusivity in CO_2	$d_{CO\text{-}CO2}$	$d_{O2\text{-}CO2}$		m^2/s	[72]
Kinetic					
Pre-exp. factor in Eq. 2.3	$A_{CO/CO2}$	2512		-	[71]
Activation energy in Eq. 2.3	$E_{CO/CO2}$	51880		J/mol	[71]
Combustion pre-exp. factor	A_{cb}	0.658		m/Ks	[102]
Combustion activation energy	E_{cb}	74800		J/mol	[102]
Gasification pre-exp. factor	A_{gf}	3.42		m/Ks	[79]
Gasification activation energy	E_{gf}	129700		J/mol	[79]

* BW: Beech wood, SBC: Sub-bituminous coal, **Diffusivities evaluated at $T = (T_c + T_{bed})/2$

CHAPTER 3. EXPERIMENTAL

In the present Chapter the experimental set-up developed in this work is presented, as well as the theoretical basis of the method used for the design and development of optical measurements, including the processing of images.

3.1. PYROMETRY WITH A DIGITAL CAMERA

Pyrometry is based on the capture and interpretation of the thermal radiation emitted from a body whose temperature is to be measured. A common digital camera can carry out this capture and interpretation if the thermal radiation includes the visible spectral band. The light from the scene is separated into three spectral bands or colors: red (0.62-0.7 μm), green (0.49-0.58 μm), and blue (0.45-0.49 μm) by a filter place over the sensor [60]. When the radiation touches the sensor, each pixel generates three values known as Digital Numbers (DN_k) that measure the radiation belonging to each mentioned spectral bands. By an image program three matrices for each image are obtained, whose elements (m,n) contain the digital numbers associated with the radiation received from the viewed scene. Fig. 3.1 shows the recreation of the capture and interpretation of the radiation from the viewed scene by the digital camera (a) and the digital numbers' example from an image of a wave on the lake's water surface (b). It should be known that the sensor has a lower limit energy level (W/m^2) and for radiation below it, the digital number assigned by a pixel is null. It also has a higher limit energy level, above from which the pixel becomes saturated and a maximum value is assigned (saturation) [88].

The water temperature shown in Fig. 3.1b cannot be measured using the visible spectral band because the light captured by the digital camera is from the sun. However, if a body emits thermal radiation within the visible spectral band due to its temperature, its temperature could be measured if the digital numbers from image are used (properly implemented in the heat transfer model). This is the basis for the temperature measurement by pyrometry with a digital camera, whose detailed discussion is given in Appendix III.

Reviewed works from literature that measure the coal/char particles' temperatures in fluidized beds by pyrometry use simultaneously the information contained in two spectral bands [32, 56-60, 65-68]. This application, named two-color pyrometry (P2C), allows calculating the temperature by Eq. 3.1. The method works provided the temperature of the object to be measured is higher than that of the background and when the surface is grey (see § AIII.2) [32, 56, 58]. It has significant advantages over other techniques used in FB, but there is a disadvantage

associated with the finite capability to measure the radiation of each pixel (as mentioned above), which could reduce the accuracy of the method: the P2C may use information from pixels that are either saturated or whose radiation is low and the corresponding digital numbers are close to zero. Nonetheless, if the surface emissivity is known and the digital numbers are used sequentially, it is possible to avoid this disadvantage, and even temperatures lower than that of the background can be measured by Eq. 3.2.

$$T_{P2C,i/j} = \frac{C_2\left(\frac{1}{\lambda_j}-\frac{1}{\lambda_i}\right)}{\left(\ln\left(\frac{DN_i}{DN_j}\right)+\ln(\beta_{i/j})\right)-5\ln\left(\frac{\lambda_j}{\lambda_i}\right)}. \quad (3.1)$$

$$T_{P1C,k} = \frac{C_2}{\lambda_k\left[\ln\left(\Phi_k\frac{\varepsilon_c C_1}{\lambda_k^5}\right)-\left(\ln\left(\beta_k DN_k-(1-\varepsilon_c)E(\Delta\lambda_k,T_w)\right)\right)\right]} \quad (3.2)$$

This approach is the one used in this work and is named one-color pyrometry (P1C, see § AIII.3). Calculating the char temperature in the digital camera's field of view requires the value of the calibration parameter β: $\beta_{i/j}$ in 3.1 for P2C and β_k in 3.2 for P1C. These parameters lump the optical and electronic parameters of the experimental set-up, as well as the hypothesis and simplification of the heat transfer model. Therefore, the accuracy and reliability of the measured temperature depends on the accuracy of the calibration, which is carried out by fitting dedicated tests as explained below (see § 3.2.2).

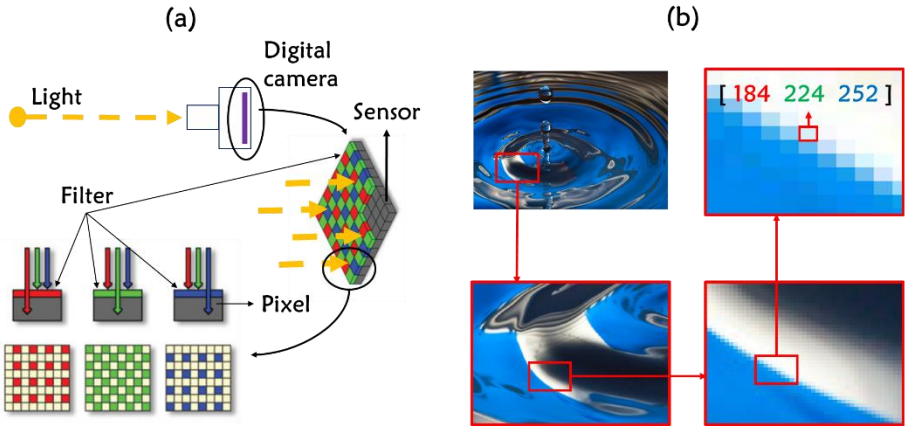

Fig. 3.1. Capture and interpretation of the radiation from the viewed scene by the digital camera (a) and the digital numbers' example from an image's pixel of a wave on the lake's water surface (b)

The char particle's size can be determined by analyzing the images obtained from the tests. This is done by relating the number of pixels (px) occupied by the initial diameter of the char particle in the firsts instants of the conversion in the bed to the known initial length in millimeter. That relation (mm/px) is used determine the char particle size throughout the tests.

One of the main assumptions made to develop Eqs 3.1 and 3.2 is that the thermal radiation received by the char particle's surface is from a surrounding black surface (see Fig. AIII.1). However, the char particle can be in the emulsion phase, bubble phase, and splash zone [32-34,

82] (see Fig. 2.2), where in addition to the background radiation (j_w), it receives radiation from the bed (j_b). To apply Eqs. 3.1 and 3.2, the bed emissivity is assumed to be unity (black body) [57], which is a reasonable assumption since the blackness is strengthened by the mutual interchange among the particles [90].

3.2. EXPERIMENTAL

The analysis of the fuels and the main characteristics of all experimental devices used are summarized in Table 3.1, whereas the description of all studies carried out in this work are summarized in Table 3.2. On the other hand, it should be keep in mind that for each experimental bed conditions in each of the studies, three tests were carried out. Most of the experimental results shown and discussed in Chapter4 are the average of these three tests. Since numerous measurements of the char particle's temperature and conversion for each test were recorded, the results are statistically representative.

Table 3.1. Fuels and experimental conditions in this work

Proximate analysis of the fuels* (mass fraction, %)			
	Beech Wood	**Bituminous Coal**	**Sub-Bituminous Coal**
Volatiles	84.9	21.1	35.6
Fixed carbon	14.5	33.7	59.2
Ash	0.6	45.2	5.2
Char density, kg/m³	405	1106	1090

Experimental set-ups	
FBC 2D	***FBC 3D***
Fluidized bed reactor	**Fluidized bed reactor**
18 x 50 x 1.8 cm, bottom and freeboard made in quartz Bed of silica sand, d_i: 0.32-0.5 mm u_{mf}: 0.18 m/s @ 25 °C	7 (i.d) x 50 cm, made in 310 steel Bed of silica sand, d_i: 0.32 - 0.5 mm u_{mf}: 0.18 m/s @ 25 °C
Electric oven	**Electric oven**
Electrical power: 11 kW 50 x 70 x 30 cm Window: 19.5 x 19.5 cm	Electrical power: 9 kW 30 (i.d.) x 70 cm
Digital camera	
JVC Everio HD, 2 Mpx	

*ASTM (dry basis)

3.2.1. EXPERIMENTAL SET-UP

Two-lab scale fluidized bed reactors have been used in this work. The first one, called FBC 2D and shown in Fig. 3.2, comprises an electric oven (high-temperature hearth's dimensions: 50 x 70 x 30 cm) equipped with a quartz window (20 x 20 x 0.5 cm), which allows direct visual observation of the bed and then to make optical measurements. The fluidized bed reactor has also a quartz window in the bottom and freeboard (18 x 21 x 0.5 cm), allowing seeing the

fluidization of the char. A black surface (a metal box located in between the internal walls of the oven and the FB reactor) makes the thermal radiation from the electric resistances (11 kW) uniform. The reactor is placed in the center of the oven, surrounded by the homogenizing black surface. The reactor geometry is approximately two-dimensional (18 x 1.8 x 50 cm) in order to obtain as many images of the char particle as possible. This design is based in the previously presented by Prins et al, [82] who showed the capability of the 2D reactor to provide information on the coal particle behavior in a FB. The second FB reactor, which is named FBC 3D, comprises an electric oven (high-temperature hearth's dimension: Ø = 30 x 70 cm) where a FB made in 310 steel (Ø = 7 x 50 cm) is placed in the center.

Silica sand was used as bed material in both reactor, where their height at rest was 8 cm (see properties at Table 3.1). The bed temperature was controlled by a thin flexible type K thermocouple (0.15 cm sheath diameter and 100 cm length) immersed into it. Pre-heated mixtures of O_2 in N_2 or in CO_2 with different O_2 concentration, or air were used as fluidization agent at different gas velocities. The device used to capture and interpret the thermal radiation from the char surface by pyrometry (see § 3.1) is a digital camera JVC Everio HD (2 Mpxs CMOS sensor), which is placed at 100 cm from the FB rector with a field of view of 24º. All tests in FBC 2D set-up were carried out in a dark-room in order to only allow radiation from the char and from the background to reach the sensor [69]. Manual mode was set to avoid differences in the way in which the software of the digital camera measures the visible thermal radiation, since differences in the images' light ratio, as the one generated from the surface reaction on the char, could change it.

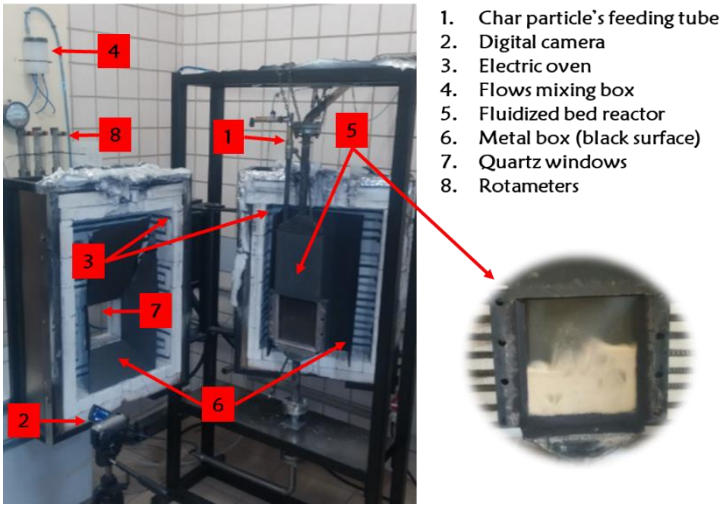

Fig. 3.2. Experimental set-up with a bi-dimensional fluidized bed reactor: FBC 2D

PREPARATION OF CHAR PARTICLES

The char particles used in this work were from beech wood and sub-bituminous and bituminous coal, whose proximate analysis is in Table 3.1. Irregular particles from these fuels (14 mm equivalent diameter) were placed inside a furnace with an inert atmosphere where they

were heated from room temperature to 800 °C with a low heating rate (8 °C/min), avoiding particle fragmentation. Each char particle was shaped into a spherical or parallelepiped form, whose weights and sizes were fixed according to the tests where they were used. While all parallelepiped char particles were drilled on their surface to make a gap (0.5 x 0.8 x 4 mm), just some of the spherical char particles were drilled from their surface to their center making a hole (0.2 x 5 mm). K-type thermocouples were embedded in the gaps and in the holes, all of them 100 cm length and with different sheath diameters: 0.25, 0.5, and 0.75 mm. In tests where the char particle were fluidized with an embedded thermocouple, a high-temperature resistant sealant was used.

RECORDING CONDITIONS

All tests carried out at FBC 2D set up were recorded using a digital camera. The recording began when the char particle was fed into the bed or into the oven (calibration and validation tests of the pyrometric measurement, see § 3.2.2). Therefore, the time of each image from the recording met with the conversion time. The images from the tests were obtained by the Adobe Premier Pro CS6 program at 25 frames per second (fps), except the ones for the calibration and validation tests of the pyrometric measurement which were analyzed at 1 fps. The decomposition rate of 25 fps gave one frame each 0.04 s, which was sufficient to follow the char particle's movement through the bed, seeing it frequently and clearly longer than the 25 % of the fluidization time. Moreover, it was proven that the results from 60 fps were not so different from the ones calculated with 25 fps.

All digital camera's parameters, such as; white balance or electronic gain, were manually set. Therefore, the way in which the software of the camera measured the visible thermal radiation received over the sensor during the tests did not change before changes in the lighting ratio of the images; for instance, because of the increase in the thermal radiation from the char particle (increase in its temperature) regarding with the background.

3.2.2. EXPERIMENTAL METHODOLOGY

TESTS AND PROCEDURE FOR THE CALIBRATION AND VALIDATION OF THE METHOD TO MEASURE OF THE TEMPERATURE

The digital device's calibration was carried out by analyzing the images of combustion tests where single char particles were placed at the center of the electric oven with the quartz window (without the fluidized bed reactor). The temperature inside the oven was 800 °C and the O_2 concentration (in N_2) ranged from 0 to 50 $\%_{v/v}$ respectively. In that way, the combustion temperatures of these char particles were at similar conditions to those in the FB working during conversion. The char particles used in these tests were parallelepipeds with an embedded thermocouple (0.75 mm sheath diameter) into the surface gap as it is shown in Fig. 3.3a. The images analysis of each test were from the time in which the char particle was fed into the oven until the thermocouple left the gap, giving a total of 1277 combustion images (one per second). The calibration procedure involves calculating for each image the average digital numbers of the ones corresponding to the char surface whose temperature was measured by the thermocouple (DN_k, one for each color or spectral band) as illustrated in the Fig. 3.3b. These average digital

numbers along with the corresponding temperature were used in Eq. AIII.17 and Eq. AIII.18 to obtain the points $\ln(\beta_{i/j})$ - $\ln(DN_j/DN_i)$ and $\ln(\beta_k)$ - $\ln(DN_k)$ respectively (see § AIII.4). Curves for the determination of $\beta_{i/j}$ and β_k when digital numbers are known, but not the temperature, were obtained by fitting those points.

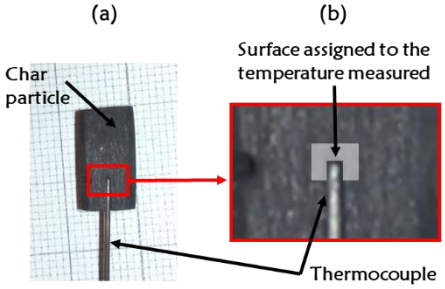

Fig. 3.3. Thermocouple into the char particle's surface (a) and the surface assigned to the temperature measured by it (b)

It should be pointed out that these calibration curves can be only used when the optical set-up is the same as the one used to calibrate. The fitting curves for P1C and P2C were used in three other validation tests (429 images). The accuracy and reliability of the pyrometer technique were analyzed by comparing the temperatures measured by pyrometer and thermocouple. A block diagram of the measurement procedures for P1C and P2C (including the calibration step) is shown in Fig. 3.4.

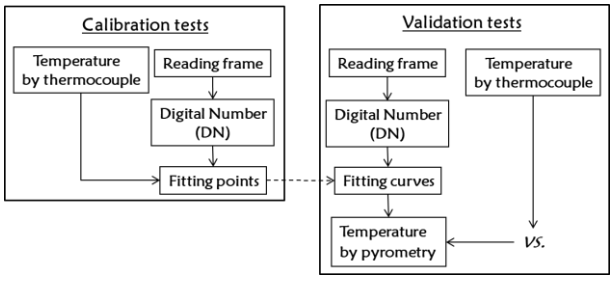

Fig. 3.4. Block diagram of the experimental procedure

TESTS AND PROCEDURE TO ANALYZE THE IMPACT OF USING THERMOCOUPLES TO MEASURE CHAR TEMPERATURE DURING COMBUSTION IN A FLUIDIZED BED

To analyze the effect of measuring the temperature by thermocouple on the conversion of a single char particle two different setups were used, the FBC 2D and FBC 3D, as sketched Fig. 3.5 and whose main design and operating data are summarized in Table 3.1. The char particles used in these tests were the spherical ones, which were fluidized with and without an embedded thermocouple. The thermocouple's length was enough to allow the char particle to sink and move throughout the bed, and the sheath diameters were 0.25, 0.5, and 0.75 mm. The mass of each char particle was fixed at 0.26 g for the beech wood char and 0.56 g for the sub-bituminous and bituminous chars.

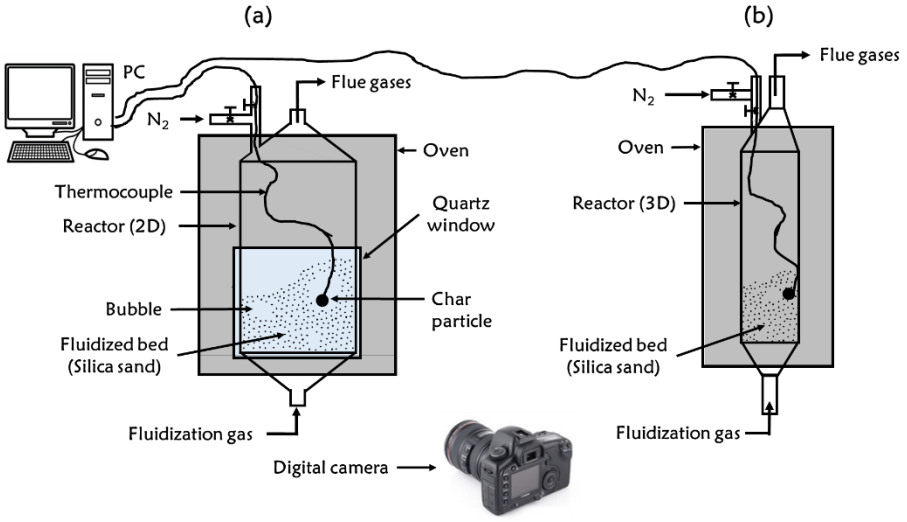

Fig. 3.5. Experimental set-up with the rectangular quartz fluidized bed reactor: FBC2D (a) and the cylindrical steel reactor: FBC 3D (b)

The images classification was carried out manually by the definitions shown in Fig. 3.6, where the locations of the different char particles and their associated phases are represented. Because of the large amount of images from each combustion test (1500 frames are generated every minute), it was not practical to classify all of them. Therefore, frames from the last 10 seconds of all minutes in each test are chosen and classified. From the selected images, the fraction of the combustion time (θ_i) during which the char particle is in a certain phase is calculated as

$$\theta_i = 1 - \frac{\sum_{j=1}^{m} N_{j,i}^{img}}{250\ m} \tag{3.3}$$

where $N^j_{ph,i}$ is the number of images where the particle is in the emulsion phase (i = ePh), or the bubble phase (i = bPh), or the splash zone (i = sPs) within the 250 frames from the 10 s associated to the j-th minute, and m is the number of minutes of each test. This analysis was applied during the time in which the char particle and the thermocouple were attached. Since most of the detachment happened when the char particle's size was around 3 mm, the comparison of these times with those obtained during conversion of a freely-fluidized char particles was made only until char particles' sizes reached approximately 3 mm. Nevertheless, the fractions of the freely-fluidized char particles were obtained until the last minute in which the char particle was seen (char's size approximately 1 mm) since they were used to characterize the char particle's movement through the bed needed for the conversion model discussed in Chapter2. Knowing the position and the size of the char particle at any time, it is possible to quantify the effect of the thermocouple on the location of the char particles in the bed for different sizes.

The effect of the thermocouple on the surface consumption was analyzed by extracting particles from the reactors at different times. The size reduction was

$$\delta_k = \frac{d_{c,o} - d_{c,k}}{d_{c,o}} \tag{3.4}$$

where $d_{c,o}$ is the initial char particle's diameter, quantified in both perpendicular ($k = \perp$) and parallel ($k = //$) directions with respect to the insertion of the thermocouple into the particle from the surface to the center. The results from the FBC 3D set-up were compared with those from FBC 2D.

According to the definitions in Fig. 3.6 a char particle on the bed's surface is associated with the splash zone when more than half of its volume is out of the bed (otherwise it is considered to be in the emulsion phase, see zooms in Fig. 3.6). By another definition, for example, a char particle on the surface of the bed is in the splash zone if part of its volume is out the bed (not necessarily more than half of its volume), the interpretation of the images would be different, and therefore, the fractions of the combustion time when the char particle is in these places (θ_i, Eq. 3.3). However, the differences between the fractions calculated for the cases with and without a thermocouple would be equivalent. Moreover, even if the definition is changed, it would not influence the percentages associated with the bubble phase as Chapter 4 discusses (see § 4.2), since one of the differences between the conversion of a char particle with and without a thermocouple is that the thermocouple increases the presence of the char particle in the bubble phase.

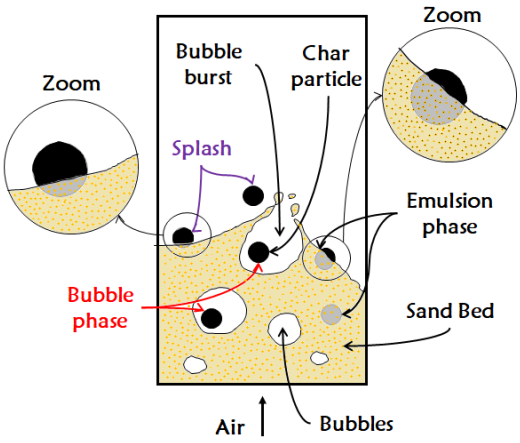

Fig. 3.6. Definition of the char particle's position in the bubbling fluidized bed reactor

TESTS AND PROCEDURE FOR EXPERIMENTAL MEASUREMENT AND THEORETICAL PREDICTION OF CHAR TEMPERATURE OSCILLATIONS

Combustion tests of single char particles freely-fluidized into the FBC 2D were carried out to study the effect of the char particle's movement through the emulsion phase, bubble phase, and splash zone on its combustion temperature. The bed temperature was set at 800 °C and the fluidization agent was a mixture of O_2 and N_2, where the O_2 concentration was either 11 or 21%$_{v/v}$. The char particles were from beech wood and sub-bituminous coal with spherical form ($d_{c,o} \sim 8$ mm), whose weights were fixed at 0.09 and 0.28 g respectively. The images analyzed by pyrometry were in the form of sequences shorter than one second, during which the char particle changes its location. These experimental results (not just the char particles' combustion

temperatures, but their oscillation as consequence of their movement through the bed) were compared with the theoretical prediction of the conversion model presented in Chapter 2.

As Chapter 2 explains (see § 2.3), the theoretical analysis needs the char particle's trajectory and velocity passing through the bed as input data. Characterizing this char particle's movement involves the fitting of the combustion time fractions during which the char is in each bed phase (θ_i, by Eq. 3.3) with its size (d_c, by pyrometry):

$$\theta_{i,T} = m_i d_c + n_i \tag{3.5}$$

where m_i and n_i are fitting constants (note that in this study m in Eq. 3.3 is the number of minutes whose images are classified and the char particle's size is approximately similar). In this way, as Appendix I describes, the time spent for the char particle to complete a cycle (T) and its distribution among the different phases ($t_{i,T}$) can be calculated. Fig. 3.7 shows an example for a char particle from beech wood (8 mm), where the residence time in each phase has been lumped (Fig. 2.2b vs. Fig. 3.7). Therefore, the theoretical analysis assumes that the particle is in the emulsion phase at the initial time and with its initial size calculates its movement through the bed (the time spent in each phase). The conversion is simulated until the end of the first cycle. Then the simulation continues with a new description of the cycle by the char particle's size reached after T seconds of conversion. The process is repeated until the conversion reaches 99 %.

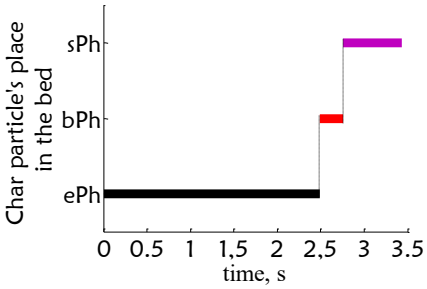

Fig. 3.7. Time and location of a char particle from beech wood (8 mm) during a cycle comprising its movement through the bed: emulsion phase (ePh), bubble phase (bPh), and splash zone (sPh) under the experimental conditions shown in Table 3.1

Note that the cyclic movement is calculated for a given char size. This size gives the residence time in each bed phase ($t_{j,T} = \theta_{i,T}\ T$, see Eq. AI.I) where the conversion takes place. However, during these T seconds, the char size is reduced, changing $t_{j,T}$ (since $\theta_{i,T}$ changes with the char size, see Eq. 3.5), and that change is not taken into account until the new cycle. Because the cycle time is much shorter than the total combustion time (burnout time), this simplification seems reasonable. On the other hand, lumping the residence times of the char particle in each bed phase reduces the char/emulsion and char/bubble interruptions to a single one: once the char leaves the emulsion phase, the bubble time starts (Fig. 2.2b vs. Fig. 3.7). This simplification makes the conditions for char conversion to change instantaneously. The results in Chapter4 (see § 4.3.1) prove that the temperature variation as result of changing the location of the char in the bed is produced in hundredths of a second.

TESTS AND PROCEDURE FOR THE EXPERIMENTAL AND THEORETICAL ANALYSIS OF THE CO_2 EFFECT ON THE CHAR PARTICLE'S TEMPERATURE AND CONVERSION

Oxy-fuel combustion and combustion tests of single char particles in FBC 2D were carried out to address their conversion in an O_2/CO_2 atmosphere with high O_2 concentration. The bed temperature was either 800 or 850 °C, and the O_2 concentration in the fluidization agent were either 11, 21, 30, 40, and 50 $\%_{v/v}$ in N_2 or CO_2. The char particles were from beech wood and sub-bituminous coal with spherical form. For each type of char, two different weights were fixed at 0.09 and 0.28 g to the char from beech wood, and 0.28 and 0.66 g to the char from sub-bituminous coal, where the diameters were 8 mm for the lighter weight and 13 mm for the heavier one. The images analyzed by pyrometry are sequences where the char particle changed its positions in the bed. In this way, the variation (oscillations) in the temperature of the char particle's surface and its size (external diameter) could be tracked. Note that the char particle's size could be measured just for some of the images where the particle is completely seen (see Fig. 4.10). The ratio of these diameters (d_c) and the initial one ($d_{c,o}$) were used to estimate the experimental conversion by

$$x_c = 1 - \left(\frac{d_c}{d_{c,o}}\right)^3 \tag{3.6}$$

The last image of the char particle is the last time when it was seen, whose time was set as burnout. Since that the char particle's size in this image was lower than two millimeter (see Table 4.2), the experimental conversion in all the tests was higher than 99 %. On the other hand, the apparent consumption rate can be estimated using the burnout time, and the char particles' content of carbon ($x_{c,fx}$), masses ($m_{c,o}$) and initial external surfaces ($s_{c,o}$) by

$$\Gamma_c = \frac{x_{c,fx}\, m_{c,o}}{s_{c,o} t_{burnout}} \tag{3.7}$$

to analyze the CO_2 effect on the char particle conversion.

The theoretical predictions by the model are checked comparing them with both experimental temperatures and burnout times from this work and others from the literature. The chosen works used different measurement techniques and experimental oxi-firing and air-firing conditions, covering different ranks of coals, fluidization velocities, bed temperature, etc. (see Table 4.4 where there are the main characteristics of these works).

Table 3.2. Experimental and theoretical studies carried out in this thesis

Calibration and validation of the pyrometry with a digital camera Combustion of single char particles placed in the oven (FBC 2D, without FB) with an embedded thermocouple (d_{th} = 0.75 mm) into the char's surface gap Rectangular char from beech wood: 7 x 7 x 14 mm O_2/N_2 atmosphere @ $[O_2]$: 0-50 $\%_v$ T_{oven}: 800 °C
Impact of using thermocouples on the char particle combustion in a FB Combustion of single char particles in FBC 2D and in FBC 3D with an embedded thermocouple and freely fluidized Spherical char from beech wood, and sub-bituminous and bituminous coal: $d_{c,o} \sim 10$ mm d_{th}: 0.25, 0.5, and 0.75 mm u_f / u_{mf}: 2 (bubbling conditions) Air as fluidization flow T_{bed}: 800 °C
Oscillation in the char particle's temperature in a FB Single char particle combustion in FBC 2D Spherical char from beech wood and sub-bituminous coal, $d_{c,o} \sim 8$ mm O_2/N_2 fluidization flow, $[O_2]$: 11 and 21 $\%_v$ u_f / u_{mf}: 2 (bubbling conditions) O_2/N_2 atmosphere @ $[O_2]$: 11 and 21 $\%_v$ T_{bed}: 800 ºC
Influence of CO_2 gas concentration on the char conversion during oxy-fuel combustion in a FB Single char particle combustion in FBC 2D Spherical char from beech wood, and sub-bituminous coal: $d_{c,o}$: 7-8 vs. 12-13 mm u_f / u_{mf}: 2 (bubbling conditions) O_2/N_2 vs. O_2/CO_2 fluidization flows @ $[O_2]$: 11, 21, 30, 40, 50 $\%_v$ T_{bed}: 800 ºC vs. 850 ºC

CHAPTER 4. RESULTS AND DISCUSSION

This chapter presents the results organized into four parts: in the first part, the method developed to measure the temperature of the char particle's surface during conversion in a FB using a digital camera are discussed (calibration and validation tests and results). In the second part, the method is applied to analyze the impact of using an embedded thermocouple into a char particle in a FB, by comparing the conversion characteristics (temperature and rate of conversion/burnout times) from experiments using freely-fluidized particles with those using char particles with an embedded thermocouple. In the third part the method is applied to capture oscillations in the char temperature during conversion, and the measurements are compared with a model developed taking explicitly into account the movement of char particle through the phases of the FB. In the fourth part, the measurement method is used in dedicated experiments to study the influence of the CO_2 concentration in a gas with high O_2 concentration atmosphere (up to 50%$_{v/v}$) useful for the analysis of FB oxy-fuel boilers.

4.1. MEASUREMENT OF THE CHAR PARTICLE'S SURFACE TEMPERATURE BY PYROMETRY WITH A DIGITAL CAMERA

4.1.1. CALIBRATION OF PYROMETRIC TEMPERATURE

Measuring the char particle's temperature needs the value of the calibration parameter: $\beta_{i/j}$ in Eq. 3.1 for P2C and β_k in Eq. 3.2 for P1C, that is, the DN_k - T_c - β_k relation of the digital camera (see § 3.1). Therefore, images from ten combustion/calibration tests (1273 images) were analyzed relating the digital numbers from the char particle's surface to the corresponding temperatures measured by the thermocouple as sketched Fig. 4.1. The temperature (radiation) detected by the sensor in each spectral band or color is shown in Fig. 4.2a, where it can be seen that the digital numbers (DN_k) increase with the surface temperature. The bands at longer wavelengths have lower saturation temperature (temperature when the maximum value of DN_k is reached), since the emitted and/or received radiation ($W/m^2\mu m$) increases with temperature and wavelength [91]. The DN_r dispersion at temperatures 600-725 °C is caused by the fast increment of surface temperature at the beginning of the combustion. The temperature measured by thermocouple and the images were recorded with a rate of one per second, so the small time-

difference between two measurements explains this dispersion. There is no dispersion in DN_g or DN_b because at these temperatures the sensor does not detect the thermal radiation. The relation between the temperature of char particle's surface and the ratio of the red/green (DN_r/DN_g) and green/blue (DN_g/DN_b) digital numbers for temperatures higher than the background (800 °C), is shown in Fig. 4.2b. The DN_g/DN_b ratio versus temperature lower than 850 °C is not plotted because of the high noise-to-signal ratio in the blue digital numbers at lower temperature than 850 °C.

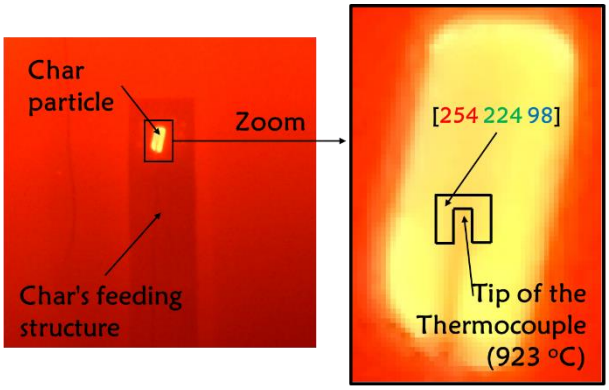

Fig. 4.1. Relation between the average digital numbers of the char particle's surface whose temperature is measured by thermocouple

Introducing the relations shown in Fig. 4.2a and Fig. 4.2b into the Eq.AIII. 17 and Eq. AIII.18 respectively, are obtained the points $\ln(DN_i/DN_j) - \ln(\beta_{i/j})$ and $\ln(DN_k) - \ln(\beta_k)$ shown Fig. 4.3, whose fitting by

$$\ln\left(\beta_{i/j}\right) = a_{i/j}\left(\ln(DN_i/DN\,j)\right)^2 + b_{i/j}\ln(DN_i/DN\,j) + c_{i/j} \quad (4.1)$$

and

$$\ln(\beta_k) = a_k\left(\ln(DN_k)\right)^2 + b_k\ln(DN_k) + c_k \quad (4.2)$$

give the calibration curves (also shown in Fig. 4.3) to measure the pyrometric temperature by two-color pyrometry (P2C) and one-color pyrometry (P1C) respectively. The coefficients values of Eq. 4.1 and Eq. 4.2 are in Table 4.1, where the of the wood char's emissivity in Eq. AIII.18 (P1C) was assumed to be 0.85 [54, 60].

Table 4.1. Calibration curves' coefficients in Eq. 4.1 for P2C and in Eq. 4.2 for P1C

	a	b	c	r^2
P2C				
red/green	- 0.0098	- 0.6949	3.1392	0.9969
green/blue	- 0.0464	- 0.6599	2.2199	0.9958
P1C				
red	1.2998	- 12.475	22.978	0.8280
green	0.1665	- 1.2089	- 5.4118	0.8178
blue	0.3136	- 2.4066	- 5.3567	0.8634

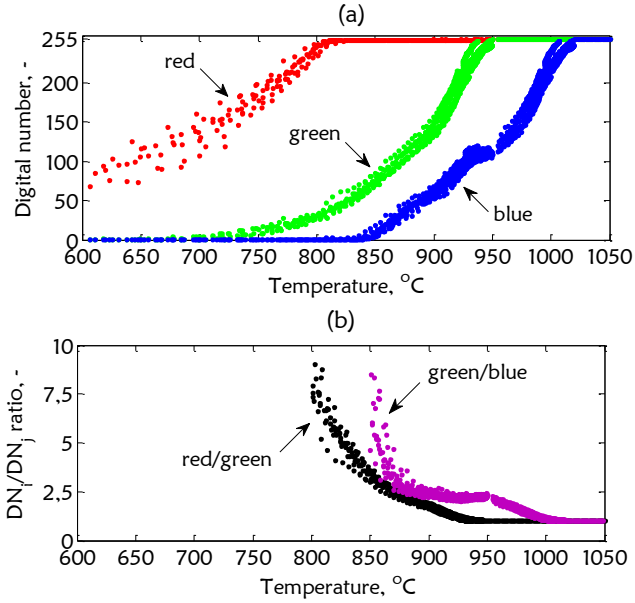

Fig. 4.2. Char particle's surface temperatures measured by thermocouple versus digital numbers (a) for red (DN_r), green (DN_g), and blue (DN_b) and versus ratio of the digital numbers (b) for red/green (DN_r/DN_g), and green/blue (DN_g/DN_b)

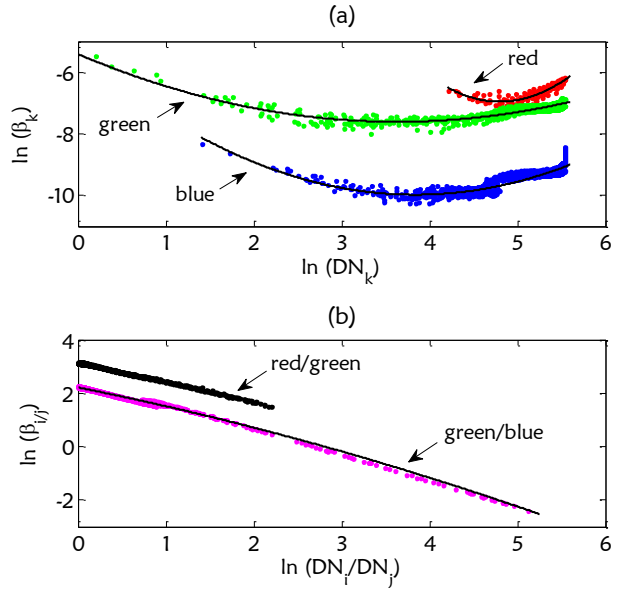

Fig. 4.3. Calibration curves by fitting $\{\ln(DN_k) - \ln(\beta_k)\}$ and $\{\ln(DN_i/DN_j) - \ln(\beta_{i/j})\}$ for P1C (a) and P2C (b) respectively

As shown Fig. 3.4, once the calibration curve are known (the relation between the radiation received on the sensor and the digital number generated), the char particle's surface temperature can be measured. The results of measuring it on the validation tests (429 images) using the information contained in the red spectral band (P1C R), in the green spectral band (P1C G), and simultaneously both (P2C R/G) are shown in Fig. 4.4. The measurement of the char particle's surface temperature by P1C R agrees with the one by thermocouple for temperatures from 600 to 800 ˚C. Above 800 ˚C, the pixels are saturated (see Fig. 4.2a) and P1C R cannot measure temperature (radiation) higher than the radiation that saturates the pixels. Measurement by P1C G has a lower limit approximately at 700 ˚C since the weak captured radiation at lower temperature than that ($DN_g < 1$, Fig. 4.2a). From this temperature (radiation) to 950 ˚C, the accuracy of P1C G is good, but then saturation occurs. The temperature measured by P2C RG can measure surface temperatures higher than the background (see § AIII.2), and its accuracy is good enough until the most energetic spectral band is saturated at 950 ˚C (see Fig. 4.2a). On the other hand, if the measurements by P1C G and P2C R/G are compared, it can be seen a similar predictive capability. This is due to the saturation of the pixels in the red spectral band (DN_r, see Fig. 4.2a), while the associated digital numbers of the green (DN_g, see Fig. 4.2a) remain active at higher temperatures. Two-color pyrometry relates the thermal radiation from two spectral bands; once the radiation associated with the less energetic spectral band saturates, the digital numbers of the most energetic spectral band determine the measurement [69].

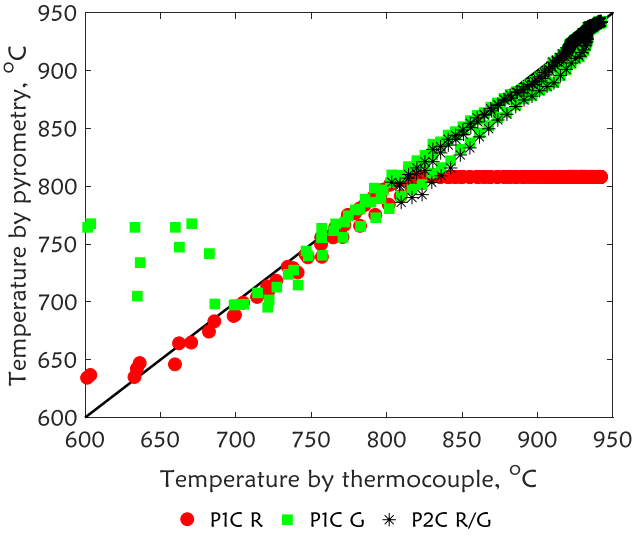

Fig. 4.4. Char particle's surface temperature by thermocouple and by one-color (P1C R and P1C G) and two-color (P2C R/G) pyrometry

4.1.2. SEQUENTIAL ONE-COLOR PYROMETRY

Fig, 4.4 shows that if the measurements by P1C R and P1C G are combined sequentially, the temperature range that can be measured and its accuracy are improved compared to the traditional simultaneous use of P2C R/G. The result is shown in Fig. 4.5, where P1C R is used until the radiation received by the red spectral band was close to saturation ($DN_r \sim 245$). After reaching this value, the algorithm calculates the temperature by P1C G. Note that while P2C

R/G uses the information from thermal radiation contained in different colors simultaneously, the algorithm proposed here (P1C RG) employs this information in a sequential way according to the digital numbers.

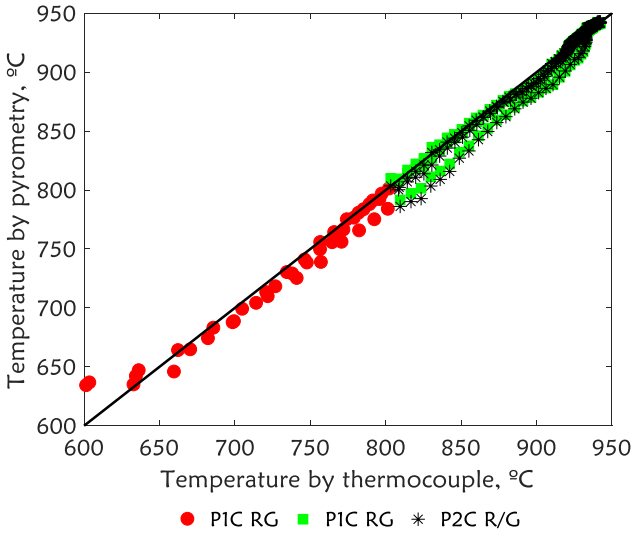

Fig. 4.5. Char particle's surface temperature by thermocouple and by pyrometry using the red and green spectral band sequentially (one-color pyrometry, P1C RG) or simultaneously (two-color pyrometry, P2C R/G)

As shown Fig. 4.5, within the most interesting temperature range for char particle combustion in a fluidized bed (800-950) ˚C, both methods (P1C RG and P2C R/G) are similar. However, the char particle's surface temperatures during oxy-combustion could be higher than the maximum temperature reached and measured in this work 950 ˚C. At temperatures higher than that, DN_g is saturated (saturation depends on the camera as well as on the working conditions; WD, FOV). One solution to measure even higher temperatures could be the use of the information from the blue digital numbers (P1C B). Fig. 4.6 shows the result from the blue spectral band (even when the green digital numbers are not saturated) validating the proposed solution because the blue digital numbers at this temperature were around 130 (see Fig. 4.2a), so there are still more than 100 values until saturation and higher temperature than 950 ºC can be measured. Another solution could be to use simultaneously green and blue (P2C G/B). In this way, the algorithm would change from P2C R/G to P2C G/B according to the DN_r/DN_g value. In order to avoid the reduction in the accuracy of the measurement, the change from P2C R/G to P2C G/B should be made when DN_r/DN_g is close to unity. If the change is made at higher values than that, the thermal radiation belonging to the blue spectral band is weak (see Fig. 4.2a), and the associated DN_g/DN_b value is very large and it is not reflected in $\beta_{g/b}$, as shown in a mathematical way by

$$\left(\frac{DN_g}{DN_b}\right)_1 \gg \left(\frac{DN_g}{DN_b}\right)_2 \rightarrow \ln\left(\frac{DN_g}{DN_b}\right)_1 \sim \ln\left(\frac{DN_g}{DN_b}\right)_2 \rightarrow \ln\left(\beta_{g/b}\right)_1 \sim \ln\left(\beta_{g/b}\right)_2 \quad (4.3)$$

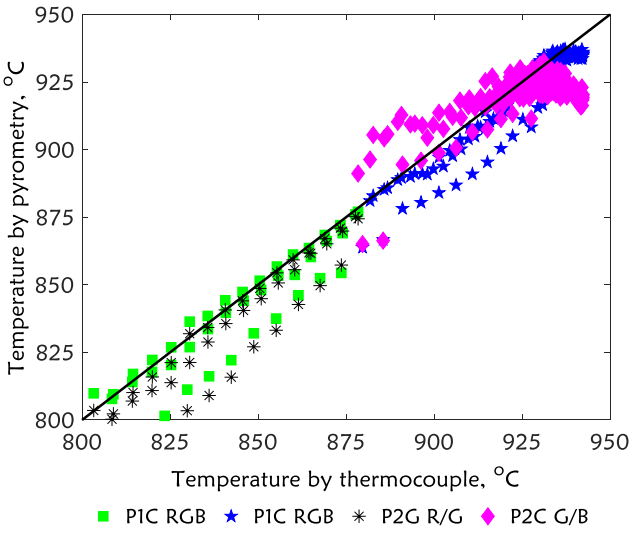

Fig. 4.6. Char particle's surface temperature by thermocouple and by pyrometry using the red, green and blue spectral band sequentially (one-color pyrometry, P1C RGB) or simultaneously (two-color pyrometry, P2C R/G)

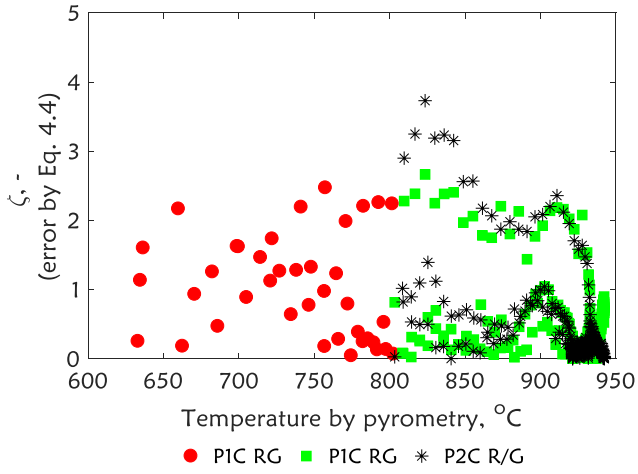

Fig. 4.7. Uncertainty of the pyrometric measurement by one-color pyrometry (P1C RG) and two-color pyrometry (P2C R/G) by Eq. 4.4

The relative error between the temperature measurements by pyrometry and the ones by thermocouple as

$$\zeta_p = 100 * \frac{\|T_{pyrometry} - T_{thermocouple}\|}{T_{thermocouple}} \tag{4.4}$$

allows analyzing the accuracy of the sequential use of the red and green spectral band proposed here (P1C RG) versus the simultaneous one that is commonly applied (P2C R/G). The result shown in Fig. 4.7 proves that P1C RG is a more reliable and accurate method for measuring the temperature of the char particle's surface than the P2C R/G.

As pointed out before, the surface emissivity has to be known to apply P1C (see § AIII.3) and the beech wood char's emissivity is assumed to be 0.85. However, the emissivity may depend on the body's temperature and the wavelength [92], and the assumption of a constant value could decrease the accuracy of the temperature calculated. From literature [32, 54, 56-58, 93, 94], it can be concluded that the char emissivity may range from 0.85 to 1 in the visible spectral band and at relevant combustion temperatures. To evaluate the effect of the emissivity assumed on the temperature measured by pyrometry, the relative error between the pyrometric temperatures assuming that the char particle's emissivity is 0.85, and the one measured by varying the emissivities from 0.85 to 1 given by

$$\zeta_{\omega}\,(\%) = 100\,\frac{\|T_{P1C}\,(\omega_c{=}0.85) - T_{P1C}\,(\omega_c)\|}{T_{P1C}\,(\omega_c{=}0.85)} \tag{4.5}$$

was calculated using 141 frames from the images of one of the validation tests. As shown in Fig. 4.8, while the differences between the two temperature measurements could be unacceptable when the char particle's surface temperatures are lower than the background (Fig. 4.8a), they are not significant when these temperature are higher than the background (Fig. 4.8b) since the reflected radiation is negligible. Therefore, a good estimation of the emissivity is needed. However, the emissivity of char is well known, and it is concluded that P1C can be used without risk.

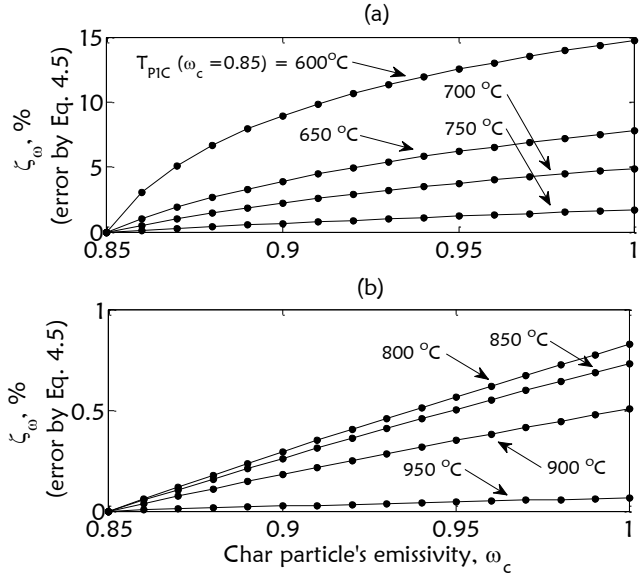

Fig. 4.8. Effect of the emissivity value on the temperature measured (P1C RG) by analyzing the change in it (by Eq. 4.5) when different emissivities values are assumed respect to the temperature measured when the emissivity is 0.85

4.1.3. Application of the One-color Pyrometry to a Single Char Particle Combustion in a FB

Once the technical development of the method is finished, the surface temperature and size of a char particle fed into the FB can be measuring during combustion. Fig. 4.9 shows a few combustion images of a single char particle in the emulsion phase, bubble phase and splash zone. Moreover, these images show that there are fractions of the char particle's surface with different brightness, which might cause by surface temperature gradient, and/or by an ash layer on the surface, and/or reaction close to it. In any case, these images prove the capability of the technique to detect details that others cannot measure, and to analyze the different steps during the combustion of solid fuel particles, such as, devolatilization, and combustion of the volatiles (flame) and char.

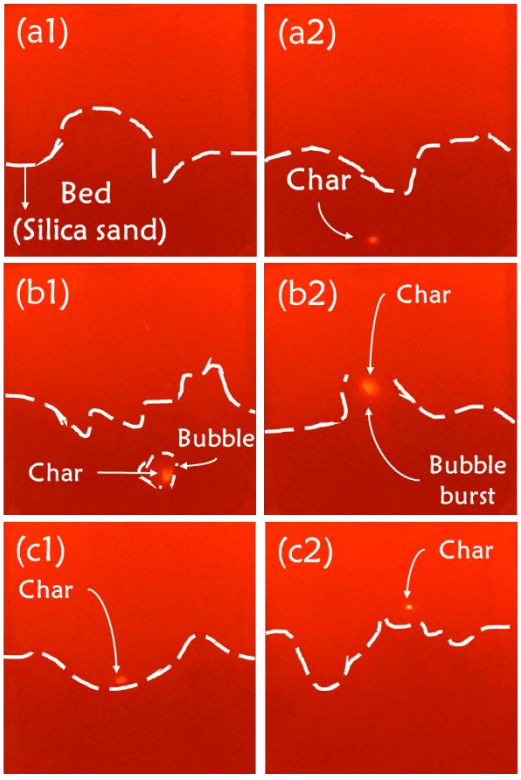

Fig. 4.9. Images of a single char particle from sub-bituminous coal in the emulsion phase (a), bubble phase (b), and splash zone (c). The dashed line is drawn to mark the bed's surface and bubbles

An example of the char particle's temperature and size measurement by analyzing combustion image is shown in Fig. 4.10 Note that for measuring the particle's size not all images are right since it is needed an image where the char particle is seen completely. The number of pixels occupied by the surface of the char particle (beech wood, $d_{c,o} \sim 8$ mm) during combustion in

the fluidized bed reactor varied approximately from 794 to 70 pixels^2 after 22 and 307 seconds of being fed onto the bed. Therefore, the sensitivity of this sizing technique can be estimated to 2.5 pixels/second, showing the capability of the method to detect and measure the events happening in a short period, such as fragmentation.

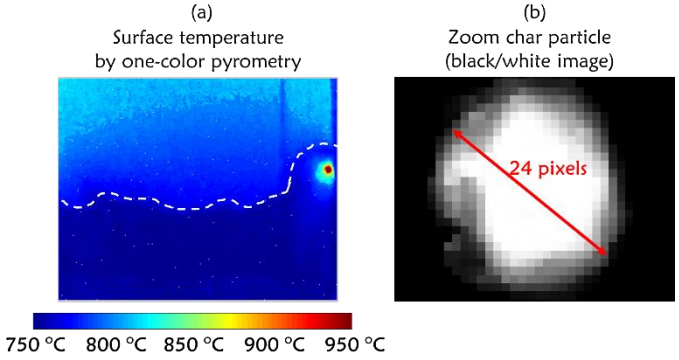

Fig. 4.10. Pyrometric temperature (a) and size (b) of a single char particle from beech wood in the bubble phase. The dashed line is drawn to mark the bed's surface

4.2. IMPACT OF USING THERMOCOUPLES ON THE CHAR PARTICLE COMBUSTION IN A FB

4.2.1. IMPACT ON THE CHAR PARTICLE'S MOVEMENT AND LOCATION IN THE BED

The images classification from the combustion tests taking into account the char particle's place in the bubbling FB shown in Fig. 3.6, allows estimating the fraction of the combustion time during which the char is in the emulsion phase, bubble phase, and splash zone. Therefore, if this classification is carried out when the char particle is fluidized with and without an embedded thermocouple (free and restricted fluidization respectively), it can be analyzed the effect of thermocouples on the char's movement through the bed. The results are shown in Fig. 4.11 for two types of chars: beech wood and sub-bituminous coal, two fluidization velocities: u_f/u_{mf} = 2 and 3, and three different sheath diameters: d_{th}= 0.25, 0.5, and 0.75 mm.

Freely-fluidized char particles (Fig. 4.11, empty symbols) are not always in the emulsion phase, but depending on the particle's density and the fluidization velocity, the fraction of time that they are out of it is longer than 15 %. When the char density increases (405 kg/m3 beech wood char vs. 1090 kg/m3 sub-bituminous char, compare Fig. 4.11a vs. Fig. 4.11b.1), the particle sinks into the bed, reducing the time of stay in the splash zone, increasing that in the emulsion and bubble phase. The longer time in the bed, arising from the higher char density, is not distributed in the same proportion in the bubble and the emulsion phases. Most likely, the drag of the bed material dominates the movement of the char particle as result of the up-ward motion of the bubbles, keeping it longer in the emulsion than in the bubble phase. At higher fluidization velocity (u_f) the porosity of the bed increases and its density is lower. The reduction of the bed density should enhance the sinking tendency of the char in the bed and so, increase the fraction of time the char is in the bed and in the bubble phase. For the sub-bituminous char at different

fluidization velocities (u_f/u_{mf} = 2 and 3), Fig. 4.11b.2 shows just an increase of 1 % of the residence time in the bubbles and a corresponding reduction in the emulsion, while the time in the splash zone remains constant. A larger change was expected, but the drag force of the bed could have a mitigating effect, as explained above. Fluidization with a thermocouple (Fig. 4.11, filled symbols) makes the char particle sink into the bed, increasing its presence in the bubble phase by more than 40 % compared to the freely fluidized particle. When there is a thermocouple attached, the presence of the particle in different places of the bubbling FB does not depend on the particle density (Fig. 4.11a vs. Fig. 4.11b.1, d_{th} = 0.25 mm). The use of thicker thermocouple sheath is seen to keep the particle longer time inside the bed, even avoiding the splash zone (Fig. 4.11b.1, d_{th} = 0.25 vs. 0.5 vs. 0.75 mm). This longer time inside the bed (because of the embedded thermocouple with thicker sheath) results to a longer time in the bubble.

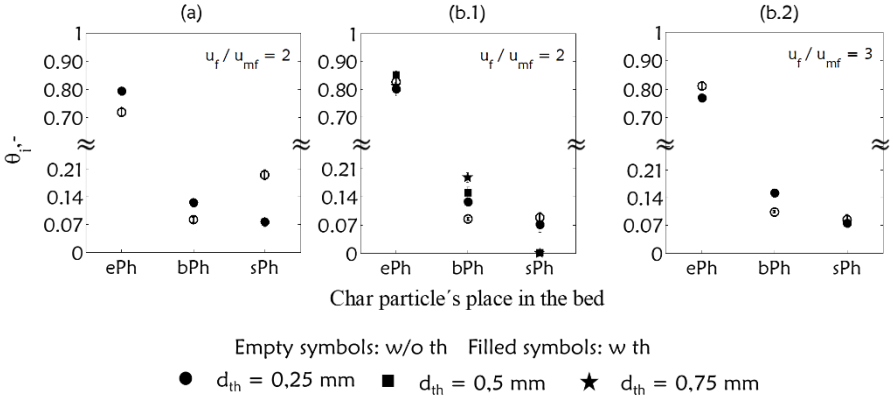

Fig. 4.11. Fractions of the combustion time by Eq. 3.3 (θ_i) during which a char particle from beech wood (a) and sub-bituminous coal (b) are in the emulsion phase (i = ePh), bubble phase (i = bPh) or splash zone (i = sPh)

As Chapter 3 explains (see § 3.2.2), these fractions are from the combustion time during which char and thermocouple are attached, that is, from the beginning of the tests until the char particles' size reach 3-4 mm. However, the particle size is reduced by combustion, and its presence in each bed phase could change. Fig. 4.12 shows the change of these fractions with respect to the size of the char particles. The size is measured by the relation mm/px from the image at the beginning of the tests and the pixel occupied by the particle during combustion (see § 3.1 and Fig. 410b). The effect of the thermocouple on the particles' location during combustion and the longer presence in the bubble phase are seen.

The results show that the thermocouple resists the drag of the bed material on the particle. The effect of this resistance on the char particles' movement (because of the thermocouple) is shown in Fig. 4.13, where a bubble reaches the char particle burst at the bed's surface. The distance traveled by the char particle, fluidized with an embedded thermocouple, is shorter (Fig. 4.12b), and obviously the thermocouple resists the impact of the bubble burst, forcing the particle to move against the push of the bed related to the collapse of the bubble.

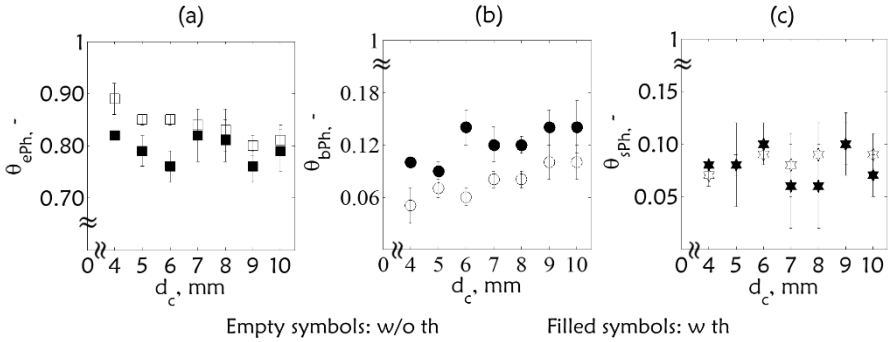

Fig. 4.12. Fraction of the combustion time during which a sub-bituminous char particle is in the emulsion phase (a), bubble phase (b) and splash zone (c) vs. its size (diameter, d_c) fluidized with (filled symbols) and without (empty symbols) an embedded thermocouple of 0.25 mm sheath diameter (u_f/u_{mf} = 2)

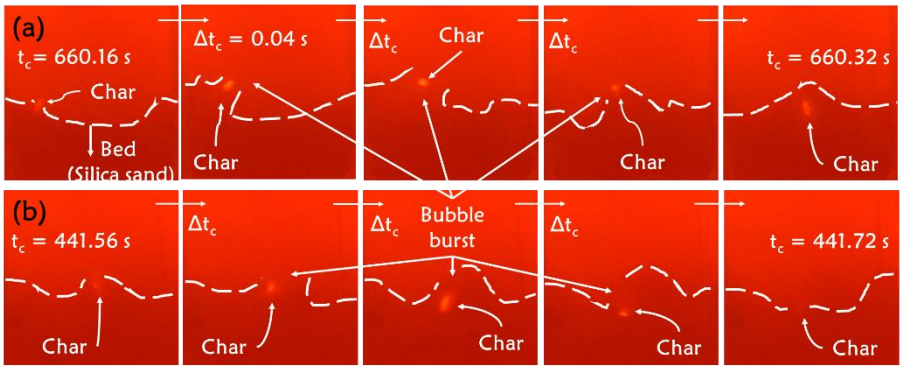

Fig. 4.13. Impact of the thermocouple on the char particle's movement: (from a sub-bituminous) fluidized without (a) and with (b) an embedded thermocouple of 0.25 mm sheath diameter (the dashed line is drawn to mark the bed's surface and the bubbles)

The location of coal/char particles out of the emulsion phase has been reported previously in literature. It was visualized the presence of coal particles (4-9 mm) in the bubbles, and on the bed surface during fluidization of alumina particles (600 μm) in a 2D FB (20 x 40 x 1.5 cm) at temperatures from 200 °C to 850 °C [82]. It was shown by examination of approximately 3000 photographs in a cold 2D FB (40 x 150 10 cm) of silica sand (420 – 590μm) fluidized with air at 0.9 and 1.3 m/s, that coarse biomass particles (cylinders with different densities), besides being in the emulsion phase, were located in the bubbles and in the splash zone [34], reporting a time outside the emulsion phase from 2 to 15 % of the total fluidization time, lower value being associated to the smaller particle size and higher density. These times are shorter than those shown in Table 3 for a biomass char particle (about 28 %), which could be explained by considering the wider reactor used in [34], where most likely a large proportion of the particles in the bubbles is not visualized. This hypothesis is in agreement with the results reported by Linjewile et al, [32], who measured the temperature of a batch of freely-fluidized coke particles

by an optical probe during combustion in sand particles (182 and 1090 μm) fluidized at two velocities (u_f/u_{mf} = 1.3 and 2), and at bed temperatures between 700 and 827 °C, noticing that the burning particles are associated with the emulsion phase for only 60 % of the time in the FB. Agarwal et al, [33] theoretically estimated a residence time in the emulsion of 80 % for the conditions conducted by La Nauze et al, [95] (size of the sand particle of 655 μm, gas velocities u_f/u_{mf} from 2 to 3.5 and bed temperatures of 700, 800 and 900 °C). The above discussion makes questionable the usual hypothesis assumed in FB models that the active particle is only converted in the emulsion phase [96], particularly if the char particle is fluidized with an embedded thermocouple.

4.2.2. Impact on the Char Particle's Surface Temperature

The effect of the thermocouple on the char particle's movement and, particularly, the increase in the residence time in the bubble phase (where the combustion temperatures are higher [32]), have consequences on char conversion that must be studied and quantified. To study this effect, sub-bituminous char particles (~10 mm, 0.56 g) were burnt with a thermocouple (w th) and without it (w/o th). The result is shown in Fig. 4.14, where the temperature in the center of the char particle measured by thermocouple (T_{th}) is compared with the surface temperatures measured by one-color pyrometry (T_{P1C}). Moreover, the burn-out time is shown.

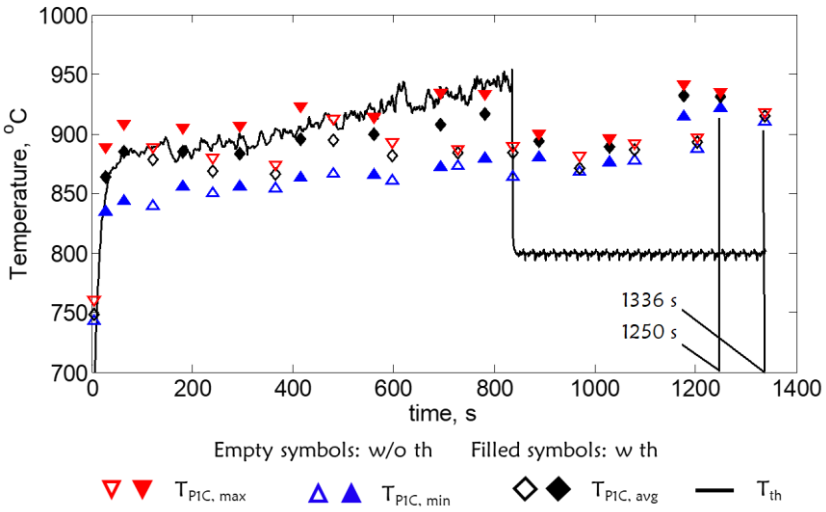

Fig. 4.14. Temperatures by thermocouple (T_{th}) and by one-color pyrometry (T_{P1C}) during combustion of two single char particles fluidized with an embedded thermocouple (d_{th} = 0.25 mm, w th) and without it (w/o th) in a fluidized bed (T_{bed} = 800 °C, u_f/u_{mf} = 2). The times indicated are the burnout time of char with (1250 s) and without (1336 s) thermocouple

The temperature recorded by the thermocouple reveals one of the main problems associated with a contact technique: the detachment of the char particle from the thermocouple. The thermocouple reads the end of combustion at 840 seconds, when the recorded temperature becomes equal to the bed temperature (T_{th} = T_{bed} = 800 °C). However, the char combustion is

far from finished, as shown by the surface temperature recorded by pyrometry. The differences between the surface temperatures measured by pyrometry when a thermocouple is embedded or not (T_{P1C} in Fig. 4.14, w th vs. w/o th) reveals that the temperature is always higher when a thermocouple is used. This difference between the two cases is more pronounced when the thermocouple is attached (t_c< 840 s). This is due to the longer time the char particle with a thermocouple spends in the bubble phase where the combustion temperature is higher because of the higher mass transfer [83]. Once the detachment char particle– thermocouple has occurred (t_c > 840 s), the difference between the surface temperatures of the char with and without a thermocouple is reduced, because the fluid-dynamic effect of the bed (quenching) is similar on both particles. However, the surface temperature of the char particle, which had a thermocouple, remains higher than that without a thermocouple, and also the end of the combustion is reached earlier: at 1250 vs. 1336 s (reduction higher than 5 % in the burnout time). A similar result has been published in [42], where a reduction of 8 % was recorded, using a thermocouple with a 0.5 mm sheath diameter. The char particle with a thermocouple attained has a higher temperature than the freely-fluidized particle, because its size is smaller due to the higher surface temperature during the time when the thermocouple was attached. This is shown in Table 4.2, where the size of both char particles is measured just after the detachment, and at the end of both combustion processes (in the last image where the char particle is seen).

Table 4.2. Char particle's sizes during combustion with an embedded thermocouple (d_{th} = 0.25 mm, w th) and without it (w/o th), at detachment time (15 min), and at the end of both combustion events (20 and 22 min)

d_P*,mm	15 min	20 min	22 min
w th	4.5	1.8	-
w/o th	5.2	2.8	1.7

*Sizing method's uncertainty: ±0.3 mm,- Complete consumption

The temperature-gradient on the char particle' surface, which ranges from $T_{P1C,max}$ to $T_{P1C,min}$ in Fig. 4.14, is larger when the char particle is attached to the thermocouple (t_c< 840 s) than on the freely fluidized char particles: 50-80 vs. 20-50 °C respectively. Once the detachment has taken place (t_c > 840 s) this difference is reduced, and the gradients fall within the same range for all particles, which is due to the higher surface temperatures caused by the longer time in the bubble phase (see Fig. 4. 11). This is proved in Fig. 4.15 where is shown the surface temperatures of the char particles with (a) an embedded thermocouple and without it (b) at some combustion times taken from Fig. 4.14. On the other hand, Fig. 4.15 points out that the higher temperatures are always in the same surface region: the one opposite to where the thermocouple is inserted. Because of the thermocouple, the char particle is not allowed to rotate freely, and the same part of the char particle's surface always faces the fluidization flux and bubbles.

4.2.3. IMPACT ON THE CHAR PARTICLE'S SURFACE CONSUMPTION

The char particle's orientation is characterized by the angle φ between the direction of insertion of the thermocouple into the char particle and the direction of the fluidization flux (from the reactor's distributor to upwards). The effect of the thermocouple on this orientation is sketched in Fig. 4.16a, where the fraction of the char particle's surface with higher temperature

is shown. The restriction of the particle's free rotation means that the same surface is always at higher temperature during the entire conversion and, as shown in Fig. 4.16b, this affects the consumption of the surface. Therefore, the reduction of the char particle's size in the perpendicular direction (⊥) relative to the insertion direction of the thermocouple should be higher than the one in the parallel direction (//). Moreover, if the char particle is attached to the thermocouple long enough, the temperature recorded by the thermocouple would attain the bed temperature (indicating the end of the combustion $T_{th} = T_{bed}$), still attached to the particle.

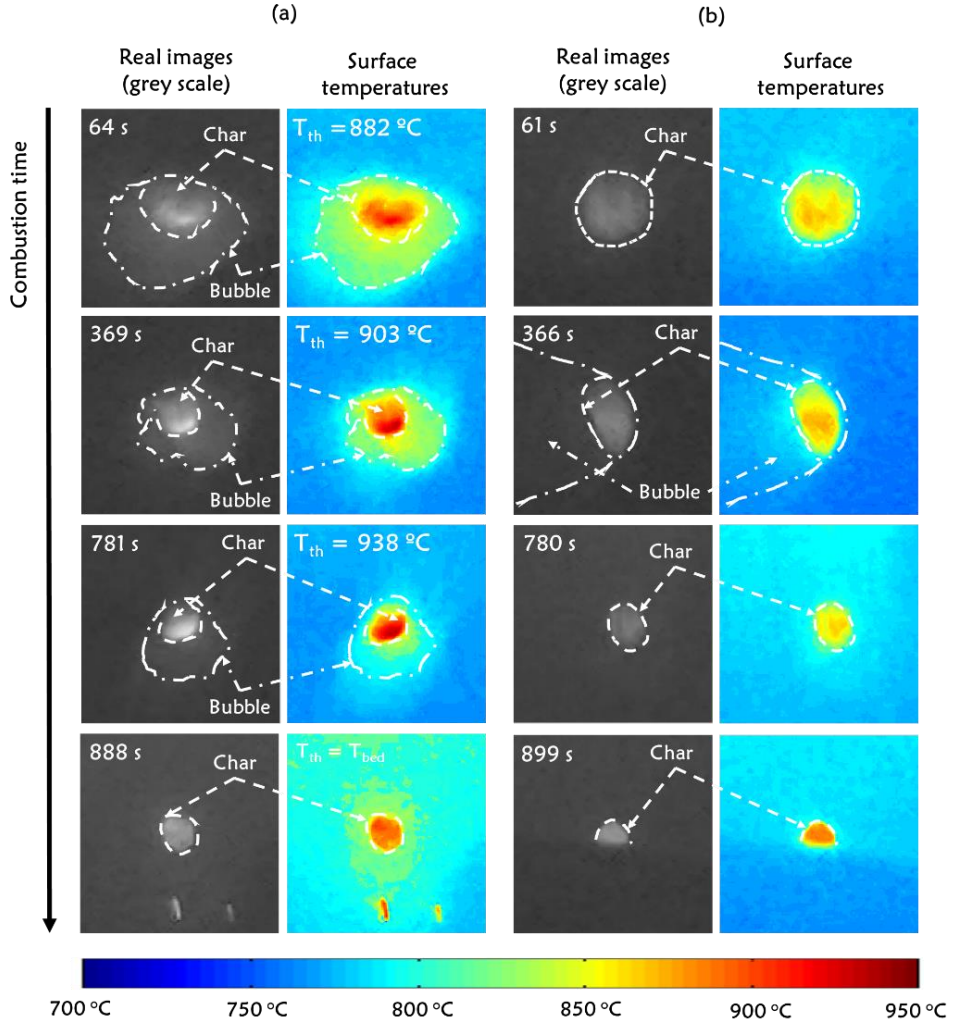

Fig. 4.15. Impact of a 0.25 mm thermocouple on the surface temperature of a sub-bituminous char particles fluidized with (a) and without (b) it (T_{bed} = 800 °C, u_f/u_{mf}= 2)

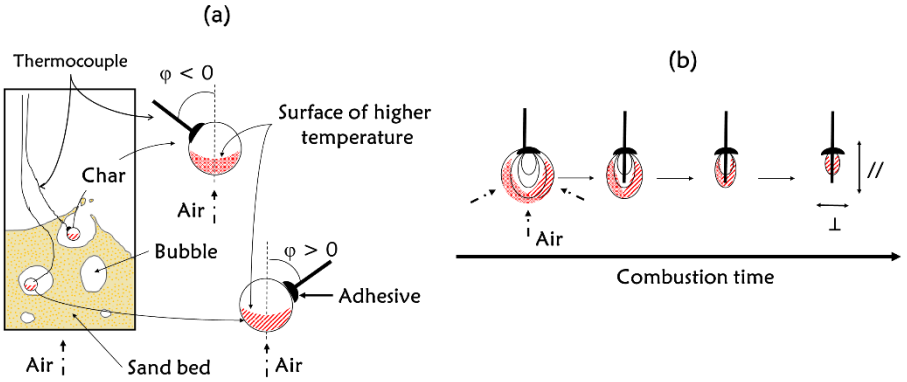

Fig. 4.16. The effect of the thermocouple on the char particle's orientation (a) and surface consumption at perpendicular (⊥) and parallel (//) direction relative to the insertion direction of the thermocouple into the char particle (b)

To prove that, char particles fluidized with an embedded thermocouple are burnt. The particles are extracted from the bed at different combustion times (t_c), and their diameters are measured in the perpendicular (⊥) and parallel (//) direction with respect to the directions of the insertion of the thermocouple. Fig. 4.17 shows the sub-bituminous (a) and bituminous (b) char particles after 12 minutes from the beginning of the combustion, and a char particle from beech wood (c) extracted after 6 minutes where the thermocouple is fixed with enough high-temperature resistant sealant to avoid the detachment at high char conversion. Moreover, the direction of the fluidization air is drawn. Higher consumption in the perpendicular direction than in the parallel one can be seen, supporting the hypothesis of non-homogeneous consumption caused of the thermocouple illustrated in Fig. 4.16b.

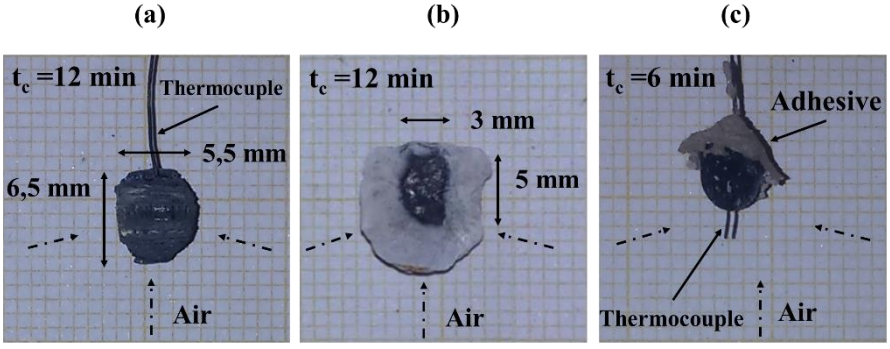

Fig. 4.17. Char from sub-bituminous (a), bituminous (b), and beech wood (c) fluidized with a 0.25 mm thermocouple, and extracted from the bed at different combustion times (t_c) (bituminous char is cut through the middle, and the direction of the fluidization air is shown)

To discard the possibility that the results obtained are affected by the rectangular geometry of the CFB 2D reactor (see Fig. 3.4), char combustion tests were carried out also in a 3D cylindrical FB reactor (see Fig. 3.5b). Char particles (from beech wood, sub-bituminous and

bituminous coal) were extracted from the reactor at various combustion times (t_c), and their diameters in the perpendicular (⊥) and parallel (//) directions with respect to that of the thermocouple insertion were measured (δ_k, by Eq. 3.4). The sheath diameter of the thermocouple was 0.25 mm. Fig. 4.18 compares these results and shows that there is a non-homogeneous surface consumption in both set-ups: FBC 2D, and FBC 3D, and therefore, it is verified that the thermocouple affects the conversion of the char. In particular, the size reduction in the perpendicular direction (⊥) is more than 10 % faster than the reduction in the parallel direction (//) in all cases.

The results shown in Fig. 4.18, involve that if the geometry of the 2D reactor is affecting to the place of the char particle and its movement through the bed, such extra restriction (the one introduced by the width of the reactor 2D) is negligible with respect to the restriction to the movement of the char particle by the embedded thermocouple, at least in the experimental conditions of this work. Although the evolution of the size of a freely-fluidized char particle was not systematically followed during conversion in this study, the shrinkage of the char is qualitatively assessed below (see Fig. 4.26) by visualizing the volume of the particle at different instants (see Fig. 4.10), verifying that the size reduction was uniform along time. These observations are in agreement with previous work [53, 97], indicating that the non-uniform consumption of the char particle reported in Fig. 4.18 is produced by the use of the embedded thermocouple.

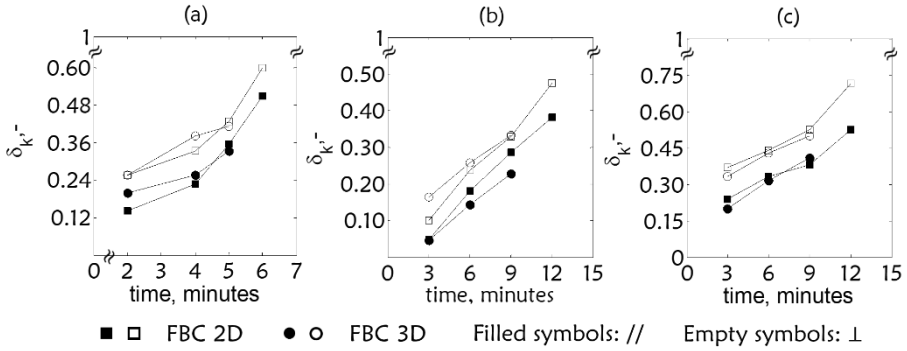

Fig. 4.18. Beech wood (a), Sub-bituminous (b), and Bituminous (c) char particle's reduction in the perpendicular (⊥) and parallel (//) directions to the thermocouple insertion at different combustion times (t_c) in the FBC 2D and 3D set-ups (0.25 mm sheath diameter)

4.3. MEASUREMENT AND THEORETICAL PREDICTION OF THE OSCILLATION IN THE CHAR PARTICLE'S TEMPERATURE IN A FB

4.3.1. EFFECT OF THE CHAR PARTICLE'S MOVEMENT THROUGH THE BED ON THE COMBUSTION TEMPERATURE

A sequence of images during 0.6 seconds from the combustion of a char particle from beech wood and its surface temperature are presented in Fig. 4.19. These images show the position of the char particle in the bed and the intermittent residence in the emulsion and bubble phases

when the char moves upward through the bed (74.60″ - 74.80″). After that, there is a period in the splash zone (74.84″ - 75.20″) where the char particle is affected by the bursting of the bubble. This bubble collapse can throw the char a few centimeters above the bed (74.84″ - 74.88″; 75.00″ - 75.08″), or cover it with sand projected (74.96″; 75.20″). The measurement of the char's surface temperature allows analyzing and quantifying its variation during the movement through the bed: higher char temperature in the bubble and/or splash zones than that in the emulsion phase (74.68″ vs. 74.7″; 75.16″ - 75.20″) and temperature oscillation of tens of degrees in periods shorter than eight hundredths of a second (74.64″ vs. 74.68″ vs. 74.72″).

Since these tests concern a single char particle, there is no difference in the O_2 concentration in the emulsion phase, bubble phase, and splash zone. Therefore, the temperature variations are due to the different heat and mass transfer from/to the char particle depending on its position in the bed: the mass transfer is decreased when the particle is immersed in the bed of particles where the heat transfer rises [55]. The heat generated at the char's surface could also change with the char position in the bed, because the sand particles of the bed inhibit the CO oxidation to CO_2 [42], but this is not considered the main reason for the measured temperature oscillations. If this happened, the measured temperature variations would be higher (317 kJ/mol for $C + O_2 \rightarrow CO_2$ vs. 133 kJ/mol for $C + O_2 \rightarrow 2CO$, @ T_c = 800 °C), and it can be seen in Fig. 4.19 that the char particle is surrounded by a cloud of sand particles.

After applying the analysis discussed above describing the time intervals during which the char particle changes its location in the bed, emulsion phase (ePh) ↔ bubble phase (bPh) ↔ splash zone (sph), the surface temperature oscillations during the entire conversion can be quantified. Fig. 4.20 shows these oscillations from the conversion of char particles from beech wood (a) and sub-bituminous coal (b) (O_2/N_2, at an O_2 concentration of 11 and 21 $\%_{v/v}$), where the length of the time intervals analyzed was shorter than 0.4 seconds. The figure bars show the temperature range measured for particles of the same size and in the same phase hundredths of second before, or after changing their place in the bed. Therefore, it is concluded that the temperatures are more stable when the particle is in the emulsion phase than in the bubble and/or splash zone. This result, which has already been pointed out elsewhere [32], is due to the stronger heat convective transfer by the sand particles in the bed, making the temperature of char staying in the emulsion phase uniform, as well as to the different conditions for convective mass transfer to a char particle outside of the emulsion phase. Note that the gas velocity surrounded the particle, u_g, is different if the char is reached by a bursting bubble at the bed's surface, $u_g >> u_{mf}$ (74.80″ in Fig. 4.19), or if it is on the bed's surface, $u_g = u_f$ (75.12″ in Fig. 4.19), or inside a bubble, $u_g = u_{th}$ (74.68″ in Fig. 4.19). On the other hand, Fig. 4.20 shows that the temperature oscillations as result of changing the location of the char in the bed, i.e. the difference in the char temperatures in different phases, vary from 10 to 100 °C. The amplitude of these oscillations increases with higher O_2 concentration and smaller char particle's size because external mass transfer controls the char consumption and these changes increase the O_2 molar flux to the char surface.

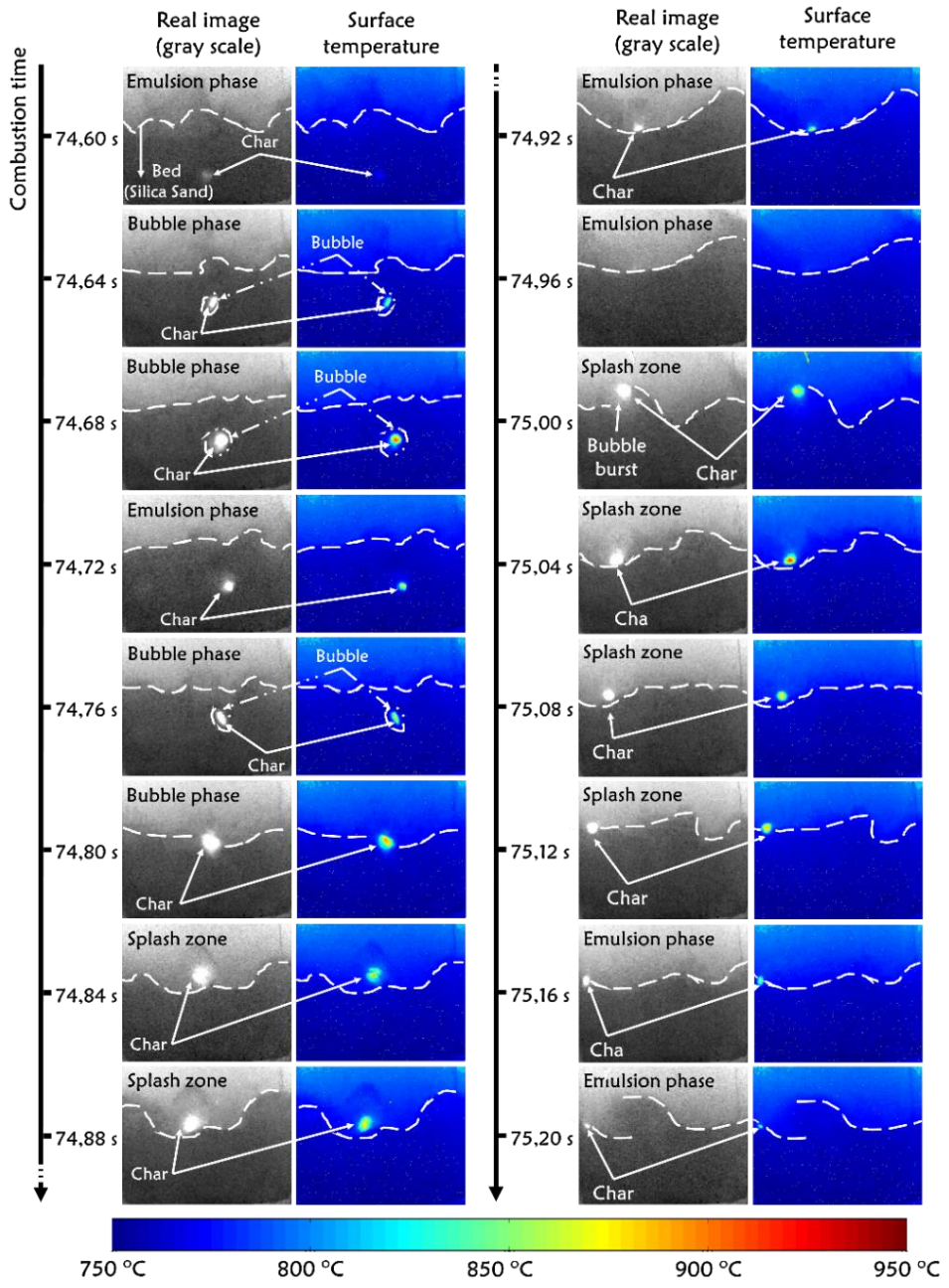

Fig. 4.19. Image (grey scale) sequences of 0.6 seconds from combustion of beech wood char in fluidized bed (T_{bed} = 800 ºC, u_f/u_{mf} = 2, 21%$_v$ O_2 in N_2) and its surface temperature by one-color pyrometry with digital camera (the dashed line is drawn to mark the bed's surface and bubbles)

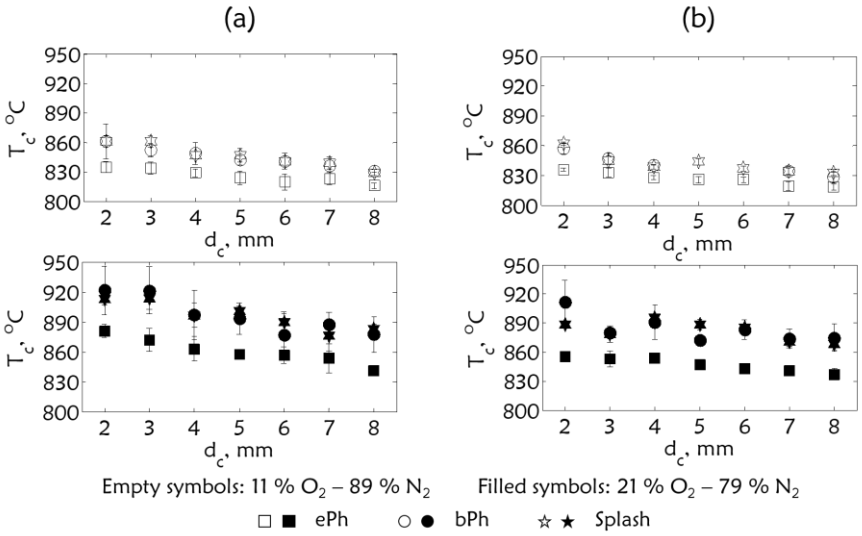

Fig. 4.20. Surfacetemperatures of char from beech wood (a) and sub-bituminous coal (b) in the emulsion phase (ePh), bubble phase (bPh), and splash zone (sPh) during combustion at 11 $\%_{v/v}$ (empty symbols) and 21 $\%_{v/v}$ (filled symbols) O_2 concentration in N_2 in a bed at 800 °C

As discussed in Chapter 1 (see § 1.2), there are publications showing temperature oscillations during coal/char combustion [32, 35, 56, 58], some of them are even associated to different char positions in the bed (emulsion or bubble phase) [32, 35]. However, those oscillations were recorded by thermocouple and are slower than the ones presented here; that is, the time from the minimum to the maximum temperature in an oscillation is longer than that shown in Fig. 4.19: seconds vs. hundredths of a second. It is possible that a thermocouple records the effect of a complete cycle of char particle's movement on the combustion temperature (see Fig. 2.2a). Therefore, the maximum temperatures would be from the time when the char particle is on the bed surface, or close to that (at the highest location of the movement shown in Fig. 2.2a) and the minimum one would be from the moment when the particle is close to the lowest point of its downward motion through the emulsion phase. On the other hand, the results from pyrometry with an optical probe show different combustion temperatures because of the intermittent char residence in the bubble and emulsion phases, and the size distribution of the char/coal particle in the bed. Although it is difficult and uncertain to estimate the particle size by pyrometry with optical probe [57], results related to the maximum particle size of 1 mm reveal a temperature oscillation of 100 °C [56].

4.3.2. Prediction of the Oscillation in the Char Particle's Temperature

The combustion model needs the implementation of the char particle's movement through the bed (see § 3.2.2). This movement is characterized using the fractions of the combustion time during which the particle is in each bed phases (see Fig. 4.12), whose sizes range from 10 mm to 1 mm. The fractions is related to the char particle's size by Eq. 3.5 whose fitting coefficients values are in Table 4.3. Using these fitting lines, along with the estimations of the bubble velocity and

the upward char velocity, the cycle time (T) and the time spends for a char particle with a given size in each bed phases (see Eq. AI.1) are calculated. These cycles for char particles from beech wood (a) and sub-bituminous coal (b) are shown in Fig. 4.21. Note that the period increases slightly as the char size decreases, which is due to the increase in the residence time in the emulsion phase as consequence of lower velocity of the descending char (Eq. AI.10, Appendix I).

Table 4.3. Fitting coefficients in Eq. 3.5

	Beech wood char	Sub-bituminous char
m_{ePh}	- 46.26	- 15.81
n_{ePh}	1.00	$9.50 \cdot 10^{-1}$
m_{bPh}	9.81	9.75
n_{bPh}	$1.91 \cdot 10^{-2}$	0.0111
m_{sPh}	39.69	6.06
n_{sPh}	$-5.47 \cdot 10^{-2}$	$3.85 \cdot 10^{-2}$

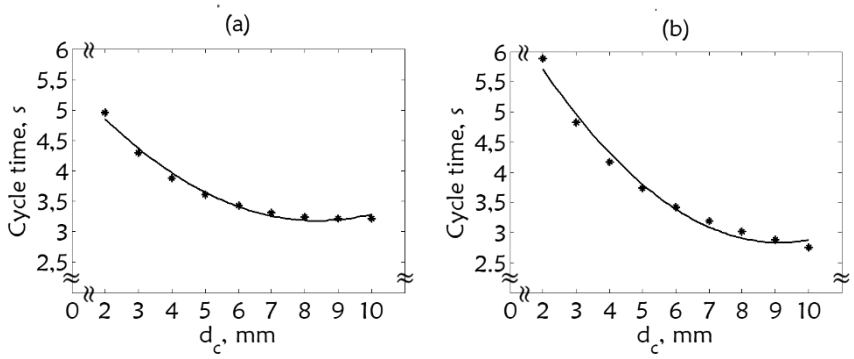

Fig. 4.21. Periods of the char particle's movement through the bed: char from beech wood (a) and sub-bituminous (b)

The theoretical temperature for a single char particle (from beech wood, 0.09 g) combustion in a sand bed fluidized with a mixture of O_2 and N_2 (21 $\%_{v/v}$ O_2) is shown in Fig. 4.22. The higher and lower temperatures of the oscillations are delimited by curves. The zoom from 301 to 309 seconds shows how the temperature is affected as the position of the char particle in the bed changes during two cycles. During the downward movement of the char through the emulsion phase, the combustion temperature decreases because of the weaker mass transfer and stronger heat transfer compared to those in the bubble/splash zone. Note that, if the temperature of the char is lower than the bed temperature, it increases during the first seconds after the feed. Once the particle is in the bubble phase and/or in the splash zone, the higher mass transfer increases the carbon consumption and the heat generated on the char surface makes the char temperature to increase. In this way, the maximum and minimum temperatures delimited by the curves in Fig. 4.22 meet the char temperatures at the highest and lowest point of the char cycle in the bed [43] (see Fig. 2.2). Moreover, the model result predicts lower char temperature in the emulsion phase, something that was already mentioned above (see § 4.3.1).

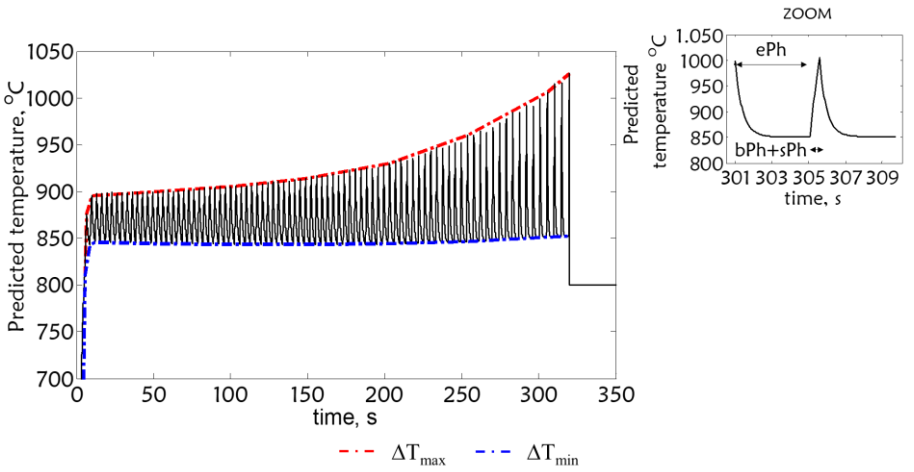

Fig. 4.22. Predicted temperature (—) of a char particle from beech wood (8 mm) during combustion in the fluidized bed described in Table 3.1, where the ΔT_{max} and ΔT_{min} curves (–·–) meet the maximum and minimum oscillation temperature. The zoom shows the time-temperature oscillation during two cycles of movement

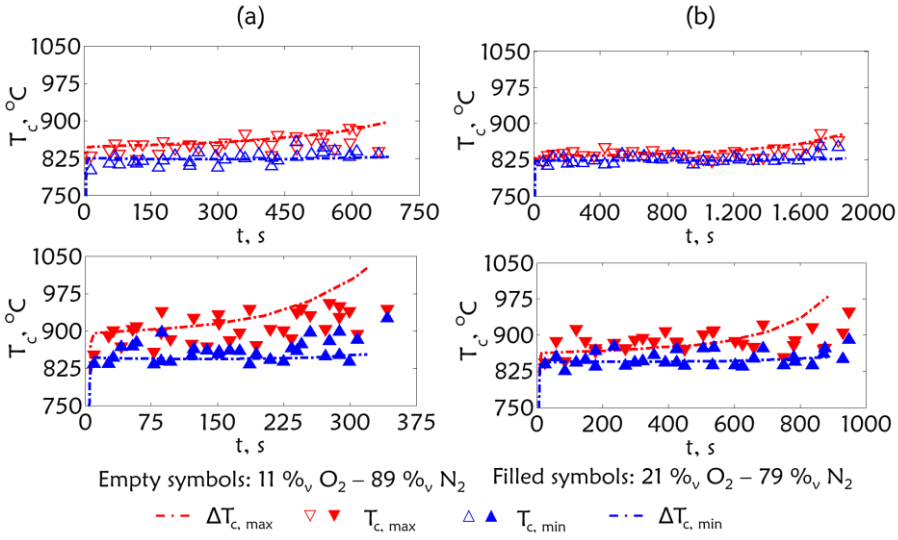

Fig. 4.23. Predicted and measured combustion temperature oscillation: ΔT_c and T_c respectively, from beech wood (a) and sub-bituminous (b) coal char particles (8 mm) at 11 $\%_{v/v}$ (empty symbols, upper diagrams) and 21 $\%_{v/v}$ (filled symbols, lower diagrams) O_2 concentration in N_2

The experimental and predicted temperature oscillations for the combustion of the char particle from beech wood (a) and sub-bituminous coal (b) are shown in Fig. 4.23, testing the model capability to explain and/or predict the experimental results. The agreement is seen from the above experimental results (Fig. 4.19 and Fig. 4.20). The theoretical analysis predicts fast

temperature changes related to the char's movement and the increase in the amplitude of the oscillation as the particle size decreases (the increase in the combustion time implies the reduction of carbonization according to Eq. 2.17) and when the O_2 concentration increases. The presented model fits the experimental results quite accurately. The results support the significance of taking into account the char particle's movement through the bed, which explain the uncertainties found in temperature and burnout times predicted in oxy-combustion processes [31]. The higher O_2 concentration in those FB reactors could increase the temperature oscillation shown here, and if the char movement is not taken into account, the errors between experimental and predicted results could be high.

4.4. THE INFLUENCE OF CO_2 GAS CONCENTRATION ON THE CHAR TEMPERATURE AND CONVERSION DURING OXY-FUEL COMBUSTION IN A FB

4.4.1. DISCUSSION OF THE EXPERIMENTAL MEASUREMENT

The apparent consumption rate (Γ_c, Eq. 3.7) and the maximum temperature ($T_{c,max}$) during conversion of single beech wood and sub-bituminous char particles with different O_2 concentration in the O_2/CO_2 fluidization flow are in Fig. 4.24 and 4.25, showing the effect of the char particle's size and the bed temperature on these experimental measurement respectively. Note in Fig. 4.24 that for sub-bituminous char particle the higher particles' size was only tested at 40 $\%_{v/v}$ of O_2. As pointed out above (see § 4.3.1) the char temperature oscillates during its combustion in a FB resulting from the change in the location of the char in the bed, so the maximum temperature presented in Figs. 4.24 and 4.25 are reached when the char is out of the emulsion phase (see Fig. 4.20).

Fig. 4.24 and 4.25 show an almost linear increase of both apparent consumption rate and maximum temperature with O_2 concentration, at least up to 40 $\%_{v/v}$ O_2 concentration and/or when the maximum char temperature is lower than 925 °C. These relations agree with those obtained using O_2/N_2 mixtures with different types of char at bed temperatures above 750 °C [53, 58, 98, 99] and also with more recent results on O_2/CO_2 mixtures at O_2 concentrations up to 40 $\%_{v/v}$ [29]. The increase in initial char's size reduces the conversion rate significantly, but it barely influences the maximum temperature (Fig. 4.24, lower part); the latter because the maximum temperature is reached at the latest stages of conversion where the size of the char is almost the same no matter the initial size [98].

Fig. 4.24 and 4.25 show an almost linear increase of both apparent consumption rate and maximum temperature with O_2 concentration, at least up to 40 $\%_{v/v}$ O_2 concentration and/or when the maximum char temperature is lower than 925 °C. These relations agree with those obtained using O_2/N_2 mixtures with different types of char at bed temperatures above 750 °C [53, 58, 98, 99] and also with more recent results on O_2/CO_2 mixtures at O_2 concentrations up to 40 $\%_{v/v}$ [29]. The increase in initial char's size reduces the conversion rate significantly, but it barely influences the maximum temperature (Fig. 4.24, lower part); the latter because the maximum temperature is reached at the latest stages of conversion where the size of the char is almost the same no matter the initial size [98].

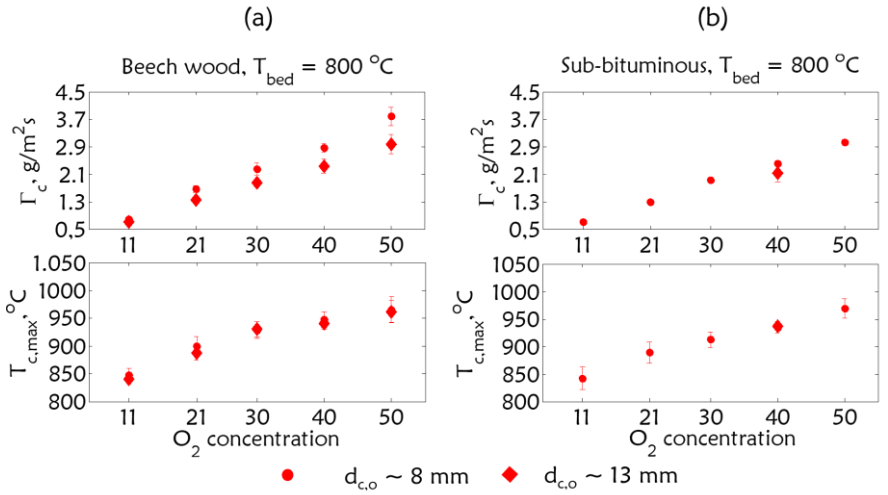

Fig. 4. 24. Effect of the initial char particle's size on the apparent conversion rate (Γ_c, Eq. 3.7) and maximum temperature ($T_{c,max}$) of char particles from beech wood (a) and sub-bituminous coal (b) as function of O_2 concentration in CO_2 at 800 °C. (Note that for sub-bituminous char particle, 13 mm was only tested at 40 $\%_v$ of O_2)

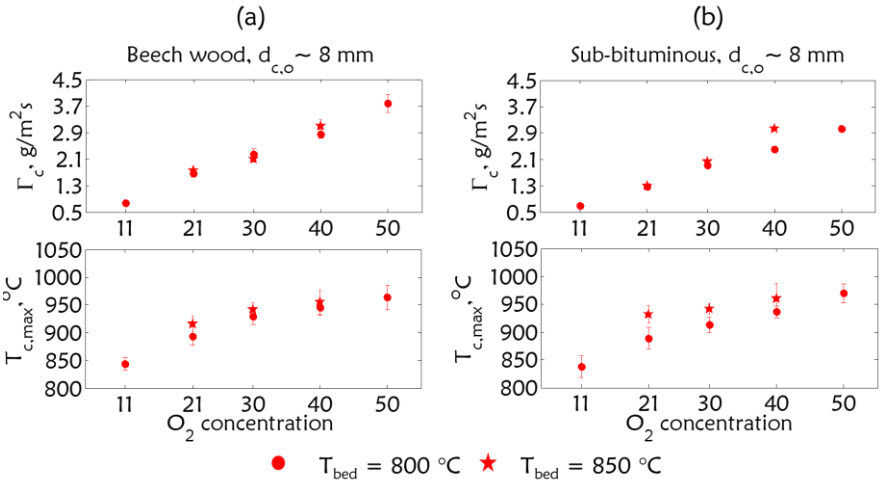

Fig. 4.25. Effect of the bed temperature on the apparent conversion rate (Γ_c, Eq. 3.6) and the maximum temperature of the char particle ($T_{c,max}$) as function of O_2 concentration in CO_2 for char from beech wood (a) and sub-bituminous coal (b) with an initial size of 8 mm

As shown Fig. 4.25, the apparent consumption rate only slightly increases with the bed temperature for O_2 concentration lower than 30 $\%_{v/v}$, but more significantly at 40 $\%_{v/v}$ (at 50 % the test was not carried out due to the possible saturation of the pixels so there is no results available). Another way to interpret the results in Fig. 4.25 is that the apparent consumption rate increases only slightly as long as the maximum char particle temperature is lower than 925

°C. This increase in the apparent consumption with the bed temperature has been theoretically pointed out by simulating the conversion of a single lignite char particle in a FB with O_2/CO_2 at 5 $\%_{v/v}$ O_2 (at this low O_2 concentration it can be assumed that the char temperature coincides with that of the bed [23]), predicting a reduction in the burnout time of about 20 % when increasing the bed temperature from 800 to 900 °C, while the O_2 diffusivity (in CO_2) was increased around 15 % [30]. On the other hand, the excess of the maximum char particle's temperature over that of the bed ($T_{c,max} - T_{bed}$), which can be seen implicitly in Fig. 4.25, decreases with the bed temperature, as also occurs in mixtures of O_2/N_2 at temperatures above 750 °C [22, 68]. The behavior of the two chars in Figs. 4.24 and 4.25 shows that the apparent consumption rate of the beech-wood char is higher than that of sub-bituminous coal. This was expected, as the reactivity of woody char is higher than that of char from coals. Overall, the results displayed are consistent with those from literature showing that the resistance to mass transport in the gas boundary-layer controls the overall rate of char conversion [22-30].

The observed behavior of the maximum char temperature at O_2 concentrations higher than 30 $\%_{v/v}$ (lower graphs in Fig. 4.24 and 4.25), as well as the increase in the apparent consumption rate with bed temperature at 40 $\%_{v/v}$ O_2 (upper graphs in Fig. 4.25), cannot be explained just by the increase in O_2 diffusivity (in CO_2) with temperature in the gas layer where the diffusion occurs (note that this temperature depends on the bed and char temperatures). To clarify this, Fig. 4.26 shows the effect of changing from O_2/N_2 to $O_2/CO2$ on the apparent consumption rate (r_c, Fig. 4.26a) and maximum temperature ($T_{c,max}$, Fig. 4.26b) as a function of O_2 concentration for the two bed temperatures and 8 mm char particles from both beech wood and sub-bituminous coal. While at a bed temperature of 800 °C the consumption rate is barely affected by changing from O_2/N_2 to O_2/CO_2, at 850 °C and an O_2 concentration higher than 30 % (for these conditions the maximum char temperature is higher than 925 °C) the apparent consumption rate in O_2/CO_2 is higher than those in the O_2/N_2 for both types of char.

The fact that similar rates measured in the two atmospheres (O_2/N_2 and O_2/CO_2) are highly remarkable since the lower diffusivity of O_2 in CO_2 than in N_2 (about 20 %, see Table 2.1). A corresponding reduction of the conversion rate could be expected, because the overall rate is controlled by the external O_2 transport, and the reduction should be roughly proportional to the diffusivity of O_2. Thus, there must be an additional carbon consumption by gasification superimposed to that of oxidation. Although char gasification with CO_2 was expected to be significant at high char temperatures, Fig. 4.26 shows that even at the lowest O_2 concentration, and at a bed temperature of 800 °C (the maximum char temperature is around 850 °C), the role of gasification is significant. The decrease in the char temperature observed in O_2/CO_2 compared to O_2/N_2 in all cases supports this fact (as the reaction is endothermic, the gasification reaction reduces the surface temperature compared to the corresponding case in O_2/N_2). It is worth noting that when O_2 is higher than 30 $\%_{v/v}$ in CO_2, the maximum temperature follows a slightly different tendency to those at lower O_2 concentration, in agreement with other experimental observations [29]. The results show that when the char surface-temperature is higher than 925 °C, the additional carbon consumption by gasification makes the overall rate higher in O_2/CO_2 than in O_2/N_2, and this additional consumption by gasification reduces the difference in burnout time in both atmospheres when the char temperature is between 850 and 900 °C. These results confirm

the significant role of gasification at high CO_2 concentration when the char temperature is higher than 850 °C.

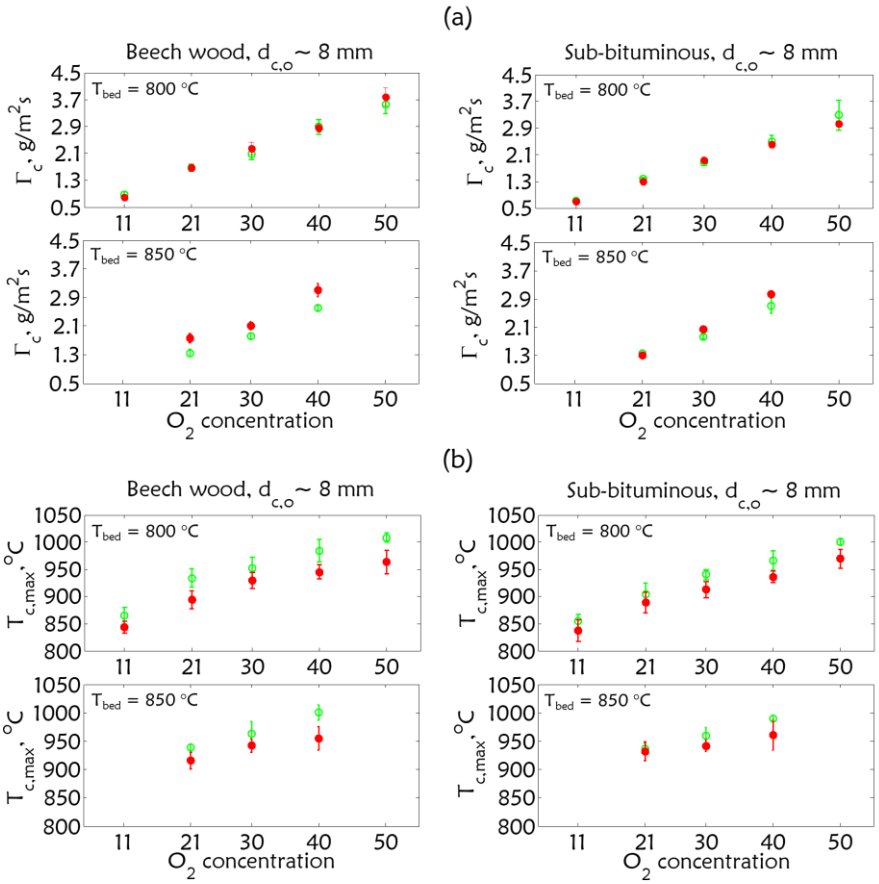

Fig. 4.26. Effect of the fluidization flow: O_2/N_2 vs. O_2/CO_2 on the apparent conversion rate (a, Γ_c by Eq. 3.6) and the maximum temperature (b, $T_{c,max}$) of char particles from sub-bituminous coal and beech wood at different O_2 concentration

This conclusions are in agreement with the results by Scala F et al., [24] who measuring the outlet CO and O_2 concentration estimated the total carbon consumption of a char particle (from bituminous coal, 6-8 mm) in a sand bed (T_{bed} = 800, 850 and 900 °C) fluidized with an O_2/CO_2 flow at 2, 5 and 15 $\%_v$ O_2 concentration. Assuming that this carbon consumption was the contributions from oxidation and gasification, they concluded that although carbon gasification was slower than oxidation, it should be taken into account. A similar conclusion could be established from the work of Roy B et al., [26] who applied the same experimental methodology as Scala F et al., [24] during the conversion of a single char particle (from Victorian Brown coal, 8-10 mm) in a sand bed at 890 °C fluidized with an O_2/CO_2 gas mixtures at 5, 10, and 15 $\%_{v/v}$ O_2 concentration. Also Bu et al. [30] calculated a contribution to overall carbon consumption of 15 % by gasification for 6 mm char from lignite at a bed temperature of 950 °C and 5 $\%_{v/v}$ O_2

(also in this case the temperature of the char surface is close to the bed temperature for the same reason as in [23]).

While the upper part of Fig. 4.27 shows the surface temperature of single sub-bituminous char particles at an O_2 concentration of 11, 21, and 40 $\%_{v/v}$ both in N_2 and in CO_2, for sequences shorter than 1 second where the location of char in the bed changes (emulsion phase ↔ bubble phase ↔ splash zones), the lower part of Fig. 4.27 presents the conversion according to Eq. 3.6. The increase in the char temperature with time (independent of the location in the bed and atmosphere) is due to the reduction of the char's size during conversion, since then the convective mass and heat transfer increase [48, 100]. Higher mass transfer increases the heat generated by oxidation, and unless the increase in the heat transfer compensates it, the temperature will increase. The contribution of the bed particles to heat transfer by convection (quenching) explains the softer increase in the temperatures of the char in the emulsion phase. In both atmospheres the differences between char temperatures outside of the emulsion phase (bubble phase/splash zone) are greater than in the emulsion phase. This is due to the different gas velocities surrounding the char in the bubble phase and splash zone as discussed above (see § 4.3.1). It should be pointed out that these differences seem to increase with the O_2 concentration.

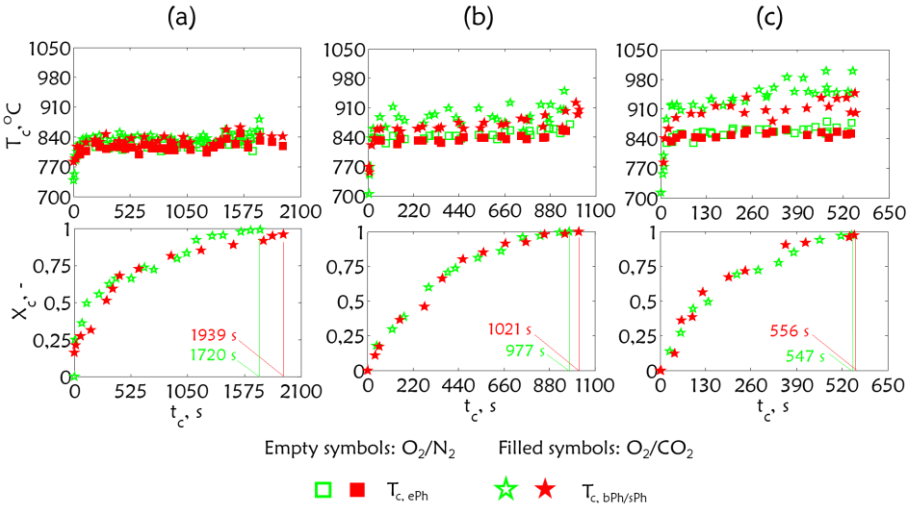

Fig. 4.27. Surface temperature (upper part) and conversion by Eq. 3.6 (lower part) of the char particle from sub-bituminous coal (8 mm, 0.28 g) in fluidized bed at 10 (a), 21 (b), and 40 % (c) in N_2 (empty symbols) or CO_2 (filled symbols)

Comparing the results between both atmospheres, Fig. 4.27 shows that the char temperatures are quite similar when the char is in the emulsion phase, but the differences are much more significant when the char particle in the bubble and/or splash zone. This is because of the increased particle convective heat-transfer in the emulsion phase, making the char temperature similar, while out of the emulsion phase, carbon consumption by oxidation is lower (lower O_2 diffusivity in CO_2 than in N_2) and also resulting for the additional carbon consumption by gasification (endothermic reaction). Moreover, the increase in the O_2 concentration of 10, 21,

and 40 $\%_{v/v}$ reduces the difference between the burnout times by 13, 5, and 2 % respectively, since the contribution from gasification to the overall carbon consumption increases. Therefore, this discussion on the experimental results shows that the difference in char temperature observed in both atmospheres is mainly controlled by the time during which the char particle is out of the emulsion phase, underlining the importance of accounting for the movement of the char particle through the different phases of the bed to understand the oxy-fuel behavior in a FB.

Although there are publications showing that the carbon consumption by gasification is not negligible at char temperatures higher than 850 °C and high CO_2 concentrations [24, 26, 30, 76], there are also experimental results differing slightly from the ones shown here. For instance, Bu et al. [28] found lower char temperatures in O_2/CO_2 in agreement with our measurements (Fig. 4.26b), but the apparent consumption rate in O_2/CO_2 was lower than that in O_2/N_2. They concluded that gasification is not negligible, but its contribution to the total carbon consumption was lower than the one found here. However, in that work the char particle was fluidized with two embedded thermocouples and it has been shown above (see § 4.2.1) that when the char particle is fluidized with an attached thermocouple, the movement of the particle and the time during which the particle is in the different bed phases changes and this restriction most likely affects the results.

4.4.2. Prediction of the Conversion Temperature and Burnout Time

It has been shown that the char particle's movement through the bed varies their temperatures and that the time during which the char is out of the emulsion phase is when occurring the bigger differences on the char conversion in O_2/CO_2 regarding the one in O_2/N_2. Therefore, the theoretical approach presented in Chapter 2 is used to study the influence of the CO_2 on the char particle's temperatures and conversion during oxy-fuel combustion in a fluidized bed. The experimental temperature from the conversion of a sub-bituminous char particle both in O_2/N_2 (a) and O_2/CO_2 (b) atmospheres at 21$\%_{v/v}$ O_2 along with the prediction of the model is shown in Fig. 4.28. The measurements (symbols) are from sequences where the char changes its position in the bed, so the surface temperatures of the char both in and out of the emulsion phase are shown (as was done in Fig. 4.27). The predicted temperatures (dotted lines) are the ones derived from solving Eqs. 2.3-2.27, assuming that the char is isothermal.

Fig. 4.28 shows the capability of the theoretical approach to describe the fast changes on the char temperature related to the movement of the char, and the increase in the amplitude of these oscillations as the size of the char decreases with conversion. As the zoom in Fig. 4.28b shows, the model calculates a decrease in the char temperature during its downward motion through the bed (see Fig. 2.2), reaching the minimum temperature in each cycle. The higher temperature occurs when the particle is in the splash zone (after its upward motion through the bed, see Fig. 2.2). It should be noted that the predicted temperature oscillation (differences between the maximum and minimum temperature of the char particle in each cycle) for the single char particle air-combustion (O_2/N_2, Fig. 4.28a) are higher than those for the single char particle during oxy-combustion (O_2/CO_2, Fig. 4.28b), in agreement with the experimental observations in the upper part of Fig. 4.27. Moreover, the lower predicted char temperature in oxy-combustion also agrees with the experimental results. The burnout time is well predicted, it is just slightly over-predicted,

which could be due to the estimation of a faster carbon consumption by oxidation at the end of the conversion.

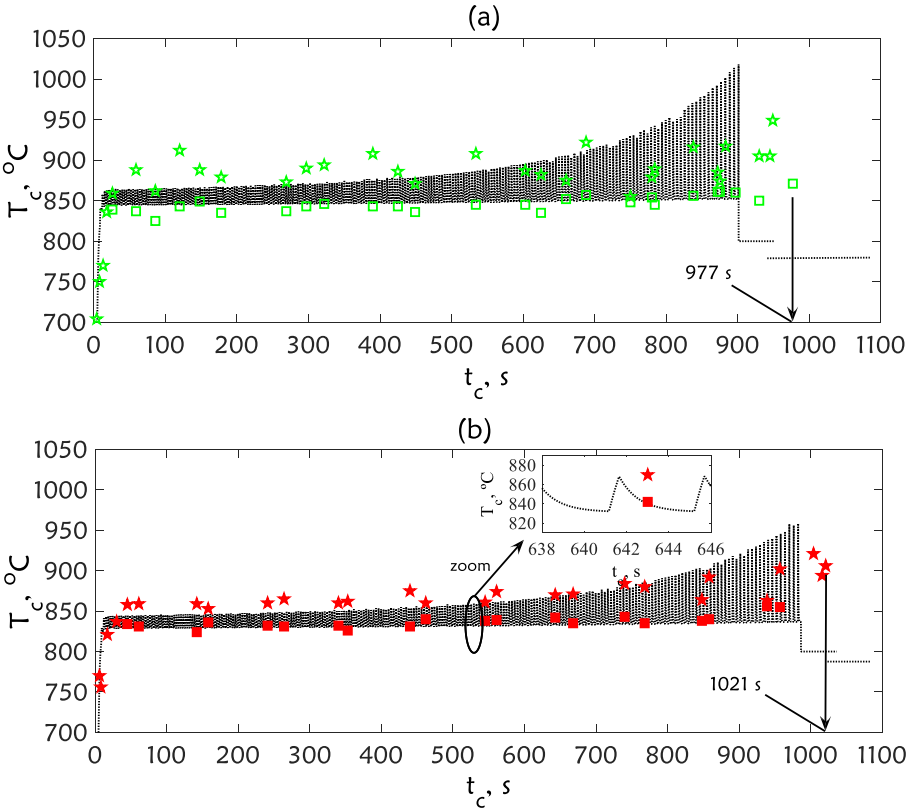

Fig. 4.28. Predicted temperature (T_c) of the single char particle conversion (from sub-bituminous coal, $d_{c,o}$ = 8 mm) in the sand bed described in Table 3.1 with an O_2/CO_2 fluidization flow at 21%$_{v/v}$ O_2 concentration

The comparison of some experimental results from literature: maximum combustion temperature (a) and burnout times (b) versus the model's predictions are in Fig. 4.29. The results predicted are from different bed-particle sizes and temperatures, type of carbon/char particles and sizes, O_2 concentrations in N_2 and CO_2, and fluidization velocities. Moreover, they were measured by different techniques, such as thermocouples, pyrometer with optical probe or digital camera, photographs, and visual analysis. The main experimental conditions of these works are in Table 4.4. The predictions of results from investigations using thermocouples were carried out until the particle reaches the size of 2-3 mm, given that this is the maximum size whose temperature can be recorded using thermocouples (see § 4.2).

The present model fits the experimental results quite accurately, improving the predictions given by some authors [30]. The maximum temperature (Fig. 4.29a) seems to be over-predicted since most of the points are close to the +15 % line. This could be a consequence of an over-estimation of the carbon consumption by oxidation. It should be pointed out that the measured

temperatures from the present work, whose predictions show uncertainties greater than 15 %, are from beech-wood char at 50 $\%_{v/v}$ O_2 concentration. In those tests, the char particle reached the maximum temperature measurable by the method used (1020 ºC, see Fig. 4.2a), and possibly it is higher. The results support the significance of taking into account the movement of the char through the bed, which could be an explanation of the uncertainties found in literature related to the prediction of temperature and burnout times in oxy-combustion [31].

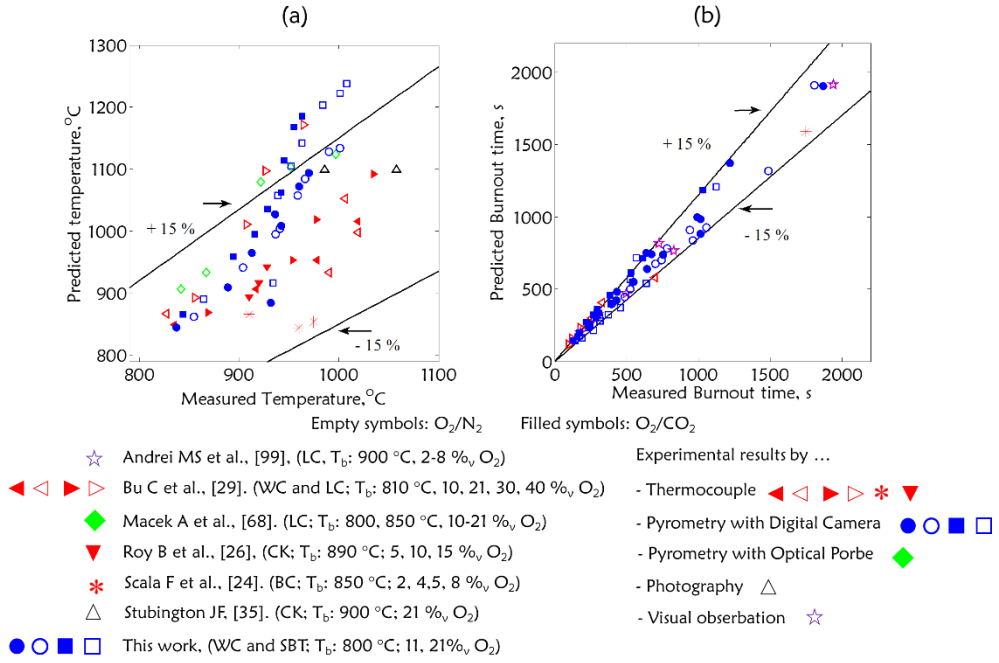

Fig. 4.29. Comparison of the maximum combustion temperatures (a) and burnout times (b) from published experimental work (see Table 3.2) versus model predictions. The lines show ± 15% deviations in the estimation

Table 4.4. Observations and experimental conditions from works where the char particles conversion in FB are addressed

Ref.	FB	Fuel	Conditions studied	Techniques	Measurement
Andrei MA et al., [99]	Silica sand, d_i: 0.2 mm u_{mf}: 0.02 m/s h_{mf}: 0.12 m	LC	O2-N2, [O2]: 2, 5, 8 $\%_v$ T_{bed}: 750, 900 °C u_f/u_{mf}: 3.2 Batch, d_c: 1.8, 3 mm	Photography Char particle weighing	Burn-out time
Bu C et al., [29]	Silica sand, d_i: 0.3-0.5 mm u_{mf}: 0.19 m/s h_{mf}: 0.15 m	AC BC LC SBC WC	O2-N2 vs. O2-CO2, [O2]: 10–40 $\%_v$ T_{bed}: 810 °C u_f/u_{mf}: 1.8 d_c: 6 mm	Thermocouple, 2 x d_{th}: 0.25 mm CCD camera	Char particle's temperature and burnout time
Macek A et al., [68]	Silica sand d_i: 1.6 mm u_{mf}: 0.8 m/s h_{mf}: 0.9 m	LC	O2-N2, [O2]: 12.5-23 $\%_v$ T_{bed}: 780-880 °C u_f/u_{mf}: 1.6 Batch, d_c: 3.7 mm	Two-color pyrometry by optical probe Flue gas analyzer	Char particle's temperature
Roy B et al., [26]	Quartz sand d_i: 0.13 mm U_{mf}: 0.05m/s h_{mf}: 0.1 m	BrC	O2-N2 vs. O2-CO2, O2]: 5–15 $\%_v$ T_{bed}: 890 °C u_f/u_{mf}: 1.4 d_c: 8-10 mm	Thermocouple, d_{th}: 0.5 mm Flue gas analyzer	Char particle's temperature and consumption rate
Scala F et al., [24]	Silica sand d_i: 0.55 mm U_{mf}: 0.13 m/s h_{mf}: 0.1 m	BC	O_2/N_2 (air) T_{bed}: 850 ºC u_f/u_{mf}: 2.3 d_c: 6-7 mm	Thermocouple, d_{th}: 0.5 mm Flue gas analyzer	Char particle's temperature and consumption rate
Stubintong JF, [35]	Silica sand d_i: 0.46 mm u_{mf}: 0.08 m/s h_{mf}: 0.23, 0.27 m	CK	O_2/N_2 (air) T_{bed}: 900 ºC u_f/u_{mf}:1.7, 1.3 Batch, d_c: 2.5-5 mm	Photography Thermocouple	Char particle's temperature

AC: Antracite Coal, BC: Bituminous Coal, BrC: Brown Coal, CK: Coke, LC: Lignite Coal, SBC: Sub-bituminous Coal, WC: Wood Char

CHAPTER 5. CONCLUSIONS

Oxy-fuel combustion in a fluidized bed (FB) is an interesting technology with high potential for reducing CO_2 emissions. In spite of all international groups working on this field and the number of pilot plants constructed and fundamental researches published, there are still a number of challenges to face before safe design of a 2nd generation FB oxy-boilers. Among these questions are clarifying the impact of changing from O_2/N_2 (air-firing conditions) to O_2/CO_2 (oxy-firing conditions) atmosphere on the conversion of coarse char particles. Moreover, the high O_2 concentration in the fluidization agent could produce unacceptable temperature levels both globally on the reactor and locally in a fuel particle.

In this work, the latter issue was investigated. A 2D FB device equipped with a quartz window at the bottom and freeboard was designed and coupled with a digital camera, allowing optical measurements of single char particle during conversion. Four main tasks were carried out to answer the most relevant questions related with the increase of char temperature under oxy-fuel conversion in 2nd generation oxyboilers (conversion in O_2/CO_2 gas atmosphere at high O_2 concentration):

- **In the first task** a method to measure the char particle's temperatures and sizes by pyrometry with a digital camera is developed, based on the sequential use of the thermal radiation belonging to the red, green and blue spectral bands (colors).
- **In the second task** the impact of using thermocouples on the char particle conversion was addressed. The main driving force for this investigation is to set clear whether the use of a thermocouple(s) attached to the coal/char particle to measure its temperature in a FB during conversion affects or not the accuracy of the measurement. Although it has been assumed up to now that the temperature of the char with an embedded thermocouple is similar to that of a freely fluidized char, it has shown by dedicated measurements that the thermocouple does influence the free movement of the char throughout different bed phases/zones and this considerably affects the rate of char conversion and therefore its temperature history during combustion.
- **In the third task** the effect of the char particle's movement through the bed (emulsion phase, bubble phase, and splash zone) on its combustion temperature was studied. These temperatures are also predicted by a model, which is developed taking into account the different locations at which the char particle stays in the bed during conversion. Comparison of interpretation of model outputs together with experimental measurements allowed a better understanding of the temperature variations.

- **In the fourth task** both the measurement technique and a theoretical model developed to predict single char particle conversion in a FB under oxy-firing conditions (taking into account heterogeneous reactions of char with O_2 and CO_2) was sued to investigate the influence of a high O_2 concentration in CO_2 on the rate of char conversion and temperature profile along the time.

5.1. SUMMARY OF CONTRIBUTIONS FROM THIS WORK

5.1.1. ONE-COLOR PYROMETRY WITH A DIGITAL CAMERA

To develop a measurement technique of temperatures by pyrometry with a digital camera, it was carried out combustion tests of single char particles from beech wood inside of an electric oven. The temperature of the oven was set at 800 °C or 850 °C, and the O_2 concentration ranged from 0 to 50 $\%_{v/v}$ in N_2.

1. A method that use the thermal radiation belonging to the visible spectral bands red, green, and blue in a sequential way is proposed (one-color pyrometry, P1C), in contrast with the traditional method based on the simultaneous use of two bands (two-color pyrometry, P2C). The color is selected automatically according to the intensity of the radiation reaching the digital camera,
2. For the optical and electronic configuration of the digital camera used in this work, the red color is used to measure char particle's temperature from 600 to 800 °C, the green color for the range of 800-925 °C, and the blue color for temperatures from 925 to 1020 °C.
3. P1C allows measuring the char particle's surface temperature below the background (sand bed and reactor's wall), overcoming the limitation of the traditional P2C, where only temperatures higher than that (800 and 850 °C, typical in a FB combustion) can be measured.
4. The method allows visualizing further conversion details, such as char particles' surface temperature gradient and size during combustion.
5. The apparent limitation of P1C, which is that the char's emissivity has to be known, was shown to be a minor inconvenience since the error caused by a guess between 0.85 and 1 is lower than 1%, provided that the temperature to be measured is higher than that of the bed (background). When the temperature is lower than the bed, the error can be higher and careful determination of the emissivity is required.

IMPACT OF USING THERMOCOUPLES ON THE CHAR PARTICLE COMBUSTION IN A FLUIDIZED BED

The effect of an embedded thermocouple on the char conversion was addressed by analyzing combustion (O_2/N_2) tests of single char particles from beech wood, and bituminous and sub-bituminous coal. These particles were fluidized either with an embedded thermocouple or without it, in a sand bed at 800 °C using air as fluidization agent.

6. The images analysis of the burning char in a 2D FB shows that a freely-fluidized char particle is not always in the emulsion phase, questioning one of the main assumptions in modeling of a bubbling FB. Depending on the density of the char particle and the fluidization velocity,

the presence of char particles in the bubble phase ranges between 8 % and 10 %, and light particles (wood char) spend more time on the surface of the bed.

7. The thermocouple resists the drag of the bed, increasing the time that the char particle stays in the bubble phase compared to the case without thermocouple. This increase is stronger with the thickness of the sheath thermocouple: more than 40 %, 60 %, and 100 % for 0.25, 0.5, and 0.75 mm of sheath diameter respectively.
8. The longer time in the bubble phase results in higher combustion temperatures, reducing the char's burnout time by around 5 % for an embedded thermocouple of 0.25 mm sheath diameter.
9. The char particle's free rotation is restricted by the thermocouple, and the same parts of their surface always attain higher temperature. This results in a non-homogeneous surface consumption: the reduction of the char particle's size perpendicular to the direction of the insertion of the thermocouple is more than 10 % faster than the reduction in the parallel direction. This non-homogeneous size reduction of the char particle was also obtained by measurements in a 3D FB combustor.
10. The use of thermocouples is contestable if accurate char temperature's measurements are aimed, since the temperature and consumption of the char surface are affected. Although the method can be used by keeping these deviations in mind, its effect on the char particle conversion could be higher if more than one thermocouple is used, or a thicker sheath diameter, and/or the O_2 concentration around the char particle is different from the one used here (air).

5.1.3. OSCILLATION IN THE CHAR PARTICLE'S TEMPERATURE IN A FLUIDIZED BED

The effect of the char particle's movement through the bed on the combustion temperature is experimentally and theoretically studied by combustion tests with single char particles from beech wood and sub-bituminous coal in the 2D fluidized-bed reactor at a constant temperature (800 °C) and for two O_2 concentration (11 and 21%$_{v/v}$) in N_2.

11. The images analysis by pyrometry detects variations in the temperature of the char particle's surface of tens of degrees as consequence of its movement through the bed. The temperatures oscillations take place in hundredths of second after the char changes its location in the bed. The amplitude of these oscillations increases with O_2 concentration, while it is lower for larger char size (external mass transfer controls the char consumption).
12. It is proven that char particle's temperatures is more stable (differences between temperatures of the char in the same phase of the bed and with the same size) when it stays in the emulsion phase than when it is located in the bubble phase or splash zone.
13. The results explain the scattered temperatures from investigations using pyrometry by optical probes, since that technique measures particles' temperatures with different sizes that are both in the emulsion phase and in the bubble phase. Moreover, the present work can explain the combustion temperatures measured by thermocouples showing similar temperature oscillations as the ones registered here: tens of degrees, despite their larger time constants. Since this longer time is, as long as the time needed to the char particle to complete one cycle of circulation through the bed, the maximum and minimum

temperatures reached could be those of the particle at the highest and lowest points of the cycle.

14. Predictions of the experimental results by the combustion model (proposed by Biggs et al. [43] and completed in the present work by experimental characterization of the char particle's movement) shows the capability of ta FB combustion model to describe the temperature oscillation during combustion measured in this work.

5.1.4. The Influence of CO_2 Gas Concentration on the Char Temperature and Conversion during Oxy-Fuel Combustion in a Fluidized Bed

It has been experimentally and theoretically analyzed the CO_2 effect on the temperatures and conversion of the char particle from beech wood and sub-bituminous coal in the 2D fluidized-bed reactor with different bed temperature and O_2 concentration in N_2 and CO_2 as fluidization flow.

15. The analysis of the digital images from these tests has shown that the mass transfer from the bulk gas in the bed phases to the char controls the char particle conversion in the O_2/CO_2 atmosphere.
16. Gasification contributes to char conversion even at a bed temperature of 800 °C provided the O_2 concentration is high enough, corresponding to a char temperature higher than 850 °C. This makes the apparent char consumption rate roughly equal in both O_2/N_2 and O_2/CO_2 for char temperatures between 850 and 925 °C, and higher in O_2/CO_2 than in O_2/N_2 for char temperatures higher than 925 °C
17. The main differences on the carbon consumption and temperatures recorded are from the time during which the char particles is out of the emulsion phase (shorter than 25 % of the fluidization time).
18. Taking into account the char particle's movement through the bed as an input of the theoretical model of the char particle conversion in fluidized bed reactors results in an important improvement to describe the effect of the O_2/CO_2 atmosphere on the char particle conversion.
19. The model developed gave good predictions of temperatures and burnout times measured in this work and also compared well with measurements from others sources, giving uncertainties smaller than 15 %.

5.2. Limitations of the Results and further Researches

Various aspects of the experimental devices and configuration used in this work, as well as results, deserve discussion, pointing out their weaknesses and how they can be improved by future research.

5.2.1. Measurements by One-Color Pyrometry

The maximum temperature measured with the new pyrometric technique was 1020 °C, which limited the analysis to operating conditions (mainly the bed temperature and O_2 concentration) where the char particle's temperature is below 1020 °C. The actual temperature range measured in this work (600 - 1020 °C) is a function of the set-up's optical and electronic configuration (experimental calibration of the digital device). A filter that attenuates the thermal radiation

before reaching the sensor would allow changing this range easily. In that way, keeping the same digital camera's working distance and field of view, the char particle's temperature (radiation) that saturated the pixel (without the filter) will not saturate it (with the filter). Obviously, the lower temperature measured here could not be measured anymore, since that with a filter that temperature (radiation) could not be detected by the sensor. Nevertheless, the char particles' temperature in oxy-combustion is much higher than that of the bed (typically between 800 and 850 °C), and if a new-calibration of the digital camera is carried out, char particle's temperatures higher than 1300 °C could be measured. This is an ongoing work.

5.2.2. 2D Fluidized Bed Reactor

One of the main criticism that could be argued is that the bi-dimensional geometry of the FB reactor could impact, to some extent, the conclusions derived in the present work. To clarify this aspect, the results from this work have been compared with those from the literature, and some tests were conducted with 3D lab-scale reactor. Full agreement was obtained and therefore, the conclusions of this works seems to be general to oxy-fuel and air-fuel combustion in fluidized bed reactors.

Another aspect to be discussed is that when the char particle is close to the window (made of quartz) the heat exchange is different to the one produced when the char is close to the metal reactor's wall. However, there is a metal box (black surface) that surrounding the reactor, and when the particle is close to the quartz window, this metal surface is located just a few centimeters, so the differences between the heat exchanges are negligible. On the other hand, the bed temperature is controlled by the thermal radiation from this black metal box (heated by the electric oven) to the reactor, so the quartz window in the bottom is at least at the same temperature than the bed. Therefore, the char particle is likely not cooled down when touching that part of the reactor during fluidization.

5.2.3. Modelling Approach for Single Particle Conversion

A shrinking particle model has been used to model the conversion of a single char particle in a FB under oxy-combustion. It could be extended to shrinking core model, where a new mass transfer resistance will be introduced since there is an ash-layer around the char core. Although there are not inconvenienced in the theoretical study, it is important to note that the experimental measurement carried out here is based on the thermal radiation emitted from the char particle's surface, whose difference with respect to the one from the background (bed and reactor's walls) allow seeing the particle. If there is an ash layer on the char's surface, it is possible that these differences between thermal radiations (the one from the particle and the one from the surrounding) involve difficulties measuring the char-ash temperature since could be much difficult to see the particle.

5.2.4. Further Research

It has been pointed out the importance of the time the char particle is in each bed phases on its conversion: temperature oscillation of tens of degrees in just hundredth of second and the lower O_2 flux to the char particle's surface when it is in the emulsion phase. Since the conditions of the emulsion phase (close to minimum fluidization velocity) are mainly a function of the

properties of the bed particles (size, density, shape, etc), it would be interesting to analyze the effect of these parameters on the oxy-fuel conversion. On the other hand, the maximum temperature that can be measured was limited to the O_2 concentration in the gas atmosphere (either in N_2 and CO_2) up to 50 $\%_{v7v}$, when the bed temperature was set at 800 °C, and up to 40 $\%_{v/v}$ when it was set at 850 °C. It would be interesting to analyze gas atmospheres with higher O_2 concentration and bed temperature since it seems that the char's temperature in oxy-combustion is not linearly related with the O_2 concentration when the temperature is higher than 950 °C. Moreover, it would be interesting to feed a batch of char particles into the bed in order to analyze if there are differences in their temperatures as a function of height of the bed. Wet recirculation of the flue gases from the exit involves H_2O concentration inside the boiler. It is expected that the increase in water vapor in the gas atmosphere increases the carbon consumption rate by gasification and reduce the char particle's temperature. However, the H_2 produce could be oxidized close to the char's surface an increase its temperature. Therefore, it will be interesting to study the conversion when the fluidization flow is a mixture of O_2, CO_2, and H_2O.

AGRADECIMIENTOS / ACKNOWLEDGEMENTS

Como personas individuales vivimos todos juntos, y por lo tanto, ni estamos, ni hacemos las cosas solos. Este trabajo no fue diferente, y durante su realización he contado con la ayuda, apoyo y consejo de familiares y amigos. Por ello, quiero dar mi más sincero agradecimiento a los que forman mis circunstancias y me acompañan siempre.

De manera explícita, quiero agradecer a Alberto Gómez Barea el haberme dado la oportunidad de investigar y de guiarme en el camino; el haberme permitido descubrir la utilidad de trabajar en una idea, aunque ésta fuese equivocada; y mostrarme que la satisfacción está en el trabajo que se realiza y no al final de él.

Agradecer a Bo Leckner, un genio con una asombrosa capacidad de escuchar, sus consejos, propuestas y correcciones, y el haberme mostrado como mejorar un trabajo manteniendo la personalidad del estudiante.

A David Fernández su afecto puro y desinteresado, prestándome su ayuda siempre que lo he necesitado.

A mis compañeros en esta "aventura doctoral", en especial a María Tripiana y Cristina López su disposición a discutir y escuchar cualquier idea. A mis compañeros "experimentales" Ana Berdugo, Eva Sánchez, y Manuel Luna su ayuda y paciencia en la preparación de las pruebas, y sobre todo su compromiso durante la realización de las mismas. A Israel Pardo su ayuda en la logística y control del material del laboratorio, si la cual ningún ensayo hubiese sido posible. También quisiera agradecer a Pedro Haro su ayuda, consejos profesionales y académicos, y sus sugerencias de socialización.

Agradecer a todos los miembros del departamento de Ingeniería Química y Ambiental su colaboración y apoyo, así como a la Universidad de Sevilla su labor en nuestra formación académica y personal.

Igualmente quisiera agradecer a mis padres Jesús y Conchi, a quienes dedico este trabajo, el amor y esfuerzo que me han dedicado durante toda mi vida; y sobre todo el haberme transmitido el coraje necesario para afrontar cualquier reto. A mis hermanos Inma y Adrián su alegría, paciencia y compañía de todos los días.

En último lugar quisiera agradecer a Leonor el ser el viento a favor en mi vida, sin el cual no hubiese podido realizar este viaje.

NOMENCLATURE

$a_{i/j}$	First coefficient of the P2C calibration curve in Eq. 4.1, -
a_k	First coefficient of the P1C calibration curve in Eq. 4.2, -
A_c	Surface area of char particle, m^2
A_c	Surface area of char particle, m^2
$A_{co/co2}$	Pre-exponencial factor for CO/CO_2 ratio, -
A_{cb}	Pre-exponencial factor for char combustion, m/Ks
A_{gf}	Pre-exponencial factor for char gasification, m/Ks
A_o	Area of multi-orifice distributor per hole, m^2
A_w	Surface area of the metal black box that surrounding the reactor, m^2
A_{wnd}	Surface area of the oven's quartz window, m^2
Ar	Archimedes number based on average inert particle diameter, -
$b_{i/j}$	Second coefficient of the P2C calibration curve in Eq. 4.1, -
b_k	Second coefficient of the P1C calibration curve in Eq. 4.2, -
$c_{i/j}$	Third coefficient of the P2C calibration curve in Eq. 4.1, -
c_k	Third coefficient of the P1C calibration curve in Eq. 4.2, -
c_p	Specific heat of char particle, J/kg K
$c_{p,i}$	Specific heat of inert particles of the bed, J/kg K
$c_{p,g}$	Specific heat of the fluidization gas, J/kg K
C	Molar concentration, mol/m^3
C_1	First Planck's constant: 3.742 10^8 $W\mu m^4/m^2$
C_2	Second Planck's constant: 1.439 10^4 $K\mu m$
C_d	Dimensionless isolated sphere drag force, -
d_c	Diameter of a char particle, m

d_i	Average diameter of the bed particles, m
d_{ij}	Binary diffusivity of compound i through j, m^2/s
$d_{p,k}$	Diameter of a char particle in the perpendicular ($k=\perp$) or parallel direction ($k=//$) relative to the insertion direction of the thermocouple into it, mm
d_{th}	Diameter of the thermocouple's sheath, mm
DN	Digital Number provided by the software of the digital camera, -
D_{ij}	Effective mass diffusivity of compound i through j in the emulsion phase: $d_{ij}\varepsilon_{mf}/\tau$ m^2/s
e	Energy emitted per unit area and wavelength, $W/m^2\mu m$
e°	Energy emitted per unit area and wavelength as black body, $W/m^2\mu m$
E	Energy emitted per unit area, W/m^2
$E_{co/co2}$	Activation energy for CO/CO_2 ratio, J/mol
E_{cb}	Activation energy for char combustion, J/mol
E_{gf}	Activation energy for char combustion, J/mol
$f_{i,j}$	View factor between surfaces i and j, -
h_{bed}	Expanded bed height, m
h_{mf}	Height of the bed at minimum fluidization velocity, m
h_p	Penetration depth of a char particle in the bed, m
j_i	Energy emitted and reflected from the char's surface (i = c), from the metal black box (i = w), and from oven's quartz window (i=wnd) per unit area and wavelength, $W/m^2\mu m$
k_{cb}	External combustion kinetics, m/s
k_{gf}	External gasification kinetics, m/s
$k_{d,ePh}$	Effective thermal conductivity of emulsion phase, W/mK
$k_{d,i}$	Thermal conductivity of bed particles, W/mK
$k_{d,g}$	Thermal conductivity of the fluidization gas, W/mK
m	Pixel of the sensor located at m row, -
	Number of minutes whose images are analyzed in Eq. 3.3, -
	Number of time that a char particle is capture by a bubble when it is ascending through the bed in a cycle in Eq. AI.5, -
m_j	Fitting coefficient in Eq. 3.5 for the particle in the emulsion (i = ePh), bubble (i = bPh), or splash zone (i = sPh) of the bed, m^{-1}
n	Pixel of the sensor located at n column, -
n_j	Fitting coefficient in Eq. 3.5 for the particle in the emulsion phase (i = ePh), bubble (i = bPh), or splash zone (i = sPh) of the bed, -

N_i	i molar flux in the gas-film around the char particle (> 0 from the fluidized phases to the char surface), mol/m²s
$N_{i,c}$	i molar flux at the external surface of the char particle (> 0 from the fluidized phases to the char surface), mol/m²s
$N^{img}_{i,j}$	Number of images where a char particle is in the emulsion phase (i = ePh), bubble phase (i = bPh), or splash zone (i = sPh) within the 250 frames from the last 10 seconds associated to the j-th minute in Eq. 3.3,-
Nu	Nusselt number based on char particle diameter, -
Pr	Prandtl number: $c_{p,g}\ \mu_g / k_{d,g}$, -
$q_{cv,g}$	Representation of the heat exchange by convection between char particle – fluidization gas in Fig. 2.2
$q_{cv,b}$	Representation of the heat exchange by convection between char particle – inert particles of the bed in Fig. 2.2
$q_{rd,b}$	Representation of the heat exchange by radiation between char particle – inert particles of the bed in Fig. 2.2
$q_{cv,w}$	Representation of the heat exchange by radiation between char particle – wall (black surface) in Fig. 2.2
r_c	Radio of the char particle, m
$r_{O2,cb}$	O_2 molar flux consumed by oxidation at the external surface of the char particle, mol/m²s
$r_{O2,gf}$	CO_2 molar flux consumed by gasification at the external surface of the char particle, mol/m²s
R_g	Gas constant: 8.315 J/molK
Re_{ePh}	Reynold number in the emulsion phase based on char particle size and u_{mf}, -
Re_{bPh}	Reynold number in the bubble phase based on char particle size and u_{tf}, -
Re_{sPh}	Reynold number in the splash zone based on char particle size and u_f, -
Sc	Smith number: $\mu_g / d_{ij}\rho_g$, -
Sh_{cdeq}	Sherwood number when there is equimolar counter-diffusion and the gas-film around the particle is not static: there is a convective flow, -
Sh_o	Sherwood number when there is equimolar counter-diffusion and the gas-film around the particle is static: there is not a convective flow, -
t_b	Time during which the char is inside a bubble, s
t_c	Combustion time, s
t_e	Time during which the char is in the emulsion phase between successive times inside bubbles in its upward motion through the bed, s
T	Duration of a complete cycle of the char's particle movement through the bed, s

T_c	Surface temperature of a char particle by one-color pyrometry, °C (K in Appendix III)
$t_{in,bed}$	Time during which the char particle is inside the bed (emulsion and bubble phase, Eq. AI.3) during a cycle of its movement, s
$t_{i,T}$	Time during which the char particle (Eq. AI.1) is in the emulsion (i = ePh), bubble (i = bPh), or splash zone (i = sPh) during a complete cycle of its movement, s
$T_{P1C,k}$	Surface temperature of a char particle by one-color pyrometry using the k spectral band or color in Eq. AIII.15 and in Eq. 3.2, K
$T_{P2C,i/j}$	Surface temperature of a char particle by two-color pyrometry using simultaneously the i and j spectral bands or colors in Eq. AIII.10 and in Eq. 3.1, K
T_{th}	Temperature of a char particle by thermocouple, °C
T_{bed}	Bed temperature, K
u_b	Average bubble velocity, m/s
u_d	Average descent velocity of a char particle through the bed, m/s
u_f	Fluidization velocity, m/s
u_{mf}	Minimum fluidization velocity, m/s
u_g	Gas velocity around to a char particle, m/s
u_r	Average rise velocity of a char particle through the bed, m/s
u_{tf}	Bubble through-flow velocity, m/s
$x_{c,fx}$	Char particles' content of carbon in Eq. 3.7, -
x_i	Molar concentration at any point of the gas-film surrounding the particle, -
$x_{i,c}$	Molar concentration at the char particle surface in the fluidized phases, -
$x_{i,bed}$	Molar concentration in the fluidized phases, -
z	Dimensionless parameter in AI.4, -

GREEK LETTERS

α_i	Absorbance of the char particle's surface (i = c), metal black box (i = w), or oven's quartz window (i = wnd), -
ΔH_{cb}	Heat of combustion (exothermic), J/mol
ΔH_{gf}	Heat of gasification (endothermic), J/mol
$\Delta\lambda_k$	Red (k = r, 0.62 – 0.70 μm), green (k = g, 0.49 – 0.58 μm), and blue (k = b, 0.45 – 0.49 μm) spectral bands
$\beta_{i/j}$	Calibration parameter for two-color pyrometry defined in Eq. AIII.9, -
β_k	Calibration parameter for one-color pyrometry defined in Eq. AIII.12, W/m^2DN
δ	Thickness of the gas-film around a char particle that absorbs the mass transfer, m

δ_k	Reduction of a char particle's size (diameter) in the perpendicular (k=⊥) or parallel (k = //) direction regarding the insertion direction of the thermocouple into the char in Eq. 3.4, -
ε_{mf}	Bed Porosity at minimum fluidization velocity, -
ζ_p	Relative error between the measurements of temperature by pyrometry and by thermocouple, %
ζ_ω	Relative error between the pyrometric temperatures assuming that the char particle's emissivity is 0.85 and by varying it from 0.85 to 1, %
θ	Correction factor when there is no equimolar counter-diffusion in Eq. 2.7, -
θ_i	Fractions of the combustion time during which the char particle is in the emulsion phase (i = ePh), bubble phase (i = bPh), or splash zone (i = sPh) in Eq. 3.3, -
	Fractions of the combustion time during which the char is in the emulsion phase (i = ePh), bubble phase (i = bPh), or splash zone (i = sPh) as a function of the char particle's size in Eq. 3.5, -
λ_k	Central wavelength of the red (k = r), green (k = g), and blue (k = b) spectral band, μm
μ_g	Viscosity of the fluidization gas, kg/ms
ξ	CO/CO_2 ratio at the char surface by oxidation, -
ρ_b	Density of the fluidized bed, kg/m³
ρ_c	Density of the char particle, kg/m³
ρ_g	Density of the fluidization gas, kg/m³
ρ_i	Density of the inert particles of the bed, kg/m³
ρ_{mc}	Molar density of the char particle, mol/m³
σ	Stefan-Boltzmann constant: 5.67×10^{-8} W/m²K⁴
τ	Tortuosity of the emulsion phase of the bed in Eq. 2.6, -
τ_i	Transmittance of the char particle's surface (i = c), metal black box (i = w), oven's quartz window (i = wnd), -
φ	Angle between the insertion direction of the thermocouple into the char particle and the fluidization flux direction (from the reactor's distributor upwards) in Fig. 4.16a
ω_c	Surface emissivity of the char particle, -
Φ_k	Constant of proportionality (Eq. AIII.14) between W/m² and W/m²μm in red (k = r), green (k = g), and blue (k = b) spectral band, 1/μm
Ψ_j	Dimensionless parameter for emulsion phase (j = ePh) and bubble phase (j = bPh) in Eq. AII.3, -

SUBSCRIPTS

⊥	Perpendicular direction regarding the insertion direction of the thermocouple into the char particle
//	Parallel direction regarding the insertion direction of the thermocouple into the char particle

ABBREVIATIONS

bPh	Bubble Phase
B	Blue spectral band
CCS	CO_2 Capture and Store
ePh	Emulsion Phase
fps	Frame per second
FBC 2D	Experimental set-up with a rectangular fluidized bed reactor (18 x 1.8 x 50 cm)
FBC 3D	Experimental set-up with a cylindrical fluidized bed reactor (7 (i.d.) x 50 cm)
FOV	Field of view of the digital camera
G	Green spectral band
P1C	One-color pyrometry
P2C	Two-color pyrometry
R	Red spectral band
sPh	Splash zone
w th	Char particle fluidized with an embedded thermocouple (restricted fluidization)
w/o th	Char particle fluidized without an embedded thermocouple (free fluidization)
WD	Working distance of the digital camera

REFERENCES

[1] BP Energy Outlook 2017 – BP Global, 2017 Edition

[2] Nejat P, Jomehzadeh F, Mahdi Taheri M, Gohari M, Zaimi M, Majid A. A global review of energy consumption, CO2 emissions and policy in the residential sector (with an overview of the top ten CO2 emitting countries). Renewable and Sustainable Energy Reviews 2015; 43; 843–862

[3] Buhre BJP, Elliott LK, Sheng CD, Gupta RP, Wall TF. Oxy-fuel combustion technology for coal-fired power generation. Progress in Energy and Combustion Science 2005; 31; 283-307

[4] Rubin ES, Mantripragada H, Marks A, Versteeg P, Kitchin J. The outlook for improved carbon capture technology. Progress in Energy and Combustion Science 2012; 38; 630-671

[5] Davidson J. Performance and costs of power plants with capture and storage of CO_2. Energy and Combustion Science 2007; 32; 1163-1176

[6] Saastamoinen J, Tourunen A, Pikkarainen T, Hasa H, Miettinen J, Hyppanen T, Myohanen K. Fluidized bed combustion in high concentrations of O_2 and CO_2. Proceeding of the 19th International Conference on Fluidized Bed Combustion 2006, N° 49

[7] Scheffknecht G, Al-Makhadmeh L, Schnell U,Maier J. Oxy-fuel coal combustion-A review of the current state-of-the-art. International Journal of Greenhouse Gas Control 2011; 5; 16-35

[8] Toftegaard MB, Brix J, Jensen PA, Glarborg P, Jensen AD. Oxy-fuel combustion of solid fuels, Progress in Energy and Combustion Science 2010; 36; 581-625

[9] Lupion M, Alvarez I, Otero P, Kuivalainen R, Lantto J, Hotta A, Hack H. 30 MWth CIUDEN Oxy-cfb Boiler - First Experiences. Energy Procedia 2013; 37; 6179-6188

[10] Czakiert T, Zuwala J, Lasek J. Oxy-fuel combustion: The state of the art. Proceedings of 12th International Conference on Fluidized Bed Technology, Kraków (Poland) 2017; 1: 35–46 (ISBN: 978-83-62079-16-2)

[11] Jäntti T, Parkkonen R. Lagisza 460 MWe Supercritical CFB-Experience During First Year After Start of Commercial Operation. Foster Wheeler Energia Oy Finland 2010; Presented at Russia Power at 24-26 March 2010 (Moscow, Russia)

[12] Leckner B, Gómez-Barea A. Oxy-fuel Combustion in Circulating Fluidized Bed boilers. Applied Energy 2014; 125; 308-318

[13] Günther C, Weng M, Kather A. Restrictions and Limitations for the Design of a Steam Generator for a Coal-fired Oxyfuel Power Plant with Circulating Fluidised Bed Combustion. Energy Procedia 2013; 37; 1312-1321

[14] Riaza J, Khatami R, Levendis YA, Álvarez L, Gil MV, Pevida C, Rubiera F, Pis JJ. Single particle ignition and combustion of anthracite, semi-anthracite and bituminous coals in air and simulated oxy-fuel conditions. Combustion and Flame 2014; 161; 1096-1108

[15] Singer S, Chen L, Ghoniem AF. The influence of gasification reactions on char consumption under oxy-combustion conditions: Effects of particle trajectory and conversion. Proceedings of the Combustion Institute 2013; 34; 3471-3478

[16] Marek E, Świątkowski B. Experimental studies of single particle combustion in air and different oxy-fuel atmospheres. Applied Thermal Engineering 2014; 66; 35-42

[17] Hecht ES, Shaddix CR, Molina A, Haynes BS. Effect of CO2 gasification reaction on oxy-combustion of pulverized coal char. Proceedings of the Combustion Institute 2011; 33; 1699-1706

[18] Gonzalo-Tirado C, Jiménez S, Ballester J. Gasification of a pulverized sub-bituminous coal in CO2 at atmospheric pressure in an entrained flow reactor. Combustion and Flame 2012; 159; 385-395

[19] Kim D, Choi S, Shaddix CR, Geier M, Effect of CO2 gasification reaction on char particle combustion in oxy-fuel conditions.Fuel 2014; 120; 130-140

[20] Jia L, Tan Y, Wang C, Anthony EJ. Experimental study of oxy-fuel combustion and sulfur capture in a mini-CFBC. Energy Fuels 2007; 21; 3160– 3164

[21] Czakiert T, Bis Z, Muskala W, Nowak W. Fuel conversion from oxy-fuel combustion in a circulating fluidized bed. Fuel Processing Technology 2006; 87; 531–538

[22] Scala F, Chirone R, Fluidized bed combustion of single coal char particles at high CO2 concentration, Chemical Engineering Journal 2010;165:902-906

[23] Scala F, Chirone R. Combusion of single coal char particles under fluidized bed oxyfiring conditions. Proccedings of the 20th Inernational Conference on Fluidized Bed Combustion 2009; 624-629

[24] Scala F, Chirone R. Combusion of single coal char particles under fluidized bed oxyfiring conditions. Industrial & Engineering Chemical research 2010; 49; 11029-11036

[25] Scala F, Chirone R. Combustion of single coal char particle under fluidized bed oxy-firing conditions. 63rd IEA-FBC Meeting, Ponferrada (Spain), 29th to 30thNovember, 2011

[26] Roy B, Bhattacharya S. Combustion of single char particles from Victorian brown coal under oxy-fuel fluidized bed conditions, Fuel 2016;165:477-483

[27] Bu C, Liu D, Chen X, Pallarès D, Gómez-Barea A. Ignition behavior of single coal particle in a fluidized bed under O2/CO2 and O2/N2 atmospheres: A combination of visual image and particle temperature. Apply Energy. 2014; 115: 301-8

[28] Bu C, Leckner B, Chen X, Pallarès D, Liu D, Gómez-Barea A, Devolatilization of a single fuel particle in a fluidized bed under oxy-combustion conditions. Part A: Experimental results. Combustion and Flame 2015; 162; 797-808

[29] Bu C, Pallarès D, Chen X, Gómez-Barea A, Liu D, Leckner B, Lu P. Oxy-fuel combustion of a single fuel particle in a fluidized bed: Char combustion characteristics, an experimental study. Chemical Engineering Journal 2016; 287; 649-656

[30] Bu C, Gómez-Barea A, Chen X, Leckner B, Liu D, Pallarès D, Lu P. Effect of CO2 on oxy-fuel combustion of coal-char particles in a fluidized bed: Modeling and comparison with the conventional mode of combustion. Applied Energy 2016; 177: 247-259

[31] Mathekga HI, Oboirien BO, North BC. A review of oxy-fuel combustion in fluidized bed reactors. International Journal of Energy Research 2016; 40: 878-902

[32] Linjewile TM, Hull AS, Agarwal PK. Optical probe measurements of the temperature of burning particles in fluidized bed. Fuel 1994; 73: 1880-1888

[33] Agarwal PK. The residence phase of active particles in fluidized beds of smaller inert particles. Chemical Engineering Science 1987; 42; 2481-2483

[34] Dos Santos FJ, Goldstein Jr L. Experimental aspects of biomass fuels in a bubbling fluidized bed combustor. Chemical Engineering and Processing: Process Intensification 2008; 47; 1541-1549

[35] Stubington JF. Comparison of techniques for measuring the temperature of char particles burning in a fluidised bed. Chemical engineering research & design 1985; 4; 241-249

[36] Manovic V, Komatina M, Oka S. Modeling the temperature in coal char particle during fluidized bed combustion. Fuel 2008; 87; Pages 905-914

[37] Selcuk N, Ozkan M. Simulation of circulating fluidized bed combustors firing indigenous lignite. International Journal of Thermal Sciences 2011; 50; 1109-1115

[38] Ozkan M. Mathematical modeling of circulating fluidized bed combustors, M. Sc. Thesis. Middle East Technical University, Ankara (Turkey)

[39] Agarwal PK, Mitchell WJ, La Nauze RD. Mass transfer processes around burning char particles in fluidized beds. International Symposium on Combustion 1989; 22; 279-286

[40] Agarwal PK, Mitchell WJ, La Nauze RD. Transport phenomena in multi-particle systems—III. Active particle mass transfer in fluidized beds of inert particles. Chemical Engineering Science 1988; 43; 2511-2521

[41] Agarwal PK. Transport phenomena in multi-particle systems—IV. Heat transfer to a large freely moving particle in gas fluidized bed of smaller particles. Chemical Engineering Science 1991; 46; 1115-1127

[42] Hayhurst AN, Parmar MS. Does solid carbon burn in oxygen to give the gaseous intermediate CO or produce CO2 directly? Some experiments in a hot bed of sand fluidized by air. Chemical Engineering Science 1998; 53; 427-438

[43] Biggs MJ, Agarwal PK. Mathematical modelling of oscillations in the temperature of freely moving burning carbonaceous particles in bubbling fluidized beds. Fuel 1993; 72; 805-811

[44] Broughton J, Howard JR. Combustion of coal in fluidized beds. In: Howard JR, Elliott D editors. Fluidized beds: Combustion and applications, Applied Science Publishers; 1983. p. 37-77

[45] Chirone R, Salatino P, Scala F. The relevance of attrition to the fate of ashes during fluidized-bed combustion of a biomass. Proceeding of the Combustion Institute 2000; 2279-2286

[46] Basu P. Burning rate of carbon in fluidized beds. Fuel 1977; 56: 390-392

[47] Komatina M, Manovic V, Dakic D. An Experimental Study of Temperature of Burning Coal Particle in Fluidized Bed. Energy Fuels 2006; 20: 114–119

[48] Winter F, Prah ME, Hofbauer H. Temperatures in a fuel particle burning in a fluidized bed: The effect of drying, devolatilization, and char combustion. Combustion and Flame 1997; 108: 302-314

[49] Collier AP, Hayhurst AN, Richardson JL, Scott SA. The heat transfer coefficient between a particle and a bed (packed or fluidised) of much larger particles. Chemical Engineering Science 2004; 59: 4613-4620

[50] Parmar MS, Hayhurst AN. The heat transfer coefficient for a freely moving sphere in a bubbling fluidised bed. Chemical Engineering Science 2002; 57: 3485-3494

[51] Hayhurst AN, Parmar MS. Measurement of the mass transfer coefficient and sherwood number for carbon spheres burning in a bubbling fluidized bed. Combustion and Flame 2002; 130: 361-375

[52] Linjewile TM, Gururajan VS, Agarwal PK. The CO/CO2 product ratio from the combustion of single petroleum coke spheres in an incipiently fluidized bed. Chemical Engineering Science 1995; 50: 1881-1888

[53] Scala F. Fluidized-Bed Combustion of Single Coal Char Particles: An Analysis of the Burning Rate and of the Primary CO/CO2 Ratio. Energy Fuels 2011; 25: 1051-1059

[54] Tomé N, Rangel N, Pincho C. Temperature of Wood Char Particles Burning in a Fluidized Bed Reactor. International Conference on Renewable Energies and Power Quality (ICREPQ'12), Santiago de Compostela (Spain), 28th to 30th March, 2012

[55] Prins W, Mass and heat transfer between a fluidized bed and a freely moving submerged sphere, Chapter 7.2 in Coal Science and Technology 22, Ed M Valk, Elsevier, Amsterdam (1995)

[56] Hernberg R, Stenberg J. Simultaneous in situ measurement of temperature and size of burning char particles in a fluidized bed furnace by means of fiber optic pyrometry, Combustion and Flame 1993; 95; 191– 205

[57] Heino P, Hernberg R, Stenberg J. Statistical pyrometric sizing of particles in fluidised bed combustion, Combustion and Flame 1997; 108; 315-326

[58] Joutsenoja T, Heino P, Hernberg R, Bonn B. Pyrometric temperature and size measurements of burning coal particles in a fluidized bed combustor. Combustion and Flame 1999; 118; 707–717

[59] Li D. Thermal image analysis using calibrated video imaging. Doctoral Thesis, University of Missouri-Columbia, Colombia, 2006

[60] Lu H, Leong-Teng I, Mackrory A, Werrett L, Scott J, Tree D, Baxter L. Particle surface temperature measurements with multicolor band pyrometry, AIChE Journal 2009; 55; 243–255

[61] Zukowski W, Baron J, Bulewicz EM, Kowarska B. An optical method of measuring the temperature in a fluidized bed combustor. Combustion and flame 2009; 156; 1445-1452

[62] Brown SL, Lattimer BY. Transient gas-to-particle heat transfer measurements in a spouted bed. Experimental Thermal and Fluid Science, 2013; 44; 883-892

[63] Tsuji T, Miyauchi T, Oh S, Tanaka T. Simultaneous measurement of particle motion and temperature in two-dimensional fluidized bed with heat transfer, KONA Powder and Particle Journal 2010; 28; 167-179

[64] Patil AV, Peters EAJF, Sutkar VS, Deen NG, Kuipers JAM. A study of heat transfer in fluidized beds using an integrated DIA/PIV/IR technique. Chemical Engineering Journal 2015; 259; 90-106

[65] Khatami R, Levendis YA. On the deduction of single coal particle combustion temperature from three-color optical pyrometry. Combustion and Flame 2011; 158; 1822-1836

[66] Grosshandler WL. The effect of soot on pyrometric measurements of coal particle temperature. Combustion and Flame 1984; 55; 59-71

[67] Godoy SM, Lockwood FC. Development of a two-colour infrared pyrometer for coal particle temperature measurements during devolatilisation. Fuel 1997; 77; 995–999

[68] Macêk A, Bulik C, Direct measurement of char-particle temperatures in fluidized bed combustors, In Symposium (International) on Combustion. Elsevier 20.1 (1985) 1223-1230

[69] Salinero J, Goméz-Barea A, Leckner B, Tripiana M, Bu B, Gómez-González E. Improving char temperature measurement by pyrometry with digital camera. Proceedings of 22nd International Conference on Fluidized Bed Conversion Turku (Finland), 2 (2015) 375-383

[70] Gómez-Barea A, Leckner B. Modeling of biomass gasification in fluidized bed. In Progress in Energy and Combustion Science 2010; 36; 444-509

[71] Arthur JR. Reactions between carbon and oxygen. Transaction of the Faraday society 1951;47; 164–78

[72] Förtsch D, Schnell U, Hein KRG, Essenhigh RH. The mass transfer coefficient for the combustion of pulverized carbon particles, Combustion and Flame 2001; 126;1662-1668

[73] Hayhurst AN. The mass transfer coefficient for oxygen reacting with a carbon particle in a fluidized or packed bed. Combustion and Flame 2000; 121; 679-688

[74] Scala F. Calculation of the mass transfer coefficient for the combustion of a carbon particle, Combustion and Flame 2010; 157; 137-142

[75] Sadhukhan AK, Gupta P, Kumar SR.Modeling and experimental studies on combustion characteristics of porous coal char: Volume reaction model. International Journal of Chemical Kinetics 2010; 42; 299–315

[76] Saucedo MA, Butel M, Scott SA, Collings N, Dennis JS. Significance of gasification during oxy-fuel combustion of a lignite char in a fluidised bed using a fast UEGO sensor. Fuel 2015; 144; 423-438

[77] Adánez J, de Diego LF, García-Labiano F,Abad A, Abanades JC. Determination of Biomass Char Combustion Reactivities for FBC Applications by a Combined Method. Industrial & Engineering Chemistry Research 2001; 40; 4317-4323

[78] Evans DD, Emmons HW. Combustion of wood charcoal. Fire Safety Journal 1977; 1; 57-66

[79] Hobbs ML, Radulovic PT, Smoot LD. Modeling fixed-bed coal gasifiers. AIChE Journal 1992; 38; 681–702

[80] Haseli Y, van Oijen JA, de Goey LPH. A detailed one-dimensional model of combustion of a woody biomass particle. Bioresource Technology 2011; 102; 9772-9782

[81] Hong L H, Warren R, Gregory P, Bryan R, Larry L. B. Comprehensive Study of Biomass Particle Combustion. Energy Fuels 2008;22; 2826–2839

[82] Prins W, Siemons R, Van Swaaij WPM, Radovanovic M. Devolatilization and ignition of coal particles in a two-dimensional fluidized bed. Combustion and flame 1989; 75; 57-79

[83] Prins, W, Casteleijn, TP, Draijer W, Van Swaaij WPN. Mass transfer from a freely moving single sphere to the dense phase of a gas fluidized bed of inert particles. Chemical Engineering Science 1985; 40; 481–497

[84] Palchonok G. Heat and mass transfer to a single particle in fluidized bed, Dr Thesis, Chalmers University of Technology, 1998.

[85] Cobbinah S, Laguérie C, Gibert H. Simultaneous heat and mass transfer between a fluidized bed of fine particles and immersed coarse porous particles. International Journal of Heat and Mass Transfer 1987; 30; 395-400

[86] Scala F. Mass transfer around freely moving active particles in the dense phase of a gas fluidized bed of inert particles. Chemical Engineering Science 2007; 62; 4159-4176

[87] Baskakov AP, Filippovsky NF, Munts VA, Ashichmin AA, Temperature of particles heated in a bed of inert material. Journal Engineering Physics 1987; 52; 574-578

[88] La Nauze RD, Jung K. The kinetics of combustion of petroleum coke particles in a fluidized-bed combustor, International Symposium on Combustion 1982; 19; 1087-1092

[89] Gómez González E. Guía para conocer las cámaras de fotografía digital. ed. Victoria 2012, pp 503

[90] Baskakov AP, Leckner B. Radiative heat transfer in circulating fluidized bed furnace. Powder Technology 1997; 90; 213-218

[91] Planck M. Distribution of energy in the Spectrum, Annals of Physics 1901; 4; 553-563

[92] Incropera FP, De Witt DP. Radiation: Properties and processes. In: Frank P. Incropera and David P. De Witt, Fundamentals of heat and mass. Prentice hall Ed., México, 1999, pp. 633-716.

[93] Roscoe JC, Witkowski AR, Harrison D. The temperature of coke particles in a fluidized combustor. Transactions of the Institution of Chemical Engineers 1980; 58; 69-72.

[94] Ross IB, Patel MS, Davidson JF. The temperatures of burning carbon particles in fluidized beds. Transactions of the Institution of Chemical Engineers 1981; 59; 83-88.

[95] La Nauze RD, Jung K, Kastl J. Mass transfer to large particles in fluidised beds of smaller particles. Chemical Engineering Science 1984; 39; 1623-1633

[96] Davidson JF, Harrison D. Fluidized Particles. Cambridge University Press, Cambridge, 1963

[97] Remiarová B, Markoš J, Žajdlík R, Jelemenský L, Identification of the mechanism of coal char particle combustion by porous structure characterization. Fuel Processing Technology 2004; 85; 303-321

[98] Scala F. A new technique for the measurement of the product CO/CO2 ratio at the surface of char particles burning in a fluidized bed, In Proceedings of the Combustion Institute 2009, 32; 2021-2027

[99] Andrei MA, Sarofim AF, Beér JM. Time-resolved burnout of coal particles in a fluidized bed, Combustion and Flame 1985; 61;17-27

[100] Chen C, Kojima T. Single char particle combustion at moderate temperature: effects of ash. Fuel Processing Technology 1996; 47; 215-232.

[101] Massman WJ. A review of the molecular diffusivities of HO, CO, CH, CO, O, SO, NH, NO, NO, and NO in air, O and N near STP. Atmospheric Environment 1998; 32; 1111-1127

[102] Fatehi H, Xue-Song Bai, Structural evolution of biomass char and its effect on the gasification rate, Applied Energy 2017; 185; 998-1006

[103] Klein SA. "Engineering Equation Solver Software (EES)", Academia Commercial version 10.091-3D (09-05-2017)

APPENDIX I. EXPERIMENTAL CHARACTERIZATION OF THE CHAR PARTICLE'S MOVEMENT THROUGH A FLUIDIZED BED

Taking into account the description of the movement of a char particle through a fluidized bed made elsewhere [43] and shown in Fig. 2.2, and the relation between the char residence time in each bed phase $t_{j,T}$ and the time spent to complete a cycle T, by

$$\theta_{j,T} = \frac{t_{j,T}}{T} \tag{AI.1}$$

The fraction of time in the splash zone during a period can be expressed by

$$\theta_s = \frac{T - t_{in-bed}}{T} \tag{AI.2}$$

where the time during which the particle is inside the bed (emulsion and bubble phases) is

$$t_{in-bed} = h_p \left(\frac{1}{u_d} + \frac{1}{u_r}\right) \tag{AI.3}$$

Therefore, the period can be expressed by

$$T = \frac{h_p}{1-\theta_s}\left(\frac{1}{u_d} + \frac{1}{u_r}\right) \tag{AI.4}$$

as a function of the upward and downward char particle's velocities (u_r and u_d) and the depth reached by a particle in a cycle (h_p).

Looking at Fig. 2.2, the upward velocity of the char particle through the bed can be expressed by

$$u_r = \frac{h_p}{m(t_e + t_b)} \tag{AI.5}$$

where m is the times that the char is reached by a bubble. The depth reached by the char is expressed by

$$h_p = m(t_b u_b - t_e u_e) \tag{AI.6}$$

Eqs. AI. 5-6 allow getting the time during which the char particle is inside a bubble as

$$t_b = \frac{u_d + u_r}{u_b - u_r} t_e \quad \text{(AI.7)}$$

and

$$t_e = \frac{h_p}{m} \frac{(u_b - u_r)}{u_r (u_b + u_d)} \quad \text{(AI.8)}$$

is the time during which the char is in the emulsion phase between the successive captures by the bubbles.

For a complete cycle, the ratio of the residence time in the emulsion phase and inside the bed: $\theta_{e,T} / (\theta_{e,T} + \theta_{b,T})$ can be expressed by

$$\frac{\theta_{e,T}}{\theta_{e,T} + \theta_{b,T}} = \frac{\frac{h_p}{u_d} + \frac{h_p}{u_r}\left(\frac{t_e}{t_e + t_b}\right)}{\frac{h_p}{u_d} + \frac{h_p}{u_r}} \quad \text{(AI.9)}$$

Eqs. AI. 7-9 give the descending velocity of the char particle through the emulsion phase by

$$u_d = \frac{\theta_{b,T}}{\theta_{e,T}} u_b \quad \text{(AI.10)}$$

as function to the bubble velocity given elsewhere [95] as

$$u_b = (u_f - u_{mf}) + 2.26\sqrt{d_b} \quad \text{(AI.11)}$$

where

$$d_b = \frac{0.3}{g^{0.2} h_p} \left(u_f - u_{mf}\right)^{0.4} \left(\left(h_{bed} - 4{A_o}^{0.5}\right)^{1.8} - \left(h_{bed} - h_p + 4{A_o}^{0.5}\right)^{1.8}\right) \quad \text{(AI.12)}$$

is the bubble diameter [43] and A_o = 9.25 10^{-5} m^2/hole in the gas distributor plate of the reactor used here.

Using Eq. AI. 4, Eq. AI: 11, and by the estimation

$$u_r = k\sqrt{u_f - u_{mf}} \quad \text{(AI.13)}$$

where k = 0.19 $m^{0.5}/s^{0.5}$ [40, 41], the cycle time T is calculated, and by Eq. AI 1 the distribution of time in each bed phase is calculated.

APPENDIX II. THEORETICAL HEAT AND MASS TRANSFER DURING CHAR PARTICLE CONVERSION IN A FLUIDIZED BED

The theoretical estimations presented are developed in Biggs et al. [43] and Agarwal et al. [40] for mass transfer; and in Biggs et al. [43], Agarwal et al. [41], Parmar and Hayhurst [50] for heat transfer.

Eqs. 2.22, 2.24, and 2.26 estimate the mass transfer from/to a char particle in the emulsion phase, bubble phase, and/or splash zone respectively, where ε_{mf} and τ are the bed porosity and tortuosity at minimum fluidization; Sc is the Smith number; Re_j is the Reynolds number of the emulsion phase (j = ePh), bubble (j = bPh), and splash zone (j = sPh); and C_d is the drag force to an isolated sphere in the emulsion phase

$$C_{d,ePh} = \frac{24}{Re_{ePh}}\left(\left(\frac{2z(1-\varepsilon_{mf})}{\tau}\right) + (10^{\Psi_{ePh}} - 1)\right) \quad \text{(AII.1)}$$

or bubble phase

$$C_{d,bPh} = \frac{24}{Re_{bPh}} 10^{\Psi_{bPh}} \quad \text{(AII.2)}$$

with

$$\Psi_j = 0.261 Re_j^{0.369} - 0.105 Re_j^{0.431} - \frac{0.124}{1+(\log_{10} Re_j)^2} \quad \text{(AII.3)}$$

and

$$z = \left(\frac{\varepsilon_{mf}}{1-\varepsilon_{mf}}\right)^{0.33} \quad \text{(AII.4)}$$

Eqs. 2.23, 2.25, 2.27) estimate the heat transfer from/to a char particle in the emulsion phase (ePh), bubble phase (bPh), and/or splash zone are estimated respectively, where

$$k_{d,ePh} = k_{d,g}\left(1 + \frac{(1-\varepsilon_{mf})(1-k_{d,i}/k_{d,g})}{k_{d,i}/k_{d,g} + 0.28\varepsilon_{mf}^{0.63(K_{d,i}/K_{d,g})^{0.18}}}\right) + 0.1\rho_g c_{p,g} d_i u_{mf} \quad \text{(AII.5)}$$

is the effective thermal conductivity of the emulsion phase; $k_{d,g}$, ρ_g, y $c_{p,g}$ are the thermal conductivity, density, and specific heat of the fluidization gas; $k_{d,i}$, and d_i, the thermal conductivity and size of the inert particles; ρ_{mf} the bed density at minimum fluidization velocity;

and Pr is the Prandtl number. The gas properties are calculated using the mass fraction of O_2, N_2, and CO_2 in the fluidized phase along with the values shows in Table AII. 2.

Table AII.1. Values of the gaseous compound

Specific Heat*			
$c_{p,O2}$	$-9.20\ 10^{-5}\ T_b^2 + 3.60\ 10^{-1}\ T_b + 8.20\ 10^2$	J/mol K	[103]
$c_{p,N2}$	$-3.26\ 10^{-5}\ T_b^2 + 2.43\ 10^{-1}\ T_c + 9.51\ 10^2$	J/mol K	[103]
$c_{p,CO2}$	$-2.57\ 10^{-5}\ Tb^2 + 8.42\ 10^{-1}\ Tb + 6.48\ 10^2$	J/mol K	[103]
Viscosity*			
$\mu_{p,O2}$	$-7.39\ 10^{-12}\ T_b^2 + 4.87\ 10^{-8}\ T_b + 7.62\ 10^{-6}$	kg/m s	[103]
$\mu_{p,N2}$	$-8.02\ 10^{-12}\ T_b^2 + 4.11\ 10^{-8}\ T_b + 7.11\ 10^{-6}$	kg/m s	[103]
$\mu_{p,CO2}$	$-8.33\ 10^{-12}\ Tb^2 + 4.77\ 10^{-8}\ Tb + 1.97\ 10^{-6}$	kg/m s	[103]
Thermal conductivity*			
$k_{d,O2}$	$-10^{-8}\ T_b^2 + 8.27\ 10^{-5}\ T_b + 3.28\ 10^{-3}$	W/m s	[103]
$k_{d,N2}$	$+8.80\ 10^{-9}\ T_b^2 + 3.97\ 10^{-5}\ T_b + 1.61\ 10^{-2}$	W/m s	[103]
$k_{d,CO2}$	-1.64 10-8 Tb 2 + 9.62 10-5 Tb – 1.13 10-2	W/m s	[103]
Enthalpies*			
AH_{CO2}	$-3.64\ 10^{-3}\ T_c^2 + 4.88\ 10^1\ T_c - 3.97\ 10^5$	J/mol	[103]
AH_{CO}	$-1.84\ 10^{-3}\ T_c^2 + 3.04\ 10^1\ T_c - 1.12\ 10^5$	J/mol	[103]
AH_{O2}	$1.75\ 10^{-3}\ T_c^2 + 3.22\ 10^1\ T_c - 1.52\ 10^3$	J/mol	[103]

*T_b in Kelvin from 298 to 1748 K

APPENDIX III. TEMPERATURE OF A CHAR PARTICLE MEASURED BY PYROMETRY

AIII.1 CHAR PARTICLE'S RADIOSITY

The following assumptions are needed to determine the radiosity of the char particle during combustion at the center of the electric oven shown in Fig. AIII.1:

- Internal walls behave as black surfaces (a black surface makes radiation and temperature uniform)
- Radiation is emitted and reflected diffusely
- The surface area of the internal walls of the oven is much greater than that of a particle and that of the window ($A_w >> A_c$, $A_w >> A_{wnd}$)
- The window is much greater than the particle ($A_{wnd} >> A_c$)

The mathematical model of i surface's radiosity (j_i) that exchanges thermal radiation with n surrounding surfaces can be found elsewhere [92] by

$$j_i = \omega_i(\lambda, T_i)\, e^o(\lambda, T_i) + \left(1 - \alpha_i(\lambda, T_i) - \tau_i(\lambda, T_i)\right) \sum_{j=1}^{n} f_{i,j}\, j_j \qquad \text{(AIII.1)}$$

where T_i is the i surface's temperature; λ is the thermal radiation's wavelength; α_l (λ,T_i), τ_l (λ,T_i), and ω_l (λ,T_i) are the i surface's absorbance, emissivity and transmittance; e° is the radiation emitted by the surface as black body (W/m²μm), and $f_{i,j}$ is the view factor between surfaces. Therefore, the radiosities of char particle (j_c), oven's wall (j_w), and window (j_{wnd}) are

$$j_c = \omega_c(\lambda, T_c)\, e^o(\lambda, T_c) + \left(1 - \alpha_c(\lambda, T_c) - \tau_c(\lambda, T_c)\right)\left(f_{c.c}\, j_c + f_{c.w}\, j_w + f_{c.wnd}\, j_{wnd}\right) \qquad \text{(AIII.2)}$$

$$j_w = \omega_w(\lambda, T_w)\, e^o(\lambda, T_w) + \left[1 - \alpha_w(\lambda, T_w) - \tau_w(\lambda, T_w)\right]\left(f_{w.c}\, j_c + f_{w.w}\, j_w + f_{w.wnd}\, j_w\right) \qquad \text{(AIII.3)}$$

$$j_{wnd} = 0 \qquad \text{(AIII.4)}$$

Respectively. Note that $\sigma_{wnd} = 0$, $\tau_{wnd} = 1$, $\alpha_{wnd} = 0$ since is a quartz window.

This equations system (Eq. AIII.2 – AIII.4) can be solved taking into account: (i) the ideal behavior of the surrounding walls, that is, $\omega_w = 1$; (ii) the weak dependence of char emissivity

on temperature and on the wavelengths in the visible range [66], that is, the char surface is gray [56, 57, 68]; (iii) the char particle is opaque, that is, $\tau_c = 0$ and because it is gray, $\omega_c = \alpha_c$ [92]; (iv) the char particle is convex, that is, $f_{c,c} = 0$; and (v) the relationship between the shape factors ($\Sigma f_{i,j} = 1$, $f_{i,j} A_i = f_{j,i} A_j$) [92]. Then, Eq. AIII. 2 becomes

$$j_c = \omega_c \, e^o(\lambda, T_c) + (1 - \omega_c) \, e^o(\lambda, T_w) \tag{AIII.5}$$

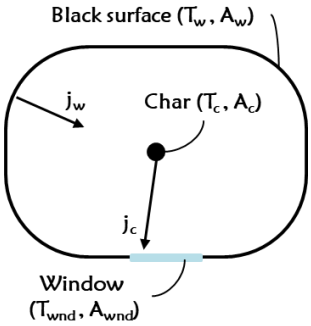

Fig. AIII. 1. Radiation exchange between black surface-char-window with temperatures T and surfaces A.

AIII. 2. TWO-COLOR PYROMETRY WITH DIGITAL CAMERA

Taking into account the high char emissivity (higher than 0.85), the radiation reflected by the char surface is negligible when its temperature is higher than the background, and the char's radiosity (Eq. AIII.5) can be simplified by

$$j_c = \omega_c \, \frac{C_1}{\lambda^5} \exp\left(-\frac{C_2}{\lambda T_c}\right) \tag{AIII.6}$$

where Wien's law

$$e^o(\lambda, T_c) = \omega_c \, \frac{C_1}{\lambda^5} \exp\left(-\frac{C_2}{\lambda T_c}\right) \tag{AIII.7}$$

has been used. If Eq. AIII.7 is applied at two wavelengths (λ_i, λ_j), both related each other, the temperature becomes

$$T_c = \frac{C_2 \left(\frac{1}{\lambda_j} - \frac{1}{\lambda_i}\right)}{\ln\left(\frac{j_c(\lambda_i, T_c)}{j_c(\lambda_j, T_c)}\right) - 5 \ln\left(\frac{\lambda_j}{\lambda_i}\right)} \tag{AIII.8}$$

where the char particle was assumed to be gray [32, 56-60,65-67].

The ratio $j_c(\lambda_i, T_c) / j_c(\lambda_j, T_c)$ is not known, but it can be estimated by the digital numbers

$$\frac{j_c(\lambda_i, T_c)}{j_c(\lambda_j, T_c)} \approx \beta_{i/j} \, \frac{DN_i}{DN_j} \tag{AIII.9}$$

using a $\beta_{i/j}$ parameter, which lumps the relation between the thermal radiation received over the sensor and the digital numbers generated (note that i and j indexes refer to the colors used). Introducing Eq. AIII.9 into Eq. AIII.8, the temperature by two-color pyrometry (P2C) is obtained

$$T_{P2C,i/j} = \frac{C_2\left(\frac{1}{\lambda_j}-\frac{1}{\lambda_i}\right)}{\left(\ln\left(\frac{DN_i}{DN_j}\right)+\ln(\beta_{i/j})\right) - 5\ln(\frac{\lambda_j}{\lambda_i})} \quad \text{(AIII.10)}$$

AIII. 3. ONE-COLOR PYROMETRY WITH DIGITAL CAMERA

By integrating Eq. AIII.5 within the spectral band (color) $\Delta\lambda_k$, it is obtained

$$\int_{\Delta\lambda_k} j_c(\lambda_i, T_c)\, d\lambda = \int_{\Delta\lambda_k} \frac{C_1}{\lambda^5}\, \omega_c\, exp(-\frac{C_2}{\lambda\, T_c}) + \int_{\Delta\lambda_k}(1-\omega_c)\, e^o(\lambda, T_w)\; d\lambda \quad \text{(AIII. 11)}$$

The first member in Eq. AIII. 11 can be estimated as

$$\int_{\Delta\lambda_k} j_c(\lambda_i, T_c)\, d\lambda \approx \beta_k\, DN_k \quad \text{(AIII.12)}$$

where β_k parameter has been introduced (the relation between the thermal radiation received over the sensor and the digital numbers generated), whereas the first term of the second member can be simplified as

$$\int_{\Delta\lambda_k} \frac{C_1}{\lambda^5}\; \exp(-\frac{C_2}{\lambda\, T_c})\, d\lambda \approx \Phi_k\; \frac{C_1}{\lambda_k^5}\, \exp(-\frac{C_2}{\lambda_k\, T_c}) \quad \text{(AIII.13)}$$

defining a proportionality constant

$$\Phi_k = \frac{\int_{\Delta\lambda_k}\frac{C_1}{\lambda^5}\, \exp(-\frac{C_2}{\lambda\, T_k})d\lambda}{\frac{C_1}{\lambda_k^5}\exp(-\frac{C_2}{\lambda_k\, T_k})} \quad \text{(AIII.14)}$$

where T_k is the average temperature of the range that can be measured using each spectral band $\Delta\lambda_k$, which is known by calibration tests (see AIII. 4). Substitution of Eq. AIII.12 and AIII.13 into Eq. AIII.11, yields the temperature of one-color pyrometry (P1C)

$$T_{P1C,k} = \frac{C_2}{\lambda_k\left[\ln\left(\Phi_k\, \frac{\varepsilon_c\, C_1}{\lambda_k^5}\right) - \left(\ln(\beta_k\, DN_k - (1-\varepsilon_c)\, E(\Delta\lambda_k, T_w))\right)\right]} \quad \text{(AIII. 15)}$$

where

$$E(\Delta\lambda_k, T_w) = \int_{\Delta\lambda_k}\, e^o(\lambda, T_w)\; d\lambda \quad \text{(AIII. 16)}$$

The accuracy of the P1C measurement depends on the simplification in Eq. AIII. 13, which assumes that ϕ_k is independent of the char's temperature. Note that for each spectral band, the value of ϕ_k is the same (see Eq. AIII.14). This simplification was evaluated by the author in a previous work [69], where the approximate temperatures $T_{P1C,k}$* (calculated by P1C using the average value of ϕ_k given by Eq. AIII. 14) were compared to the exact ones $T_{P1C,k}$ (calculated by P1C using the exact value of ϕ_k, introducing the approximate temperature $T_{P1C,k}$* in Eq. AIII.14). The comparison shown a disagreement lower than 0.5 % for black's body temperature higher than 650 °C.

AIII. 4. CALIBRATION CURVES

Equations AIII.10 and AIII.15, used to determine the char particle's surface temperature need the parameters ($\beta_{i/j}$, β_k). These parameters are given by fits to the points (DN_i/DN_j - $\beta_{i/j}$) for P2C,and (DN_k - β_k) for P1C according to Eq. AIII.17 and Eq. AIII.18 respectively, where the

temperature related to the surface region, whose radiation is measured, is substituted by digital numbers. In this way, the fitting curves store the relation between the calibration parameter and the digital numbers in the temperature range of interest.

$$\ln(\beta_{i/j}) = \frac{C_2}{T}\left(\frac{1}{\lambda_j} - \frac{1}{\lambda_i}\right) + 5 * \ln\left(\frac{\lambda_j}{\lambda_i}\right) - \ln\left(\frac{DN_i}{DN_j}\right) \quad \text{(AIII.17)}$$

$$\ln(\beta_k) = \ln\left(\Phi_k\, \varepsilon_c\, \frac{C_1}{\lambda_k^5}\, \exp\left(-\frac{C_2}{\lambda_k T}\right) + (1 - \varepsilon_c)\, E(\Delta\lambda_k, T_w)\right) - \ln(DN_k) \quad \text{(AIII.18)}$$